Aalto University
School of Engineering

Tuomas Rantanen

Rock mechanics analyses of exfoliation fractures at Långören island

Master's thesis that has been left to be inspected for the degree of Master of Science

Espoo 07.11.2016
Supervisor: Professor Mikael Rinne
Instructor: Topias Siren

Aalto University
School of Engineering

Aalto University, P.O. BOX 11000, 00076 AALTO
www.aalto.fi

Abstract of master's thesis

Author Tuomas Rantanen

Title of thesis Rock mechanics analyses of exfoliation fractures at Långören island

Degree programme Structural Engineering and Building Technology

Major/minor Foundation and Rock Engineering / Construction Economics and Management **Code** IA3028

Thesis supervisor Mikael Rinne

Thesis advisor(s) Topias Siren

Date 07.11.2016 **Number of pages** 71 **Language** English

Abstract

Exfoliation fracturing is a worldwide observed and studied fracturing phenomenon in rock. However, the true cause of this type of fracturing remains still currently unidentified. While one of the most recent exfoliation fracturing observations occurred at Långören island in South-Western Finland, the aim of this thesis was to discover the reason for this local event by employing a fracture mechanics code FRACOD^{2D}.

As the fracturing occurred at the end of the exceptionally hot summer period, the thermal conditions were considered highly important for the analysis. The weather conditions were determined based on the historical data and *in situ* monitoring, which was performed at the island. In addition, the stress field, topography and previous post-glacial conditions were estimated in order to account different exfoliation theories. As a result, three alternative theories, which were topography induced high stress, post-glacial pressure release and summertime induced thermal expansion, were selected to be modelled.

Exfoliation fractures were detected in all of the modelling cases, while the undulating convex topography and high compressive stress state were applied. In this context, the topography, which was the most capable of producing high tensile stresses was also the most appropriate regarding the development of exfoliation fractures. As the solely high *in situ* compression seems slightly unrealistic and the post-glacial conditions could not be included in the present day fracturing, the thermal expansion was evaluated as the most probable cause of the Långören exfoliation events. The long-term thermal expansion was also discovered to induce additional stresses much deeper compared to short-term thermal impact. Thus, the fractures very close to the rock surface could be generated by the expansion due to the sudden temperature peak while high average temperatures would be required for further fracture development.

The results of this study indicate that very high stresses are necessary for the exfoliation fracturing. Actually several factors can affect behind high compression and the thermal expansion represents only one of them. This master's thesis provided basis for the more profound exfoliation analyses with fracture mechanics approach. Consequently, for example, time-dependent fracture growth, pre-existing fractures, viscoelasticity, direction-dependent rock mass strength and improved accuracy can be employed in the future modelling.

Keywords Exfoliation fracturing, Fracture mechanics, Thermal expansion, Modelling, Fracod

Aalto-yliopisto
Insinööritieteiden korkeakoulu

Aalto-yliopisto, PL 11000, 00076 AALTO
www.aalto.fi

Diplomityön tiivistelmä

Tekijä Tuomas Rantanen

Työn nimi Långörenin saaren eksfoliaatiorakojen kalliomekaaninen analysointi

Koulutusohjelma Rakenne- ja rakennustuotantotekniikan koulutusohjelma

Pää-/sivuaine Pohja- ja kalliorakentaminen / Rakentamistalous **Koodi** IA3028

Työn valvoja Mikael Rinne

Työn ohjaaja(t) Topias Siren

Päivämäärä 07.11.2016 **Sivumäärä** 71 **Kieli** Englanti

Tiivistelmä

Eksfoliaatiorakoilu on maailmanlaajuisesti tunnettu kallioperän ilmiö, jonka todellista alkuperää ei ole kuitenkaan pystytty todistamaan tieteellisesti. Vaikka rakoilun yleinen syntymekanismi onkin vielä nykyisin tuntematon, tämän diplomityö tavoitteena oli selvittää syy vuonna 2014 Långörenin saarella Koillis-Suomessa tapahtuneelle eksfoliaatiorakoilulle käyttäen rakomekaanista mallinnusohjelmistoa FRACOD^{2D}:ta.

Raot syntyivät poikkeuksellisen kuuman kesäkauden päätteeksi, joten termiset olosuhteet määriteltiin olennaisiksi tekijöiksi tutkimuksen kannalta. Reunaehdot lämpötilojen osalta hankittiin käyttäen ilmatieteenlaitoksen tilastollista dataa ja *in situ* mittauksin selvitettyjä kallion lämpötilajakaumia. Lisäksi jännitystila, topografia ja jääkauden jälkeiset olosuhteet määriteltiin karkeasti, jotta eksfoliaatiorakoilua oli mahdollista simuloida eri teorioihin perustuen. Työhön mallinnettavaksi valikoituivat teoriat topografian aiheuttamasta korkeasta jännitystilasta, jääkauden jälkeisestä kuormanpoistumisesta ja kesäkauden aiheuttamasta lämpölaajenemisesta.

Eksfoliaatiorakoja syntyi kaikissa eri teorioihin perustuvissa rakomekaanisissa malleissa, kun käytettiin kumpuilevaa kuperaa topografiaa ja suhteellisen korkeaa puristusjännitystä. Eniten eksfoliaatiorakoilua synnyttänyt topografia oli se, jossa syntyi suurimpia vetojännityksiä suhteessa mallinnettuun puristukseen. Toisaalta hyvin korkea tektoninen puristusjännitys vaikuttaa epärealistiselta eikä jääkauden jälkeisillä olosuhteilla kyetty selittämään nykyisin ilmenevää eksfoliaatiota. Täten kausittainen lämpölaajeneminen valikoitui kaikkein mahdollisimmaksi rakoilun alkuperäksi Långörenin saaren tapauksessa. Pitkän aikavälin lämpölaajeneminen aiheutti mallinnuksissa lisäjännityksiä selvästi syvemmälle verrattuna lyhyen aikavälin lämpölaajenemiseen. Tästä syystä lyhytaikainen korkea lämpötila voisi synnyttää rakoja vain hyvin lähellä kalliopintaa, kun taas pitkän ajanjakson saatossa korkea keskilämpötila voisi aiheuttaa rakoja useiden metrien syvyyteen.

Työssä esitettyjen tulosten mukaisesti tietynlainen topografia ja korkea puristusjännitys ovat välttämättömiä vaatimuksia eksfoliaatiorakojen synnylle. Korkea puristusjännitys saattaa kuitenkin lämpölaajenemisen ohella aiheutua useiden eri tekijöiden seurauksena. Työn tarjoamia reunaehtoja eksfoliaation synnylle voidaan toisaalta hyödyntää tulevissa tutkimuksissa. Lisäksi esimerkiksi aikariippuvaa raonkasvua, olemassa olevia rakoja, viskoelastisuutta ja suuntariippuvaa kalliomassan lujuutta voidaan huomioida tulevaisuudessa yhä tarkemmissa analyyseissä.

Avainsanat Eksfoliaatiorakoilu, Rakomekaniikka, Lämpölaajeneminen, Mallinnus, Fracod

Preface

This master's thesis originates from the mystery of exfoliation fracturing, which has fascinated scientists over centuries. The work was conducted at Aalto university in the Department of Civil Engineering. Furthermore, the in situ experiment, described in the thesis, was part of collaborative exfoliation fracturing research between ETH Zurich, Switzerland and Aalto university and it was funded and designed by ETH Zurich.

For me, the master's thesis was the final accomplished for the degree of Master of Science. The project taught me greatly, and not only rock mechanics but also new ways to work, discover information and solve inevitable problems, as the unknown origin of exfoliation was examined. Hence, I would like to acknowledge all the people who were involved in this accomplishment. The following persons provided me guidance.

Mikael Rinne (Aalto university) – Thesis Supervisor
Topias Siren (Aalto university) – Main advisor
Johannes Suikkanen (Posiva Oy) – Advisor
Erik Johansson (Saarnio & Riekkola Oy) – Advisor
Matthew Perras (ETH Zurich) – Advisor, in situ experiment
Kerry Leith (ETH Zurich) – Advisor, in situ experiment

First of all, I would like to express my gratitude to Prof. Mikael Rinne for providing me a possibility to work for Aalto university with such an interesting topic. Secondly, I want to thank my advisor Topias Siren for his comments and assistance in the project, especially with the fracture mechanics modelling. Moreover, I express my appreciation to Johannes Suikkanen (Posiva Oy) and Erik Johansson (Saarnio & Riekkola Oy) for assisting my work with proficient comments and accurate remarks.

From ETH Zurich, I would like to thank the developers of the in situ monitoring system Matthew Perras and Kerry Leith for their support and for the opportunity of being part of a unique and fascinating experiment at Långören island. I give also my gratitude to all the people at Aalto university who I had a change to work with and who provided me help when needed.

Finally, I would like to thank my family, friends and especially my girlfriend Milla-Maria Nyman for cheering and constant support.

Espoo 07.11.2016

Tuomas Rantanen

Content

Notations

G	[J/m^2]	Strain energy release rate
G_C	[J/m^2]	Critical strain energy release rate
G_I	[J/m^2]	Strain energy release rate in mode I
G_{II}	[J/m^2]	Strain energy release rate in mode II
G_{IC}	[J/m^2]	Critical strain energy release rate in mode I
G_{IIC}	[J/m^2]	Critical strain energy release rate in mode II.
E	[GPa]	Young's modulus
K	[MPa$\sqrt{m}$]	Stress intensity factor
K_C	[MPa$\sqrt{m}$]	Fracture toughness
K_{IC}	[MPa$\sqrt{m}$]	Fracture toughness in mode I
K_{IIC}	[MPa$\sqrt{m}$]	Fracture toughness in mode II
S_H	[MPa]	Major horizontal stress component
S_h	[MPa]	Minor horizontal stress component
Sv	[MPa]	Vertical stress component
U	[J]	Energy
W	[J]	Work
Y_k		Dimensionless stress intensity factor
a	[mm]	Crack length
b_t	[mm/mm°C]	Coefficient of thermal expansion
c	[MPa]	Cohesion
c_p	[J kg^{-1} K^{-1}]	Specific heat capacity
c_t	[W m^{-1}K^{-1}]	Thermal conductivity
g	[m/s^2]	Gravitational acceleration
h	[m]	Height
k_i	[°]	Curvature
k_n	[GPa/m]	Normal stiffness
k_s	[GPa/m]	Shear stiffness
v	[m/s]	Velocity
z	[m]	Depth
Δl	[m]	Length
Δt	[s]	Time
β	[°]	Slope of the surface
θ	[°]	Direction
ν		Poisson's ratio
ρ	[kg/m^3]	Density
$\sigma_{1,2,3}$	[MPa]	Main stress component
σ_c	[MPa]	Uniaxial compressive strength
σ_{cm}	[MPa]	Rock mass strength
σ_H	[MPa]	Horizontal principal stress component
σ_{ij}	[MPa]	Stress component to ij direction
σ_n	[MPa]	Stress normal to the failure plane
σ_S	[MPa]	Shear stress
σ_t	[MPa]	Tensile strength
$\sigma_{tensile}$	[MPa]	Tensile stress
σ_v	[MPa]	Vertical principal stress component
φ	[°]	Friction angle
ψ	[°]	Dilatation angle
ϕ		Normal traction gradient

Abbreviations

2D	Two-dimensional
3D	Three-dimensional
AE	Acoustic emission
BEM	Boundary Element Method
DDM	Displacement Discontinuity Method
FMI	Finnish Meteorological Institute
GPR	Ground Penetrating Radar
GTK	Geological survey of Finland
Mode I	Tensile fracturing mode
Mode II	Shear fracturing mode
Mode III	Anti-plane shear fracturing mode
SCG	Subcritical crack growth
UCS	Uniaxial compressive strength

1 Introduction

This chapter introduces the exfoliation fracturing phenomenon in rock. Furthermore, it presents the aim of this thesis together with employed methods and written structure.

1.1 Exfoliation fracturing

Rock mass is always composed of many different types of fractures and other geological structures. One specific type of rock discontinuity is *exfoliation fracturing* and it can be identified based on its anomalous features separating it from other cracking types.

Exfoliation fractures (Figure 1), also called as sheeting joints, are large scale fractures, which usually generate parallel to the topographic surfaces (Harland 1957; Twidale 1973; Martel 2006) They can reach 200 meters lateral length and initiate in depths of 100 meters. However, fracture curvature decreases and vertical distance between fractures increases with depth. (Jahns 1943) Considering the previous features, the term *exfoliation* is appropriate for these fractures, as it refers to Latin word *exfoliāre,* which signifies surface parallel peeling (Chapman and Greenfield 1949).

Figure 1. Slightly curved exfoliation fractures at Yosemite national park in United States (Martel 2011).

The generation of exfoliation fractures is not limited to any specific climate or territorial environment (Holzhausen 1989). On the other hand, it has been realized that exfoliation commonly develops in hard rocks such as granite, gneiss and massive sandstone, which possess high uniaxial compressive strength (Jahns 1943). Exfoliation fracturing is regularly determined as a geologically young structure (Hencher *et al.* 2010), because exfoliation often occurs parallel to the surface that is formed during the last few million years (Martel 2006) and the fractures cut across other older discontinuities (Twidale 1973). Moreover, exfoliation fracturing phenomena have been recorded recently at Twain Harte in United States and at Långören island in Finland.

Exfoliation fracturing is strongly related to time-dependent rock behaviour, because, in addition to rapid fracture development, the generation of exfoliation fractures has been also observed to occur subcritically (i.e. progressively) (Bahat *et al*. 1999). *Subcritical crack growth* (SCG) is a state where a fracture grows with a slow but accelerating velocity

in stress state close but below the material ultimate strength. While this stable type of fracture propagation can be distinguished from the rapid and uncontrolled rock failures (Backers 2006), subcritical fracture propagation can eventually lead to rapid fracture development (Rinne 2008). According to Wiederhorn *et al.* (1974), the transition between subcritical and spontaneous fracturing is determined by a velocity of 10^{-1} *m/s* (Bahat *et al.* 1999). As a result, exfoliation can develop slowly during long periods of time or along instantaneous failure.

Although three hundred years of worldwide observations and research have been achieved regarding the origin of exfoliation joints, their true cause remains still unrevealed. Consequently, numerous theories exists, explaining the source of exfoliation phenomenon. According to Twidale (1973), these theories can be divided into external and internal categories. The traditional external theories rely on temperature variations, chemical weathering and pressure release. Internal explanations, on the other hand, rely on plutonic injection, metasomatic expansion, vertical uplift and lateral compression. (Twidale 1973)

Currently, the external origin of exfoliation is often considered as more convenient than internal one (Twidale 1973). However, Martel (2006 and 2011) has accomplished to construct a hypothesis on how high horizontal stresses tend to reorient and increase corresponding tensile stresses due to convex topography conditions and produce exfoliation. Thus, theory of surface-parallel compression can be considered as one of the most probable explanation for the rock exfoliation.

In external category, the theories of temperature variations and chemical weathering are also widely criticized (i.e. Twidale 1973; Holzhausen 1989; Martel 2006). Therefore, the explanations of pressure release and surface-parallel compression are commonly regarded as the two most plausible causes of rock exfoliation. On the other hand, while the high compressive stress state is evidently associated with exfoliation fracturing, it is important to realize that for example temperature variations and chemical reactions can have a major impact on the fracture development due to their compression increasing effects (Twidale 1973).

The importance of exfoliation fracturing research exists because of the rock mechanical problems induced by these fractures. Exfoliation fractures can generate serious hazards. For instance, they reduce slope stability (Terzaghi 1962), and influence strongly to the erosion rate (Wakasa *et al.* 2006) and groundwater networks (Borchers 1996).

1.2 Exfoliation at Långören island

One of the most resent exfoliation fracturing recordings occurred in 2014 at Långören island in South-Western Finland. At the end of extremely hot summer period, the island bedrock crackled and new fractures appeared, finally generating evident exfoliation slabs (Figure 2).

Figure 2. Långören exfoliation fractures located very close to the rock surface. The photo is taken a few days after the event when the fractures had achieved full openness (photo by Aleksei Sarpaneva)

The fracturing started with a cracking noise and shortly after, apparent fracture trails appeared to the rock surface. The main event continued about two hours. However, the near surface slabs reached their full openness during the following days.

While regarding the Långören fracturing phenomenon, the high temperature and solar radiation can be determined as probable triggering effects for the fracture propagation. The improved failure conditions at Långören are also achieved due to the nearby seawater, which might induce moist fracture environment leading to higher exfoliation fracturing velocities (Bahat *et al.* 1999).

1.3 The thesis

This master's thesis examines exfoliation fracturing at Långören island through fracture mechanics modelling. The aim of the study was to construct a conceptual model explaining what was the cause of the exfoliation events in 2014. The thesis does not concentrate on defining the true cause of the global rock exfoliation, but it only explores the reason of the local phenomenon.

The analyses were conducted using FRACOD^{2D} -software (*FRActure propagation CODe)* which enables fracture mechanics modelling of crack initiation and propagation in two-dimensional space. The FRACOD^{2D} employs the DDM –method *(Displacement Discontinuity Method)* and fracture propagation is predicted according to the modified G-criterion called F-criterion. (Shen *et al.* 2014) The software can also consider time dependency, thermal and hydrological effects (Shen *et al.* 2014) and it has previously been used for exfoliation fracturing observations (Lanaro *et al.* 2007).

The challenges in the research exist mainly due to the unknown origin of exfoliation fractures. Thus, while constructing fracture mechanics models, certain assumptions and various theories must be employed in order to obtain overall information of the exfoliation

phenomenon at Långören island. The risk in the analysis is that some essential basis behind exfoliation phenomenon was not considered and therefore, the results remain incomplete. Moreover, the simplifications that were required for the fracture mechanics modelling might have had a significant influence on the achieved results.

In the thesis, chapter 2 introduces the theoretical basis behind modern fracture mechanics. Furthermore, it presents the exfoliation fracturing theories, which are currently regarded as the most prominent ones. The final part of the chapter demonstrates the rock and environmental conditions at Långören island.

Chapter 3 presents the methodology for monitoring the exfoliation fracturing in the field conditions. In addition, the rock temperature behaviour at Långören is demonstrated and the temperature variation in contrast to the existing fractures is discussed.

Chapter 4 introduces the fracture mechanics modelling software FRACOD^{2D} and its capabilities and limitations to model exfoliation fracturing. Sensitivity analyses and model calibration are also presented in this chapter.

Chapter 5 reviews the complete fracture mechanics modelling for the exfoliation at Långören island. The simulations are based on the different exfoliation fracturing theories and the obtained results are evaluated after each case.

Finally, in chapters 6 and 7 the results achieved in the study are discussed and concluded. Furthermore, the uncertainties, remarks and the further improvements are presented regarding the thesis.

2 Methods and materials

Understanding the basis of fracture mechanics studies is essential for profound analyses of the achieved results. On the other hand, while features of natural rock mass make the rock discontinuous, heterogeneous and anisotropic, it is also important to consider rock mechanical and fracture mechanical theories and methods critically as they are usually developed for materials with ideal quality. (Whittaker *et al.* 1992)

This chapter concentrates on giving a short introduction to fracture mechanics and exfoliation fracturing theories. In addition, the last part of this section presents the rock and environmental conditions at Långören island.

2.1 Fracture mechanics

2.1.1 Griffith hypothesis and definitions

The modern fracture mechanics is comprehensively based on the Griffith hypothesis (Griffith 1920) of primitive micro-cracks and energy balance. However, Griffith theory has some limitations mainly restricting the concept only for tensile failures. As a result, it has been enhanced and modified considerably over last decades. (Whittaker *et al.* 1992)

In order to explain the Griffith hypothesis and other fracture mechanical principles, it is first important to define terms related to these fundamental theories. Bieniawski (1967) provided accurate explanations for the fracture mechanics terms separating the crack and fracture initiation and propagation.

Crack initiation occurs prior to actual fracturing and it is determined as a process in which microscopic defects are originated to an intact material. Analogously, *fracture initiation* is a process in which these pre-existing micro-flaws coalesce forming an apparent larger scale fracture while the stress at the flaw tips exceeds the molecular cohesive strength of a material. *Fracture propagation* takes place when a fracture inside a material is continuously extending. (Bieniawski 1967)

Griffith hypothesis examines the phenomenon of fracture initiation presenting two basic requirements for the tensile failure of a solid. *The stress requirement,* for overcoming the cohesive strength of a material, is achieved by the assumption that a material contains elliptical pre-existing flaws, referred as Griffith cracks. These cracks induce stress concentrations thus, leading to fracture initiation. *The energy requirement* on the other hand, implies that external loading applied to the structure is balanced by the potential elastic strain energy and the surface energy of the pre-existing cracks. Therefore, the amount external work must be increased in order to overcome the resistance for fracture initiation. (Bieniawski 1967)

According to Whittaker *et al.* (1992), the total energy U of the infinite cracked plane in tension can be presented using the following formula.

$$U = U_t + U_c - W + U_s = U_p + U_s \tag{1}$$

Where,

U	*is total energy of the infinite cracked plane*
U_t	*is total initial elastic strain energy of the stressed but uncracked plane*

U_c *is the elastic strain energy release caused by the introduction of the crack of length 2a and the relaxation of the material above and below the crack*
U_s *is change in the elastic surface energy due to the formation of the crack new surfaces*
U_p *is change in the potential energy*
W *is work done by the external forces*

Employing the theory of elasticity, the above equation can be solved to present strain energy release rate G, which is regarded as a highly important parameter in fracture mechanics. Strain energy release rate is expressed with a generic equation as follows and it represents the elastic strain energy release U_c per unit crack length. (Whittaker *et al.* 1992)

$$G = \frac{\partial U_c}{\partial a} = \frac{\pi \sigma^2 a}{E'} \tag{2}$$

Where,

G *is strain energy release rate*
σ *is tensile stress*
a *is half-crack length*
E' *is Young's modulus*

In tension, the necessary condition for fracture initiation is achieved when the strain energy release rate reaches the critical value G_c, which can also be presented in terms of material property parameter *fracture toughness* (Whittaker *et al.* 1992).

2.1.2 Modes of fracturing

In order to understand the function of fracture toughness, it is first essential to explain the behaviour of fractures under different loading conditions. In a solid, fractures can be divided into three main categories, which are tensile (*mode I*), shear (*mode II*) and anti-plane shear (*mode III*) modes of cracking (Figure 3). These fracturing modes represent the displacements produced by the affecting stress state, which is generally divided into three main components (Figure 4). (Whittaker *et al.* 1992)

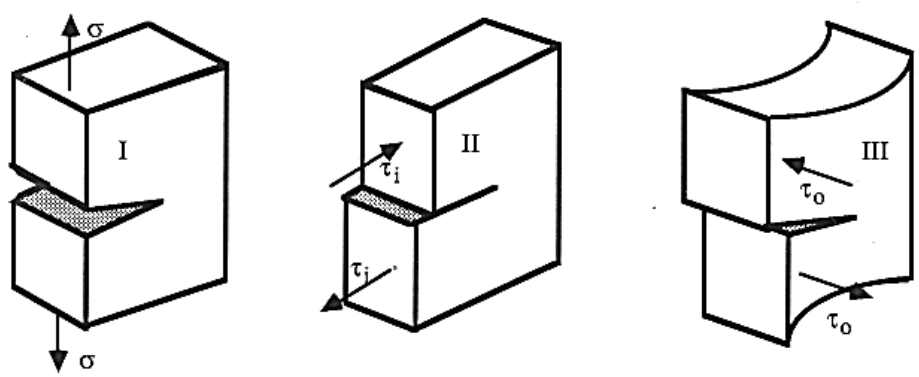

Figure 3. The different fracturing modes. From the left to the right: tensile, shear and anti-plane shear modes with corresponding displacements (Whittaker et al. 1992).

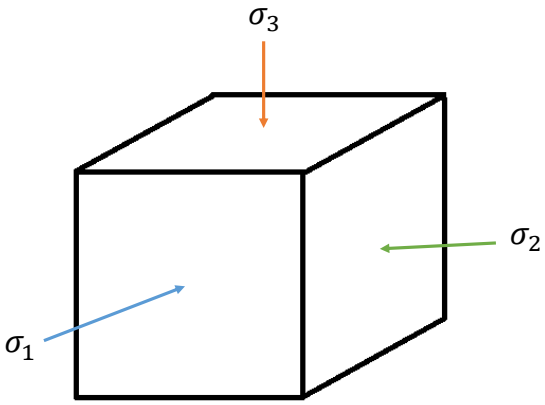

Figure 4. Affecting stress-field in rock expressed by the three main stress components $\boldsymbol{\sigma_1}$, $\boldsymbol{\sigma_2}$ *and* $\boldsymbol{\sigma_3}$.

Mode I fractures generate to the direction of the affecting normal stress at the crack tip and perpendicular to the minor principal stress component σ_3. Mode II and mode III fractures initiate in different shear stress conditions. Analogously, in-plane shear stress τ_i induces mode II failures and out-of-plane shear stress τ_o on the other hand, mode III failures. The shear stress and propagation direction of shear fractures is dependent on the main principal stress component σ_1 and the friction angle of the material. A crack displacement can also result from a combination of any two of the fracturing modes. In this case, the cracking type is called as *mixed mode fracturing*. (Whittaker *et al.* 1992)

2.1.3 Fracture toughness

In each of the fracturing modes, fracture propagation can be determined by stress intensity factor *K,* which is a local crack tip parameter (Whittaker *et al.* 1992) representing material resistance against fracture formation (Atkinson 1982). In addition to being first to propose the stress intensity factor approach, Irwin (1957) introduced the relationship between the global parameter *G* and *K*. In the different fracturing modes this relationship is presented as follows.

$$G_I = \frac{K_I^2}{E'} \tag{3}$$

$$G_{II} = \frac{K_{II}^2}{E'} \tag{4}$$

$$G_{III} = \frac{K_{III}^2(1+\nu)}{E'} \tag{5}$$

Where,

G_N	*is the mode dependent strain energy release rate*
K_N	*is the mode dependent stress intensity factor*
ν	*is the Poisson´s ratio (Whittaker et al. 1992, p. 90).*

Similar to the critical value of the strain energy release rate G_c, the resistance against fracture formation can be expressed with the stress intensity factor. As a result, when the *K* reaches its critical value K_c, called as fracture toughness, a criterion for rapid failure is achieved (Atkinson 1982).

Moreover, fracture toughness can be employed while estimating the material strength. This is achieved with the following equation.

$$\sigma_t = \frac{K_{IC}}{\sqrt{\pi a} Y_k} \tag{6}$$

Where,

σ_t	*is the tensile strength*
K_{IC}	*is the fracture toughness in mode I*
a	*is the size of the most critical crack*
Y_k	*is the dimensionless stress intensity factor depending on geometry of the most critical crack (Whittaker et al. 1992, p. 231)*

2.1.4 Subcritical crack growth

The stress intensity factor is particularly important while demonstrating time-dependent behaviour of a material (Evans 1972), because the fracture propagation can also occur below the fracture toughness limit K_c. Subcritical crack growth is a term denoting this certain type of fracture propagation. (Atkinson 1984) Subcritical fracturing can appear in all fracturing scales (Rinne 2008), and besides rock, it has been observed to exist in various materials including glass, ceramics and metals (Anderson and Grew 1977). However, while the mechanism of SCG varies in different materials, in rock, the controlling process is generally determined to be *stress corrosion* (Atkinson 1984).

Subcritical crack growth is also called as stable cracking, because the fractures often develop with a fixed speed. Moreover, according to the Griffith energy requirement, the stress must be increased in order to overcome the higher resistance induced by the generating fractures with an increasing size. Therefore, value of the stress intensity factor *K* rises if the crack growth velocity *V* increases. (Backers 2004) As a result, subcritical behaviour of a material can be efficiently described by constructing *K-V* diagrams (Figure 5) (Evans 1972).

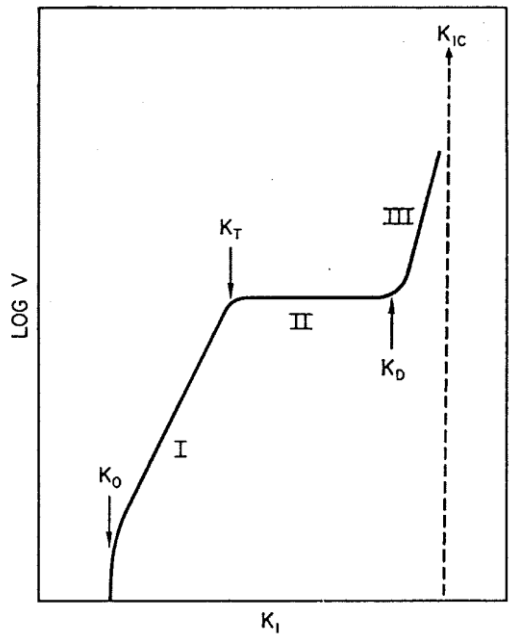

Figure 5. Idealized K-V –diagram presenting the long-time behaviour of a material in tension (Evans 1972). V is the crack growth velocity and K is the stress intensity factor.

Below *the stress corrosion crack growth limit* K_0 no fracture propagation occurs due to stress corrosion. In contrast, currently it is assumed that in the region I, the stress corrosion reactions control the fracture growth. In region II, the crack development is specified due to the rate of reactive species transportation to the crack tips, while region III is considered as unaffected by the chemical reactions and the mechanical rupture acts as the main fracture growing mechanism. (Atkinson 1984)

Subcritical crack growth velocity can be determined by equations introduced by Charles (1958) and required calculation parameters can be obtained from laboratory tests according to methods introduced by Wilkins (1980) and Backers (2006). However, this subject is not discussed in this study further and the subcritical crack growth in the fracture mechanics modelling is ignored.

On the other hand, it is important to realize that due to SCG, the exfoliation fracturing can, in reality, occur during long periods of time and the recorded Långören event might have only been the rapid phase of the long fracture generation. SCG enables fracturing also in smaller stress states, which can be considered while investigating the fracture initiation stress for exfoliation.

2.2 Exfoliation fracturing theories

Commonly, two as the most fundamental considered exfoliation fracturing theories are the explanations of pressure release and surface-parallel compression. However, while currently having a superior position over other theories, even these two concepts do not provide inclusive and perfect answer to the origin of rock exfoliation.

2.2.1 Pressure release

In the pressure release theory, the formation of exfoliation fractures is a result of the rock expansion (Harland 1957; Twidale 1973). This expansion is induced by the pressure removal or unloading, which can be achieved mainly due to erosion or melting of the glacier (Lanaro *et al.* 2007). While erosion allows rock to be released from the high cool down pressures (Twidale 1973), a glacier applies high compression to the bedrock, which is then released after the melting period.

Rock expansion after the pressure release, also referred as rebound, is well-recognized phenomenon in geological materials. In rebound, rock behaves as a viscoelastic material and the stresses from the past loading history, which are locked to a residual stress field, are reoriented and released during the rebound. Rock expansion can occur instantly or time-dependently, but the most appropriate conditions for delayed rebound are achieved if the pressure release time is short compared to the *material relaxation time.* In addition to the affecting stresses, the various rock properties and environmental conditions are also considered as influencing factors to the rebound phenomenon. (Nichols 1980)

The criticism towards pressure release theory comes from the fact that pressure release in elastic conditions does not itself produce breaking of a material. Thus, while complete three-dimensional rebound is free from any permanent deformations, other factors are required for the exfoliation fracturing. (Holzhausen 1989; Martel 2006) However, naturally rebound occurs in a geological context where *in situ* stresses are always present enabling the failure conditions for the expanding rock. In other words, the actual difficulty in the comparison between theories is to distinguish the most fundamental mechanism behind the rock exfoliation.

2.2.2 Surface-parallel compression

The theory of surface-parallel compression implies that exfoliation fractures generate parallel to the high horizontal stress σ_1 and normal to the induced tensile stress σ_3, which are reorientated according to the topography (Martel 2006). While ignoring the shape of the rock surface, this mechanism is similar to the indirect tensile strength test where fractures are produced in the direction of the applied loading.

According to Martel (2006), exfoliation fractures originate from the compression, which in convex topography conditions increases the tensile stress *T* eventually producing failures, if the stabilizing effect of the unit weight is exceeded. The normal traction gradient ϕ in this case is calculated with the following formula using parameters presented in the Figure 6. In shallow depths, tensile stress normal to the surface is activated if the resulting ϕ is positive. (Martel 2011).

$$\phi = \sigma_{11}k_1 + \sigma_{22}k_2 - \rho g * cos\beta \quad (7)$$

Where,

σ_{ij}	is the stress component acting to the *j*-direction and normal to the *i*-direction
k_i	is the principal curvature
ρ	is the rock density
g	is the gravitational acceleration
β	is the slope of the surface (Martel 2011).

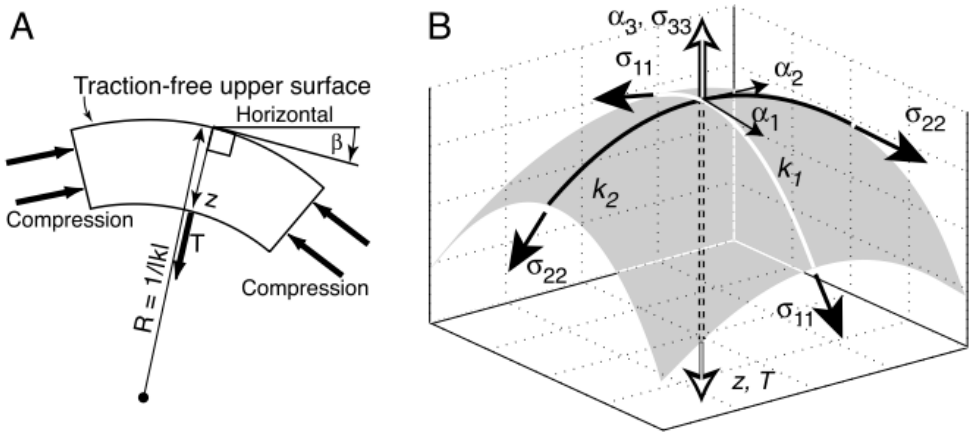

Figure 6. The left-hand side (A) presents the behaviour of a curved cross-section under compression while R is the radius of the curvature and $\boldsymbol{\beta}$ *is the slope of the surface. In the right-hand side (B) is the corresponding three-dimensional model, where the* $\boldsymbol{\alpha_i}$ *is the direction. (Martel 2011)*

The theory of surface-parallel compression is demonstrated valid for convex rock surfaces. On the other hand, also concave surfaces experience exfoliation fracturing and naturally, compressive stresses tend to decrease towards the top of convex topography. Thus, compression, which increases the tensile stress in the convex topography conditions, cannot be the ultimate solution for the exfoliation formation (Lanaro *et al.* 2007).

2.2.3 Discussion

The high compression is evidently a key factor in exfoliation fracturing (Twidale 1973), but whether it is the pressure release or convex topography, that triggers the fracture initiation, can be only debated. In addition, it is important realize that other agents can also

increase surface-parallel compression. Particularly external thermal effects influence on the top of the surface and therefore, aligned to the topography. In natural environment, the rock temperature is affected not only by the air temperature but also by the radiation from the sun. Thus, the rock temperature can have a major difference to actual air temperature (Hall and André 2001)

Temperature variations induce thermal stresses, which can reduce the rock tensile strength (Kirkkomäki 2001), while thermal expansion simultaneously increases the compressive stress state in rock. Therefore, the possibility for near-surface exfoliation fracturing can be improved in certain temperature conditions (Twidale 1973). Similarly, chemical alterations can lead to expansion in the rock mineral volume and produce incensement in the compressive stress state. Chemical environment affects also to the subcritical crack growth velocities (Evans 1972; Bahat *et al.* 1999) However, the effect of chemical reactions is only limited to the shallow depths. (Blackwelder 1925)

In the fracture mechanics modelling of the exfoliation phenomenon, it is important to understand the restrictions and modelling capabilities of the employed simulation method. In contrast to the agents behind exfoliation fracturing, the possibilities of the Fracture mechanics code FRACOD^{2D} are discussed in chapter 4.

2.3 Exfoliation conditions at Långören island

Because the modelling was performed regarding the local exfoliation phenomenon at Långören island, the local exfoliation affecting factors were required for the fracture mechanics analysis.

2.3.1 Location and geology

Långören is an island located in the archipelago of South-Western Finland (Figure 7; Figure 8), and roughly in the middle between the cities of Hanko and Turku. The ground surface at Långören is mainly exposed bedrock with stunted vegetation. In addition, the exfoliation fracturing in 2014 occurred at the west side corner of the island where the bedrock is the most revealed having an inclination towards northwest.

Figure 7. Location of the archipelago of South-Western Finland

Figure 8. Location of the Långören (red circle) island in contrast to the mainland and the nearest weather station that is set at Vänö island (red rectangular) The distance between the islands is approximately 13 kilometres.

According to GTK (*Geological Survey of Finland)*, the rock type at the island is microcline granite. However, in this study, microcline granite was assumed sufficiently similar to pegmatitic granite, which was used as the representative rock type in rock mechanics modelling. The validation of pegmatitic granite was rationalized due to the great number of existing laboratory and modelling data of Olkiluoto pegmatitic granite (Siren 2011; Kukkonen *et al.* 2011; Åkesson 2012).

2.3.2 Thermal conditions

As thermal effects were considered important in the exfoliation development, the weather history at Långören island during the exfoliation fracturing was essential to be discovered. While it was important to consider long-term and short-term temperatures in order to account both secular and impulsive stress variations, it was decided to examine Långören temperatures 10 weeks and 10 days before the exfoliation occurred in the 30th week of July, accurately 27th July 2014. Moreover, while solar radiation can increase rock temperature much higher than air temperature, it is notable that the Långören is located in the sunniest region of Finland (FMI*, Finnish Meteorological Institute* 2016).

According to the data from the nearest weather station (Vänö, Kemiösaari; Figure 8), located 13 kilometres south from Långören, the average temperatures from 10 weeks before the fracturing have been as presented in Table 1.

Table 1. Weekly mean temperatures at Långören island between the weeks 21 and 30 in 2014.

Week	Mean temperature °C
21	14.2
22	9.7
23	14.6
24	13.9
25	10.7
26	12.2
27	14.7
28	19.0
29	18.5
30	23.0

In contrary, while considering short-term thermal variations, the air temperature conditions from 10 days before the fracturing are presented in the Table 2.

Table 2. Temperature conditions at Långören island between 18.7.2014 and 27.7.2014 (FMI 2016)

Date	Maximum temperature °C	Mean temperature °C	Minimum temperature °C
18.7.2014	21.5	18.5	16.3
19.7.2014	23.1	19.7	15.8
20.7.2014	25.2	20.4	17.4
21.7.2014	27.0	20.1	17.5
22.7.2014	25.1	21.6	15.4
23.7.2014	27.9	23.2	19.7
24.7.2014	28.7	23.5	17.7
25.7.2014	28.8	23.8	18.2
26.7.2014	28.0	24.0	19.1
27.7.2014	28.5	24.9	20.2

In addition to air temperature, the temperature of the nearby seawater was also discovered. The seawater temperature was estimated based on available satellite data. As seen in Figure 9, the surface water temperature in the Baltic Sea has been over 20 °C during the exfoliation fracturing event (SYKE 2016).

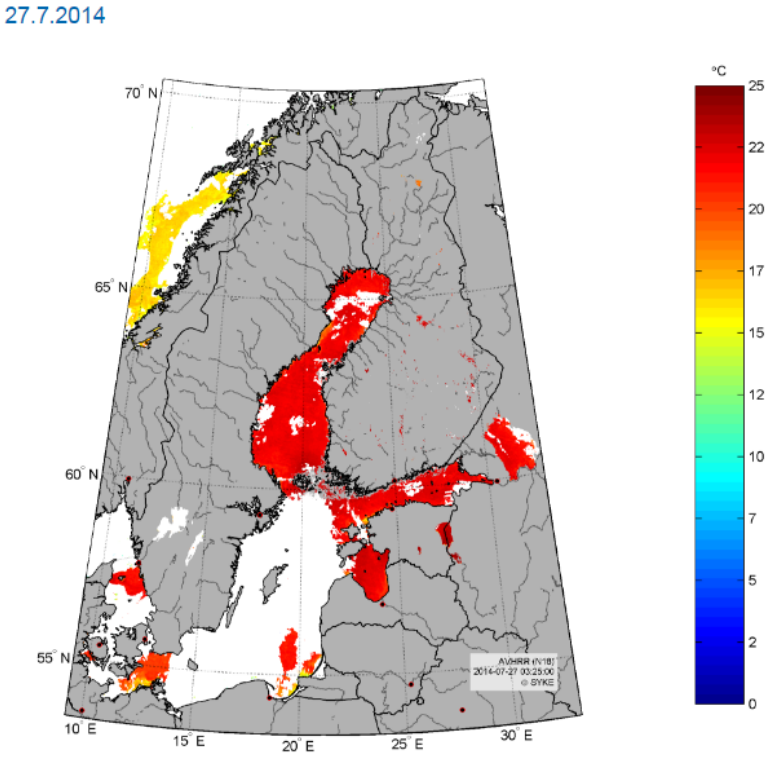

Figure 9. Surface water temperature in the Baltic Sea 27.7.2014 (SYKE 2016)

2.3.3 Glacial stresses

In Fennoscandia, the *in situ* stress-field can be affected not only by the natural tectonic forces, but also by the past glaciations. During the glacial development, the ice cover induces significant changes to the all three stress-field components. While considering exfoliation fracturing, the most prominent factor in the stress variations is that after the ice sheet retreats, the horizontal stress component reduces later compared to the vertical component. (Lund *et al* 2009) Thus, during the possible vertical rebound, the compression in bedrock can still be relatively high.

A possible stress-field at Långören, induced by the last glaciation, can be estimated roughly based on the maximum ice cover thickness (Figure 10). As confirmation, the past ice cover thickness is appropriately in respect to the current measured vertical uplift rate, which at Långören island is roughly $4mm/yr$ (Figure 11). On the other hand, the obtained stress values represent only one possible scenario, and the real glacial stress-field might have differed significantly from the estimation.

In general, the effect of the current post-glacial compression is estimated to be only a few mega pascals based on the glacial stress-field modelling (Lambeck and Purcell 2003; Hökmark and Fälth 2014). However, while simulating exfoliation due to pressure release theory, the stresses from the glacial history are important, because the conditions instantly after the retreat of the ice cover must be employed.

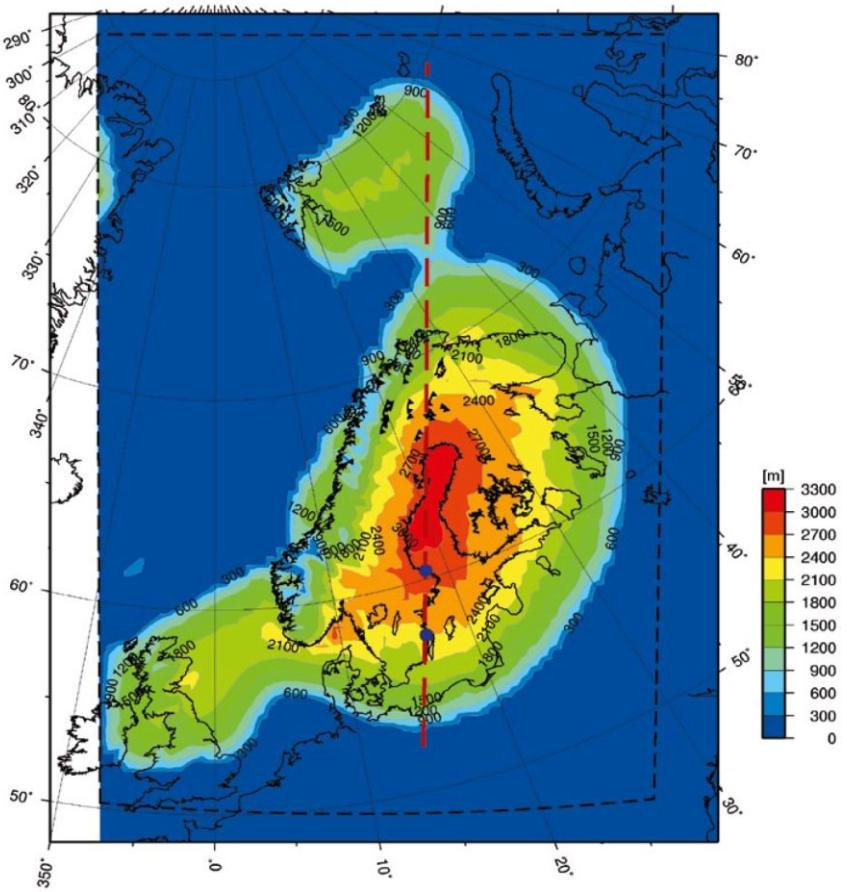

Figure 10.Maximum ice sheet thickness simulation in Fennoscandia during the last glacial, known as the Weichselian glacial (Lund et al. 2009).

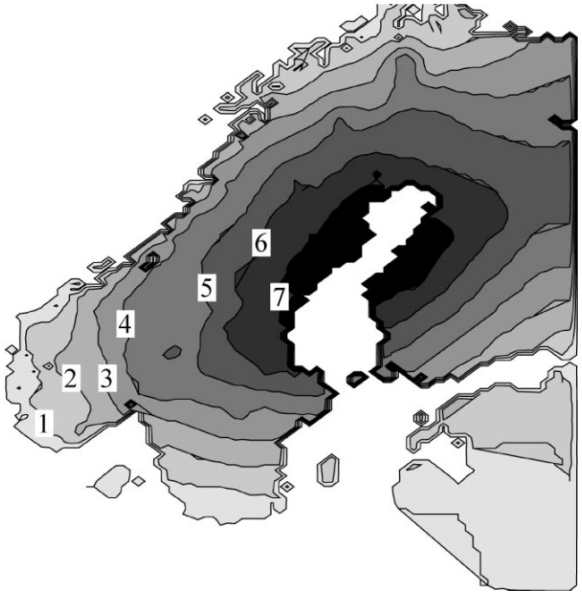

Figure 11. Vertical uplift mm/yr. (Fjeldskaar et al. 2000)

At Långören, the *in situ* stress-field at Långören during the glaciation is estimated using the ice cover thickness *h* of 2500 meters (see Figure 10). The main vertical stress component σ_v at the rock surface below ice sheet is calculated in this case by

$$\sigma_v = \rho g h. \tag{8}$$

Where,

σ_v	is the vertical stress component below the ice cover
ρ	is the density of the ice
g	is the gravitational acceleration
h	is the thickness of the ice cover.

With the values of $\rho = 900 kg/m^3$, $g = 9.81\ \frac{m}{s^2}$ and $h = 2500\ m$, the main principal vertical stress component σ_v, at the time of the glaciation on the rock surface is 22 MPa. In contrast, the principal horizontal stress component σ_H is estimated according to the glacial stress analyses. While, in the end-glacial conditions, the vertical and horizontal stress components become nearly equal (Hökmark and Fälth 2014, p. 10) the horizontal compression can be considered equal to 22 MPa vertical pressure.

In time, the estimated horizontal stress component reduces after the melting of the glacial cover. However, if the conditions directly after the ice load removal are considered, the horizontal load can be kept constant through the analysis. Based on the glacial models by Lund *et al.* (2009) the stress relaxation varies also significantly in different modelling approaches. Thus, the real glacial stresses can distinct greatly from the approximations performed 10,000 years after the real events.

2.3.4 *In situ* stresses

Although post-glacial influence is currently minimal, very high near-surface horizontal stress can be realistic in some cases, because corresponding values have been measured in Southern Finland. Based on these measurements, the highest major principal stress component has been almost 15 MPa only 15 meters from the bedrock surface (Mononen 2005). Besides glacial stresses, other factors might also affect behind high surface stress states. For example, residual stresses can be a result from the high cooldown pressures of the minerals (Mononen 2005) or currently high stress concentrations might be induced by the topography.

While the magnitude of the horizontal stress is important, also the *in situ* -direction of the maximum stress component is necessary for the fracture mechanics modelling. Basically the stress direction determines the location and the topography of the 2D-section in the fracture mechanics models, because the analysis should be performed parallel to the maximal horizontal stress. In Finland, it is generally agreed that the main principal horizontal stress has approximately northwest-southeast direction (Figure 12).

On the other hand, the topography of the Långören island was only an approximation during the creation of this study and the real directions and magnitudes of the *in situ* stress components should be acquired for more accurate analyses.

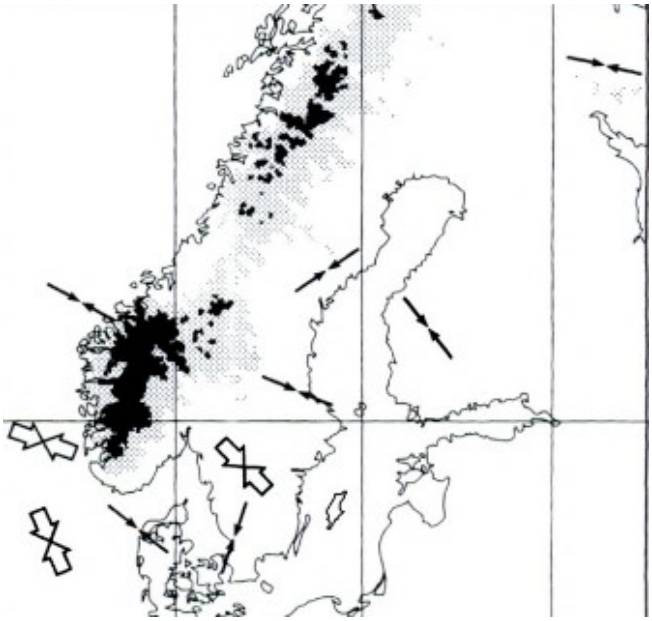

Figure 12. Direction of the main principal horizontal stress component in Scandinavia (Amadei and Stephansson 1997).

3 *In situ* –monitoring of exfoliation fractures

This chapter presents the methodology for studying the generation of exfoliation fractures *in situ*. The introduced system, which was installed at Långören, was designed to evaluate exfoliation and other fracture formation especially in contrast to the weather conditions. The experiment was a part of the collaborative research project between ETH Zurich and Aalto university and the monitoring system was designed and funded by ETH Zurich.

Since no new fracturing was observed during the testing period employed in the thesis, only the rock temperature results were used in order to model the realistic air-rock temperature relationship. Moreover, the presented air temperature profiles were obtained from the Vänö weather station as the air temperature data directly from Långören was not accessible at the time of this thesis.

3.1 Monitoring system

The monitoring system, set up at Långören island, employs the *acoustic emission* (AE) -technique to examine the development of exfoliation fractures. The advantage of the acoustic emission technique is that it can be used as a non-destructive method in observation of brittle fracture formation in rock (Lockner *et al.* 1992). While growing fractures, including microcracks, induce elastic waves, the microphones of an AE-device can detect these deformations from the top of the surface (Bruttomesso *et al.* 1993). Consequently, AE-sensors record defects also deep inside the rock mass (Grosse and Ohtsu 2008).

In addition to the AE-devices, the Långören monitoring system consists of rock temperature sensors, a weather station and a data logger computer. AE- components were also enhanced with piezoelectric signal generators, which allow the monitoring of *primary wave* (P-wave) velocity in the rock. In order to enable real-time observation, the system was connected to the mobile network. Furthermore, the power for the system was provided by a solar panel and attached batteries. The final arrangement is presented in Figure 13.

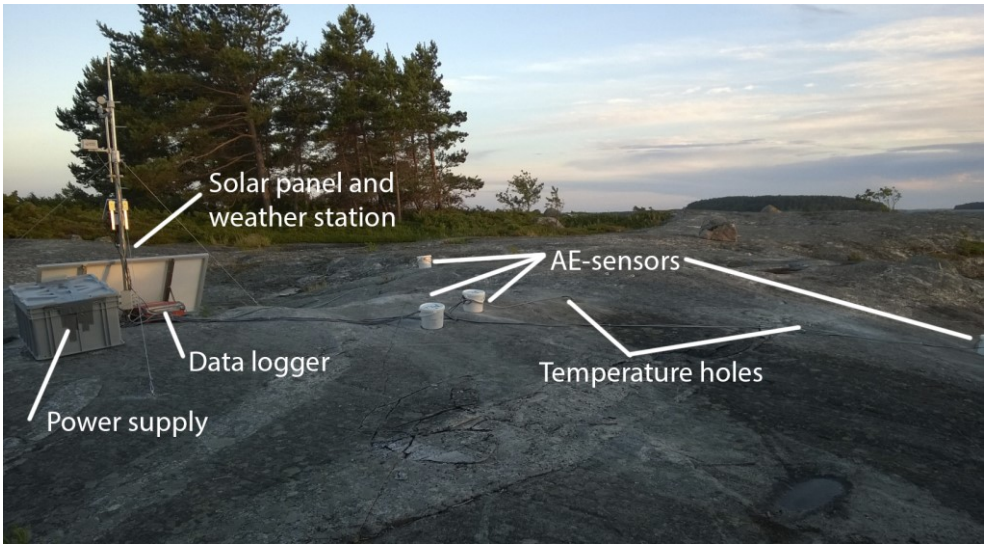

Figure 13. The final set-up of the in situ -monitoring system at Långören island.

To measure rock temperature versus depth relationship, two holes were drilled close to the AE-components and temperature sensors were grouted into these holes. The weather station was set to measure the rock surface temperature, air temperature, air humidity,

rainfall, wind speed, wind direction and solar radiation. One core sample was also taken from the investigation site and a crack meter was connected to the open fracture detected inside the borehole.

3.2 Determination of the testing area

The determination of the sensor locations was based on the visual examination during the assembly and the GPR (*Ground Penetrating Radar*) surveys executed by GTK at Långgören in 2015. The aim of the estimation was to find positions for the AE-sensors where the rock was the most intact and thus, having the greatest possibility for new fracture development. The approximated location in contrast to the GPR -measured exfoliation fractures are presented in Figure 14.

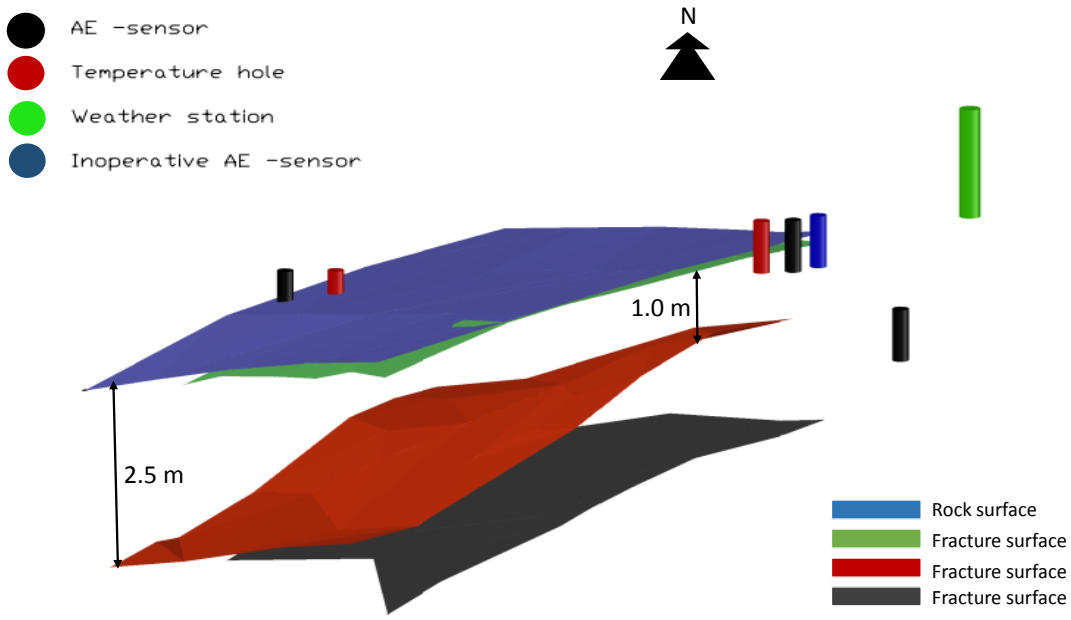

Figure 14. The locations of the monitoring components in contrast with the interpreted GPR fracture surfaces (raw GPR data provided by GTK). The blue surface is the rock surface and the green, red and grey surfaces are approximated exfoliation fracture surfaces. As seen in the figure, one of the AE -components proved inoperative.

3.3 Installation of the system

For the monitoring system, the careful installation procedure was conducted in order to acquire reliable and functional system. However, one of the AE -components proved inoperative after the installation.

The combined AE - piezoelectric components were installed to the top of the bedrock by gluing them to the defined locations. The rock surface was also refined before the gluing for avoiding any open space between the sensors and the rock. After the attachment, two plastic covers were set on the sensors (Figure 15). Furthermore, the space between these covers was filled with sand in order to prevent distraction signals above the rock surface.

Figure 15. The plastic covers protecting the AE-sensors from the noise and weather conditions.

Twelve temperature sensors were inserted to the drilled temperature holes with known vertical positions. The grout for filling the holes was selected considering as close properties compared to the rock as possible. The vertical positions of the sensors and the overall depths of the temperature holes are presented in Table 3 and Table 4.

Table 3. The sensor depths and types in the upper temperature hole (see Figure 13, on the right)

Sensor	**Depth, millimetres**	**Sensor type**
Sensor 1	40	Digital
Sensor 2	150	Analog
Sensor 3	230	Analog
Sensor 4	440	Digital
Sensor 5	770	Analog
Sensor 6	1110	Digital

Table 4. The sensor depths and types in the lower temperature hole (see Figure 13, on the left)

Sensor	**Depth, millimetres**	**Sensor type**
Sensor 1	40	Digital
Sensor 2	120	Analog
Sensor 3	250	Analog
Sensor 4	440	Digital
Sensor 5	X	Non operational
Sensor 6	1080	Digital

Because the monitoring system was constructed to be dependent on the solar energy, it is fully operational only during the summer months. On the other hand, if the power consumption would be limited by the intervals during which the system active, the operation period could be extended.

3.4 Monitoring results

The relationship between the air temperature and the rock surface temperature was examined by plotting these values in contrast to each other using a period of one week (Figure 16). The obtained weather data was considered as very accurate because the measurement interval was 10 minutes while the measurement interval of the rock temperature was 200 seconds.

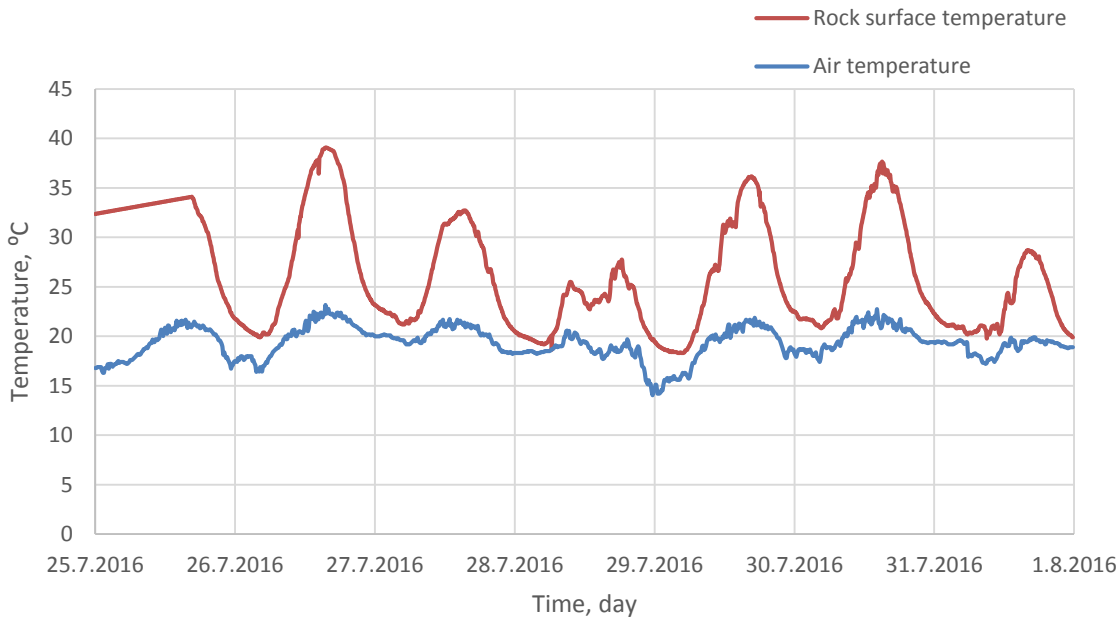

Figure 16. Rock temperature versus air temperature diagram. The time period is selected between 25.7.2016 and 1.8.2016, because during this time the air temperatures reached their highest values (FMI 2016) after the monitoring system installation. The rock temperature represents the surface temperature, as it is the temperature of the sensor 1, which was installed to 40 mm depth. The air temperature was achieved from the Vänö weather station.

As seen from the diagram, the temperature difference between air and the rock is emphasized during the daytime. The approximated maximum temperature difference in the Figure 16 is 16.5 °C while the minimum difference, measured during the nighttime, is only 0.7 °C. The average difference between the rock surface and air is approximately 7.1 °C. The diversity between the air and rock values is rationalized due to the solar radiation, which is effective daytime. Thus, also cloudiness affects to the air-rock temperature ratio. Figure 17 presents the estimated average cloudiness in contrast to the rock temperature.

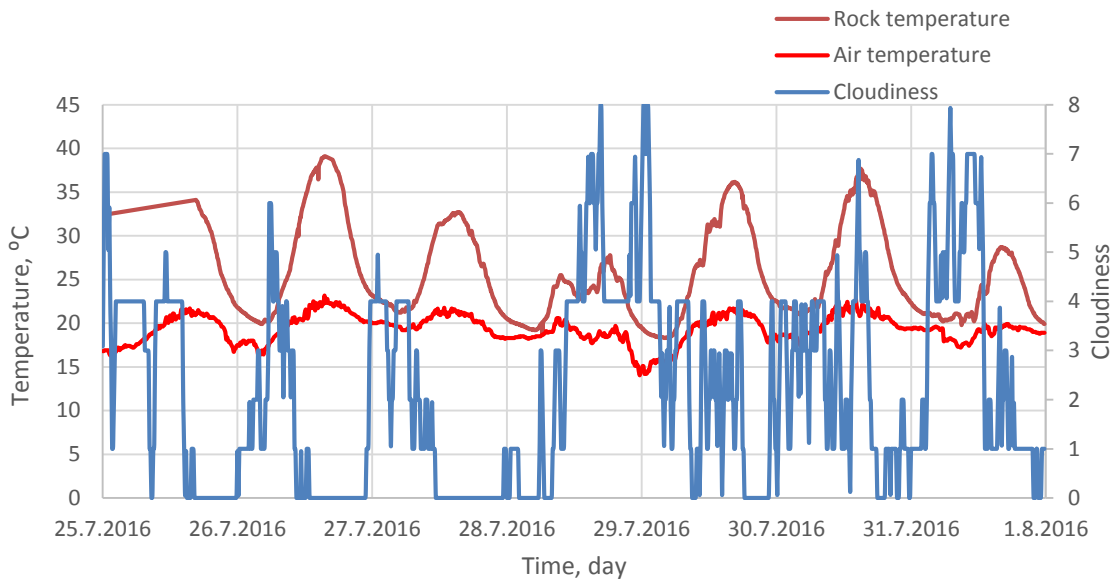

Figure 17. Average cloudiness in contrast to the air and rock surface temperatures. The cloudiness is evaluated with scale from 0 to 8, where 0 is the cloudless weather and 8 is the cloudiest weather.

If accounting the depth of the temperature sensors, the following temperature diagram is achieved from the upper temperature hole (Figure 18). Moreover, while the daily maximum rock temperature is plotted versus the depth, the temperature behaviour illustrating graph is achieved (Figure 19).

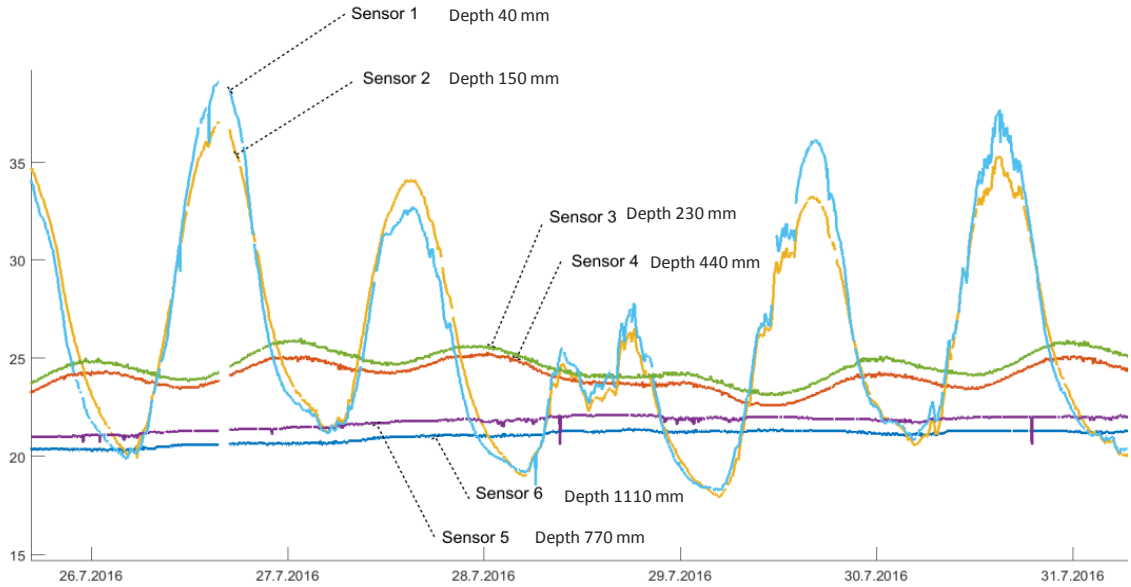

Figure 18. Rock temperature profile from the upper temperature hole between 25.8-1.8.2016.

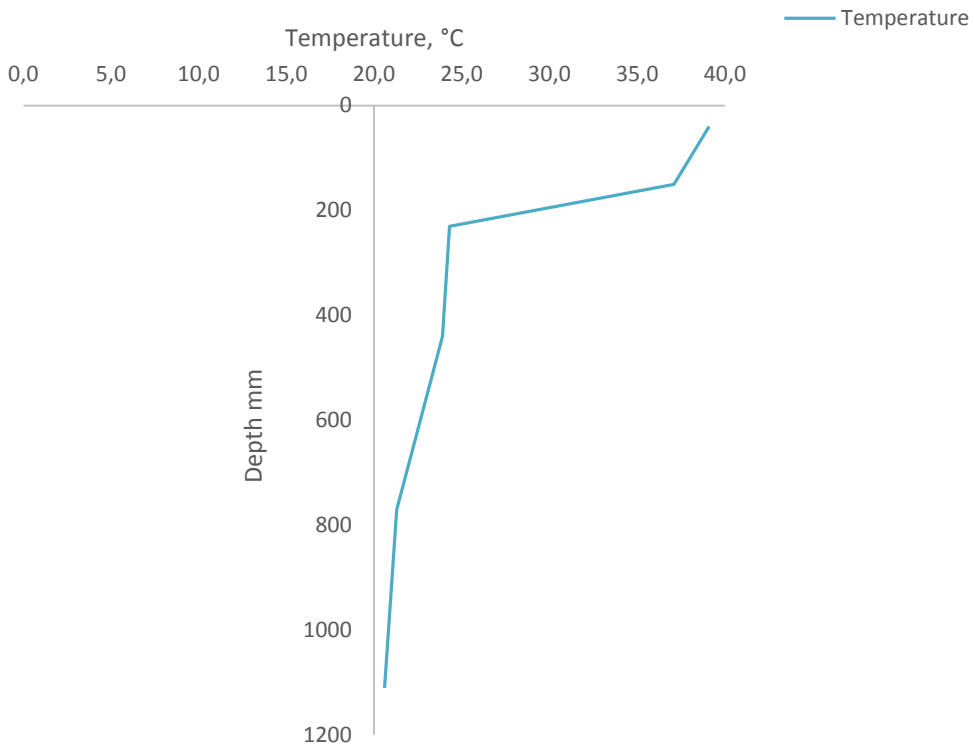

Figure 19. The temperature versus depth diagram from the upper temperature hole 26.7.2016, while the sensor 1 at the depth of 40 mm has reached its peak value.

As seen in Figure 18, the thermal properties of rock allow the daily temperature changes to have only minor effect while considering depths below 0.5 meter. However, the rock is apparently storing heat as the two bottom sensors have a steady inclination upwards. The sensors 3 and 4 have reverse daily evolution compared to the sensors 1 and 2. Thus, the temperature difference between depths of 120 mm and 230 mm is the greatest (Figure 19).

On the other hand, the cracks in the obtained core sample were also located between 150 mm and 230 mm depths from the rock surface. Therefore, the explanation for the temperature behaviour between 120 mm and 230 mm might be that the two open fractures prevent the proper thermal conduction in rock (Figure 20). Hence, there exists uncertainty in the veracity of the obtained temperature profiles.

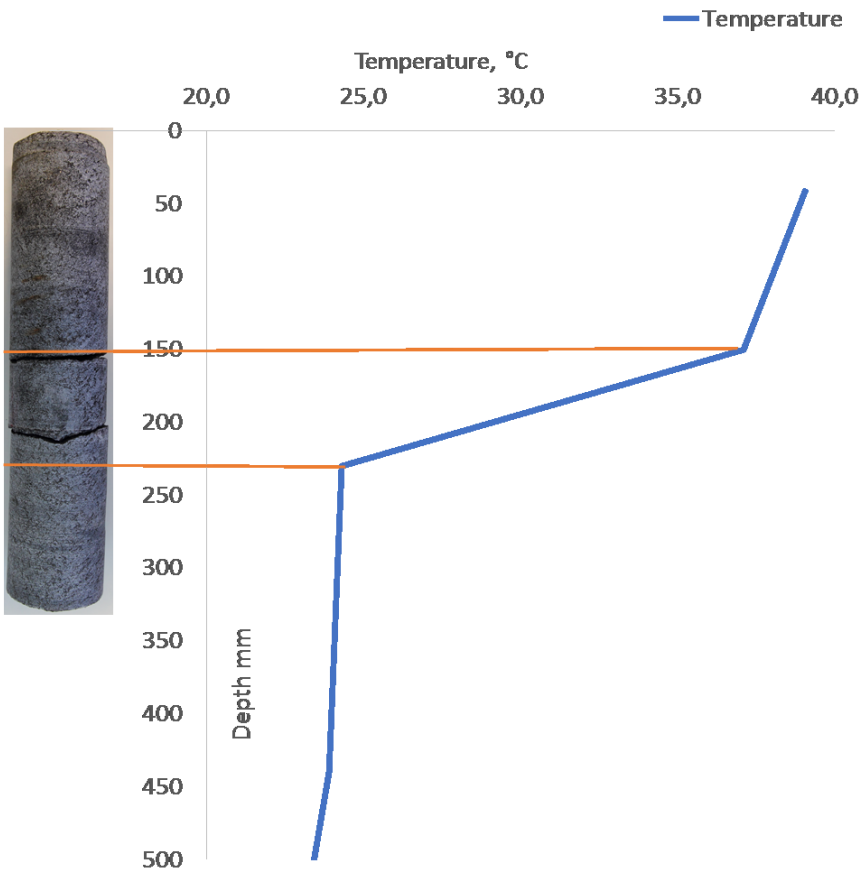

Figure 20. The locations of two near-surface exfoliation fractures in the core sample corresponding to the maximum temperature difference observed in the rock temperature monitoring.

While daily short-term temperature variations are a very likely source of the near surface exfoliation at Långören, the deeper fractures might not be explained fundamentally with thermal stresses. The weekly long-term temperature variations on the other hand, can have more profound influence as the heating during longer timespan increases horizontal compression much deeper.

4 Fracture mechanics modelling

This chapter introduces the fracture mechanics modelling of exfoliation fractures at Långören island. First, the chapter presents the FRACOD^{2D} –software and the basic concepts behind the modelling. Next, the chapter reveals the sensitivity of the software and furthermore, the model calibration, boundary conditions and essential modelling parameters.

4.1 FRACOD^{2D}

4.1.1 Overview

FRACOD^{2D} *(FRActure propagation CODe)* is a fracture mechanics modelling software, which enables observation of fracture initiation and propagation in two-dimensional space. The software is designed for analysing fracture mechanics problems inside elastic and isotropic rock medium. Thus, every initiated fracture represents a local failure in the intact rock mass. FRACOD^{2D} simulates fracturing in macro scale ignoring micro-crack processes. (Shen *et al.* 2014) Therefore, the process of crack initiation is not considered. In addition, the FRACOD^{2D} has been developed over last years and time dependent functions and thermo-mechanical coupling has been included. The software version 5.2 is used in this thesis.

The software is based on the DDM -method *(Displacement Discontinuity Method)*, which is one of the major *Boundary Element Methods* (BEM) (Shen *et al.* 2014). The selection of DDM-approach can be considered advantageous compared to other BEM-methods, because it presents fractures as elements instead of surfaces (Siren 2011). In other words, a single DD-element is composed of two crack surfaces (Shen *et al.* 2014).

New shear fractures initiate according to the Mohr-Coulomb criterion, if the influencing stresses overcome the rock mass strength. In contrast, the tensile initiation criterion is used for mode I fracturing. The shear and tensile fracture initiation conditions are demonstrated with the following two formulas (Shen *et al*. 2014).

$$\sigma_S \geq \sigma_n * \tan(\phi) + c \tag{9}$$

Where,

σ_S is the shear stress
σ_n is the normal stress to the shear failure plane
ϕ is the friction angle in the rock mass
c is the cohesion in the rock mass.

$$\sigma_{tensile} \geq \sigma_t \tag{10}$$

Where,

$\sigma_{tensile}$ is the tensile stress
σ_t is the tensile strength.

In the FRACOD^{2D}, the criterion for the fracture propagation and the propagation direction is achieved by employing the *F-criterion*, which is also called as the modified G-criterion. (Shen *et al.* 2014) Based on the work of Shen and Stephansson (1993), the F-criterion can

consider fracturing also in mode II and the resulting strain energy release rate is divided into tensile *(G_I)* and shear *(G_{II})* components.

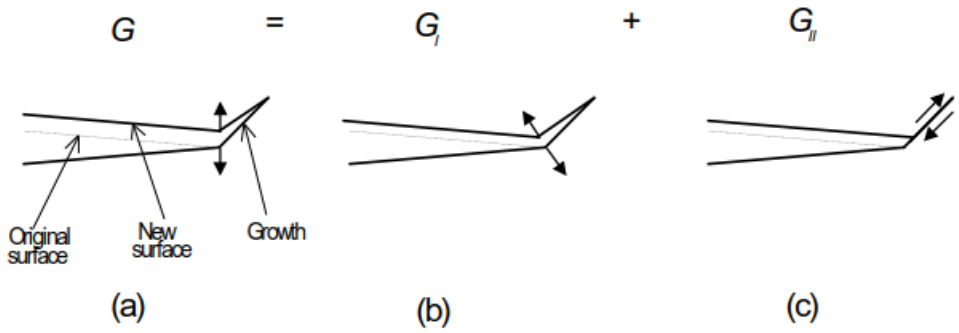

Figure 21. Different displacement modes in fracture generation. (a) The fracture has both open and shear displacements. (b) The fracture has only open displacement. (c) The fracture has only shear displacement. (Shen and Stephansson 1993)

The value of the F-criterion to an arbitrary direction can be determined with the following formula.

$$F(\theta) = \frac{G_I(\theta)}{G_{IC}} + \frac{G_{II}(\theta)}{G_{IIC}} = 1.0, \quad (11)$$

Where,

θ	is an arbitrary direction
$G_I(\theta)$	is the strain energy release rate in mode I
$G_{II}(\theta)$	is the strain energy release rate in mode II
G_{IC}	is the critical strain energy release rate in mode I
G_{IIC}	is the critical strain energy release rate in mode II.

If the F-criterion reaches values higher than 1.0, the fracture propagation begins and the direction is decided based on the direction of maximum F-value (Shen and Stephansson 1993). Moreover, if the anisotropy is considered by using direction dependent fracture toughness, the F-criterion can be presented as follows. (Shen *et al.* 2014)

$$F(\theta) = \left(\frac{K_I}{K_{IC}(\theta)}\right)^2 + \left(\frac{K_{II}}{K_{IIC}(\theta)}\right)^2 = 1.0, \quad (12)$$

Where,

θ	is an arbitrary direction
K_I	is the stress intensity factor in mode I
K_{II}	is the stress intensity factor in mode II
$K_{IC}(\theta)$	is the direction dependent fracture toughness in mode I
$K_{IIC}(\theta)$	is the direction dependent fracture toughness in mode II.

In FRACOD^{2D}, the gravity function has been included since the version 2.3, which is essential in exfoliation fracturing observations (Lanaro *et al.* 2007). In BEM, the gravity affects in the centre of every element and the gravity induced shear and normal stresses are calculated separately in each point in the medium (Shen *et al.* 2007).

FRACOD^{2D} has previously been proved suitable for exfoliation fracturing simulation and the features of the software make the versatile exfoliation examination possible for Långören phenomenon. Thus, it is regarded as an appropriate tool for the modelling conducted in this thesis.

4.1.2 Thermo-mechanical coupling

One of the FRACOD^{2D} features that is important regarding the Långören exfoliation simulation is thermo-mechanical coupling. While using the boundary element method, thermo-elastic problems can be solved by adopting two different approaches, which are called direct and indirect. In FRACOD^{2D}, the indirect thermo-mechanical approach is employed, because it has been found appropriate while coupling DDM and thermal effects. Moreover, indirect method is considered advantageous if the internal heat sources are used. (Shen *et al.* 2014)

In the indirect method, fictitious heat sources with unknown strength are created to the model and they are evaluated by solving the source to match given boundary conditions. Consequently, these fictitious heat sources determine next the temperature, stress and displacement distribution in the model. (Shen *et al.* 2014)

Thermo-mechanical time is accounted by dividing the heat source into sub-sources, which influence at the alternative time steps. Therefore, the temperature is always constant at the certain time step and the value of the step is an accumulation of previous values. This time marching scheme is illustrated in the Figure 22. (Shen *et al.* 2014)

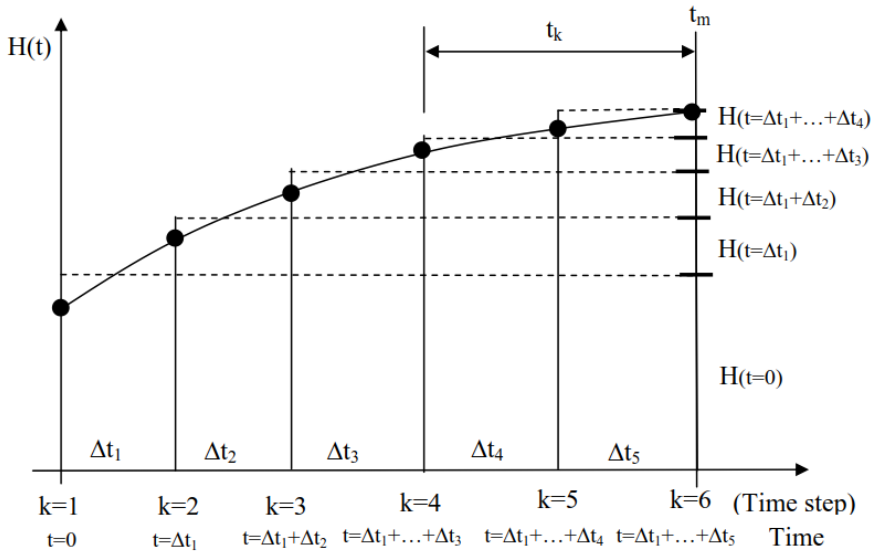

Figure 22. The solution of the time marching scheme in FRACOD^{2D}. The temperature is constant over a step and it is accumulated from the previous values. (Shen et al. 2014)

By increasing the thermal time steps in the model the calculation speed is reduced due to the increasing size of the equation system. Thus, in the newest version of FRACOD^{2D}, the maximum number of 15 time steps is allowed. The time steps must also be uniform in order to avoid errors in the calculation. (Shen *et al.* 2014)

4.1.3 Limitations and sensitivity

The most significant limitation in the current version of FRACOD^{2D} regarding exfoliation fracturing is the incapability to simulate viscoelasticity and chemical effects. Thus, although chemical environment and viscoelastic relaxation might have an influence on the fracture development, they cannot be implemented in this study directly. However, while stress conditions were widely varied, the expansion induced by chemical reactions could be hence accounted. The viscoelasticity on the other hand, is related to the pressure release theory, which can be also modelled by examining only the effects of the remaining stresses.

The sensitivity of the FRACOD^{2D} results mainly from the use of various geometric variables. These parameters are *grid point spacing*, *boundary element size*, *fracture initiation element size* and functions *SETF*, *SETE* and *SETT*. *SETF* is the cut-off level of simultaneous multiple fracture propagations. *SETE* is the check-up level for elastic fracture growth while *SETT* is the tolerance factor giving the tolerance distance between separate fractures. All the previous parameters have been observed to have considerable effects in the analysis, and different combination of these variables have been determined to give very different results. (Siren 2015)

The relationships between different geometric variables are demonstrated in the following figures on the next page. First, the different relationships between boundary element, fracture element and grid points are discovered (Figure 23). Next, the effects of different *SETF* and *SETT* functions are demonstrated (Figure 24). The correct values for the exfoliation fracturing modelling were selected based on these sensitivity analyses and the work of Siren (2015) and the default values of FRACOD^{2D}.

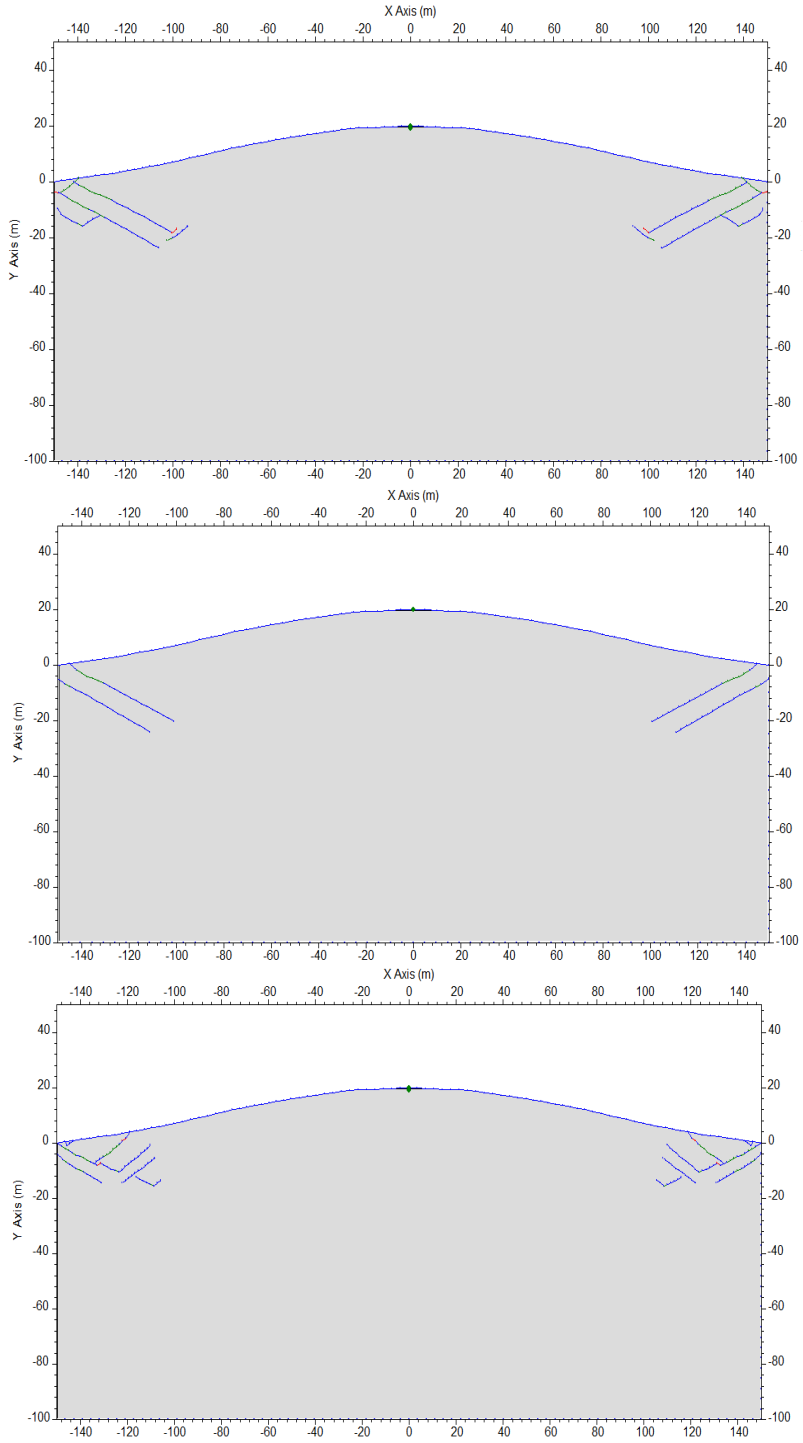

Figure 23. The sensitivity study of grid point spacing, boundary element number and fracture initiation element size. In the upper model, the grid point spacing and fracture element size are $\mathbf{1.5}$ *∗boundary element size. In the middle, all these parameters are set to equal value. In the bottom model, the fracture and boundary element sizes are the same and the grid point spacing is* $\mathbf{1.5}$ *∗boundary element size.*

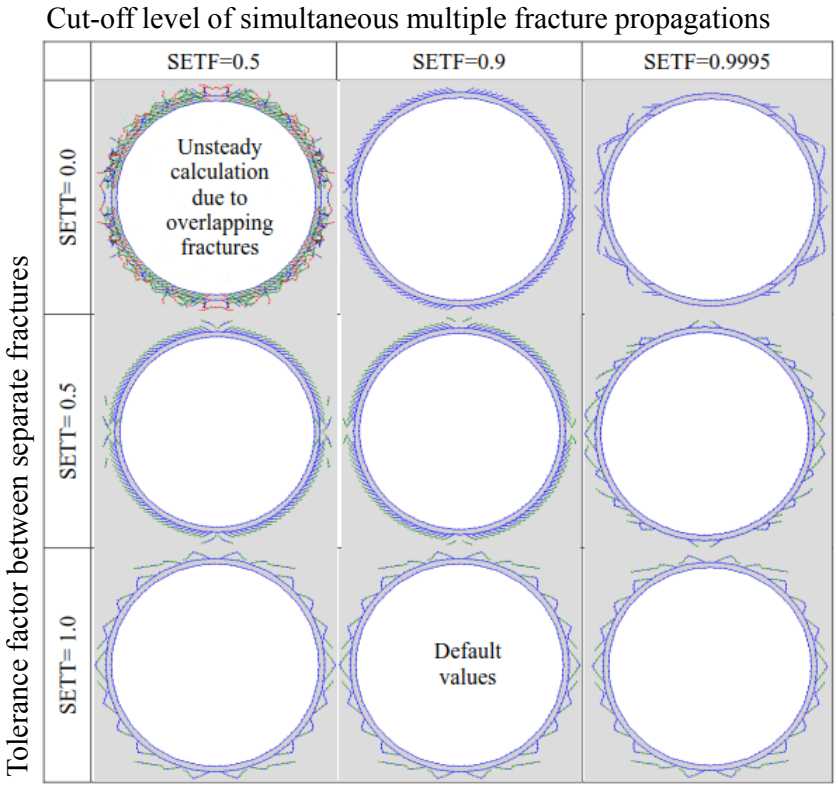

Figure 24. The relationship between different values of SETF and SETT functions (Siren 2015).

As the default values of FRACOD^{2D} were discovered to indicate realistic results, these values were chosen to the exfoliation fracturing models except the *SETF* was set to 1.0, because no remarkable effect was discovered between the default value of 0.9 and 1.0 (Siren 2015). The following table presents the final geometric parameters.

Table 5. Geometric variables in the exfoliation modelling that influence to the observed fractures.

Parameter	**Value**
Boundary element size	1.0
Grid point spacing	1.5* Boundary element size
Fracture element size	1.5* Boundary element size
SETF	1.0
SETE	0.5
SETT	1.0

In contrast to the software based variables, also the employed rock and fracture mechanics parameters have a major influence on the simulated fracturing. While this thesis was created there was no rock mechanics data available from Långören and thus, the material properties of Olkiluoto pegmatitic granite were input to FRACOD^{2D}. As a result, there exists some uncertainty in the material context.

Especially fracture mechanics parameters, such as fracture toughness, cohesion and stiffness, affect significantly to the fracture generation. In previous FRACOD^{2D} -studies, for example, cohesion values between 0 and 43 MPa and normal stiffness values between 2 and 50,000 GPa/m have been used (Shen *et al.* 2014) In this study, these parameters were

widely varied in order to obtain the parameters that best correspond to the exfoliation fracturing environment. The variables are set in calibration modelling section 4.3.

From rock mechanics parameters, the especially Poisson's ratio influences to the exfoliation fracture generation, because it determines how the rock is capable of resisting shear deformations. In the previous exfoliation modelling, the Poisson's ratio has been observed to decrease the depth at which fractures initiate (Figure 25). (Lanaro *et al.* 2007)

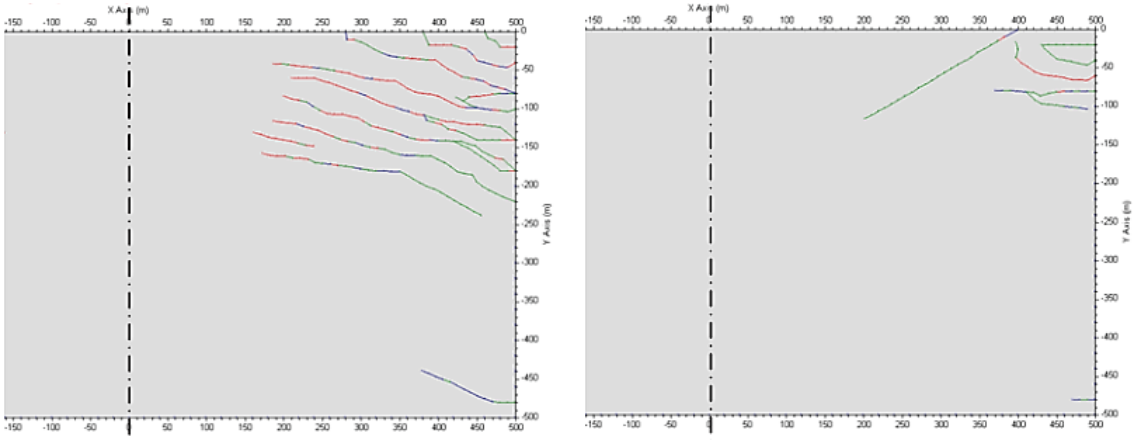

Figure 25. The influence of the Poisson's ratio on the exfoliation development. The left hand side is the model with the Poisson's ratio of 0.25 and the right hand side is the model with the value of 0.40. (Lanaro et al. 2007)

While considering thermal effects, the accuracy in FRACOD^{2D} model influences also the accuracy of the temperature distribution. In other words, the temperature behaves always less continuously between two adjacent grid points if the accuracy is decreased. Moreover, FRACOD^{2D} tends to overestimate the surface temperature in the models with larger element size (Figure 26).

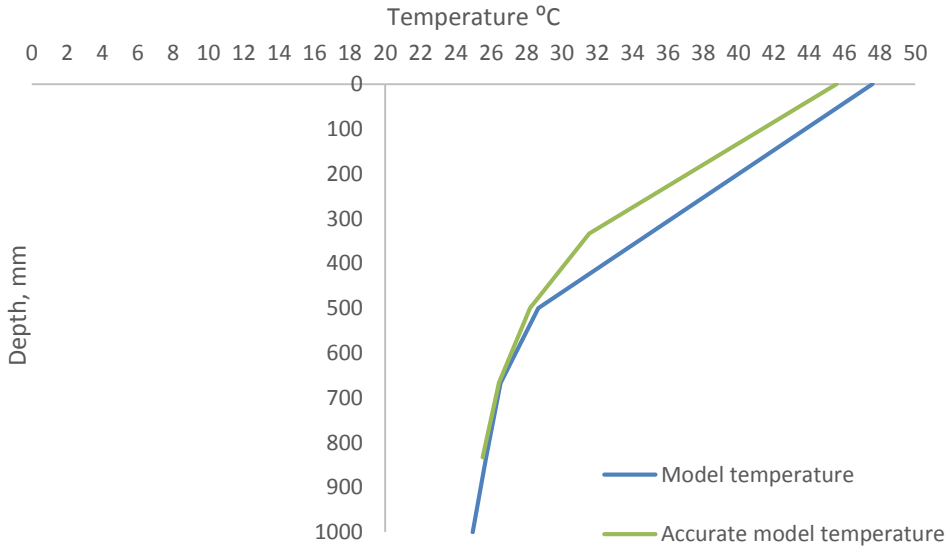

Figure 26. The temperature distribution depending on the model accuracy. In this case, the input temperature at the boundary was 44.5 °C.

4.2 Essential boundary conditions

The necessary boundary conditions regarding exfoliation modelling are presented next. These conditions are the *in situ* compression, glacial stresses and thermal environment. The validation of the values is presented in chapter 2.3.

4.2.1 *In situ* stress

In the thesis, the maximum realistic principal *in situ* stress component was estimated to 15 MPa based on the highest measured near-surface values at Southern Finland (Mononen 2005). As a result, this compression was regarded as a comparison value for the possibly higher stress states applied in the modelling. In addition, while considering pressure release and glacial induced stresses lateral compression was set to 22 MPa, which serves as the instant compression after the glacial pressure removal.

4.2.2 Pressure release

The pressure release modelling was performed by employing the initial horizontal and vertical stresses of 22 MPa estimated in section 2.3.3. The additional effect of tectonic *in situ* compression was mainly ignored in the pressure release simulations, because based on the studies of Lund *et al.* (2009) and Steffen and Wu (2011) the stress field is substantially reoriented and modified during the glacial cycle. Thus, the exact amount of compressive stress is very hard to predict. On the other hand, one pressure release model was processed with higher horizontal stress state to examine the influence of this factor.

According to the glacial stress field simulations by Lund *et al.* (2009), the latest glacial pressure was released in two phases. First, approximately 70 percent of the vertical overburden pressure was removed and consequently, the remaining pressure was released in the second phase. In this thesis, the horizontal compression was kept constant through the modelling, because according to the post-glacial stress simulations, lateral compression decreases slower behind the vertical pressure (Figure 27).

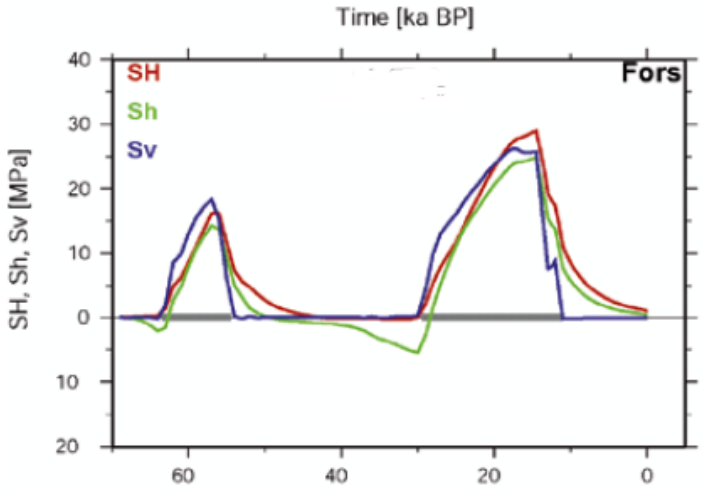

Figure 27. The estimation of the stress field behaviour during the Weichselian glacial cycle. The evaluation is performed for Forsmark in Sweden. S_H is the major horizontal stress component while S_h is the minor horizontal stress component and S_v is the vertical stress component. (Lund et al. 2009, p. 63).

4.2.3 Thermal conditions

FRACOD^{2D} can process only limited number of thermal time steps and the amount of these steps has an influence on the calculation speed. Thus, long-term (weekly) and short-term (daily) thermal effects are required to be modelled separately. In the long-term modelling, the average temperatures from 10 weeks before the fracturing event were employed (Table 1). Thus, one week represented one time step. In addition, the average air temperature was increased by 5 °C to represent the average difference between air and surface rock temperature.

In the short-term thermal models, applying the temperature variations was not however, that simple. While these models should be able to account daily temperature differences, the average values could not be used. The solution was to have separate time steps for the daily minimum and maximum temperature. However, this reduced the regarded day number to seven as each day required two time steps.

The daily rock temperatures were modelled in contrast to the historical weather data and the *in situ* rock temperature behaviour. Furthermore, the daily maximum temperature and the daily minimum temperature were chosen as the alternating time steps. Daily maximum temperature was estimated to be the maximum air temperature increased by 16 °C degrees and the daily minimum was set equal to the air temperature (see Figure 16). The modelled short-term temperatures are presented in Table 6 and in Figure 28.

While regarding sea temperature, which was input for the 25-meter-wide area at the sides of the topography, the long-term sea temperature was set to follow average air temperature directly. In the short-term models, the sea temperature was set to a constant temperature value of 20 °C corresponding to Figure 9.

Table 6. The modelled short-term temperatures while accounting the daily difference between rock and air temperatures.

Date	Step number	Thermal time, s	Air temperature, °C	Short-term rock temperature °C
21.7	1	0	27.0	43.0
21.7	2	43200	17.5	17.5
22.7	3	86400	25.1	41.1
22.7	4	129600	15.4	15.4
23.7	5	172800	27.9	43.9
23.7	6	216000	19.7	19.7
24.7	7	259200	28.7	44.7
24.7	8	302400	17.7	17.7
25.7	9	345600	28.8	44.8
25.7	10	388800	18.2	18.2
26.7	11	432000	28.0	44.0
26.7	12	475200	19.1	19.1
27.7	13	518400	28.5	44.5
27.7	14	561600	20.2	20.2

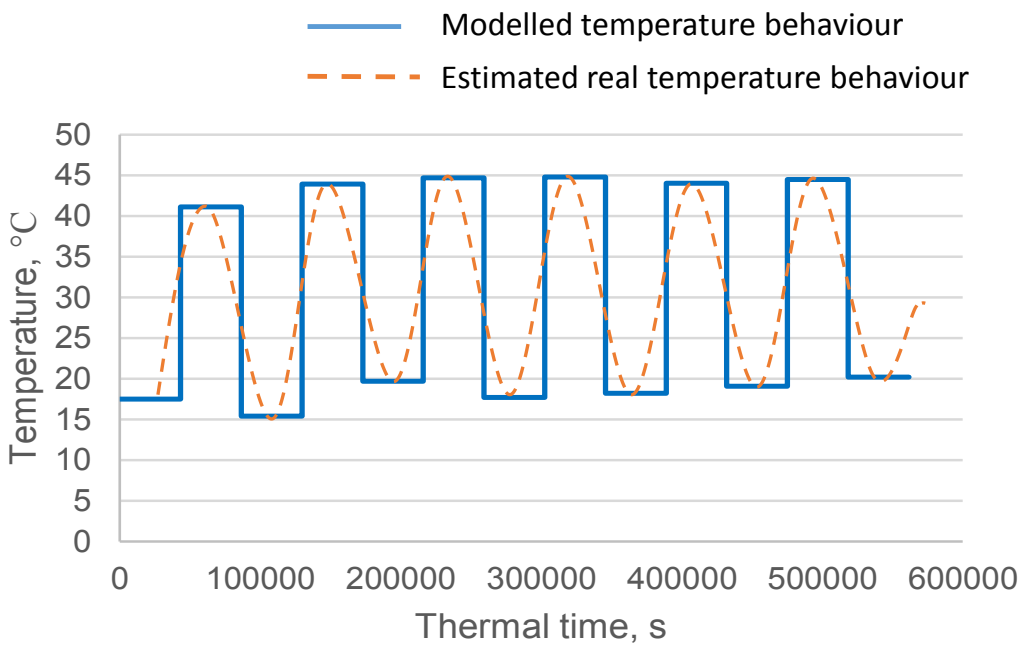

Figure 28.The modelled short-term temperature behaviour in contrast to the modelled thermal time and estimated realistic rock temperature behaviour.

The thermal properties for the modelled rock were obtained from laboratory results of Olkiluoto pegmatitic granite (Kukkonen *et al.* 2011; Åkesson 2012). The employed values are presented later in Table 7 together with other modelling parameters.

4.3 Calibration modelling

The calibration modelling was performed in order to calibrate the stress behaviour and the laboratory values of the rock mechanics and fracture mechanics parameters (Siren 2011, p. 10) to the *in situ* scale.

4.3.1 *In situ* stress behaviour

In the FRACOD^{2D}, the *in situ* stress field can be modelled by using two different approaches. These approaches are the employment a far-field stress function or a boundary stress function. The main difference between these two functions is the displacement behaviour due to the different boundary conditions. While far-field stress approach prevents displacements at the model boundaries, the boundary stress function applies the highest displacements at the same boundaries. This displacement behaviour and the boundary types for both approaches are demonstrated in Figure 29.

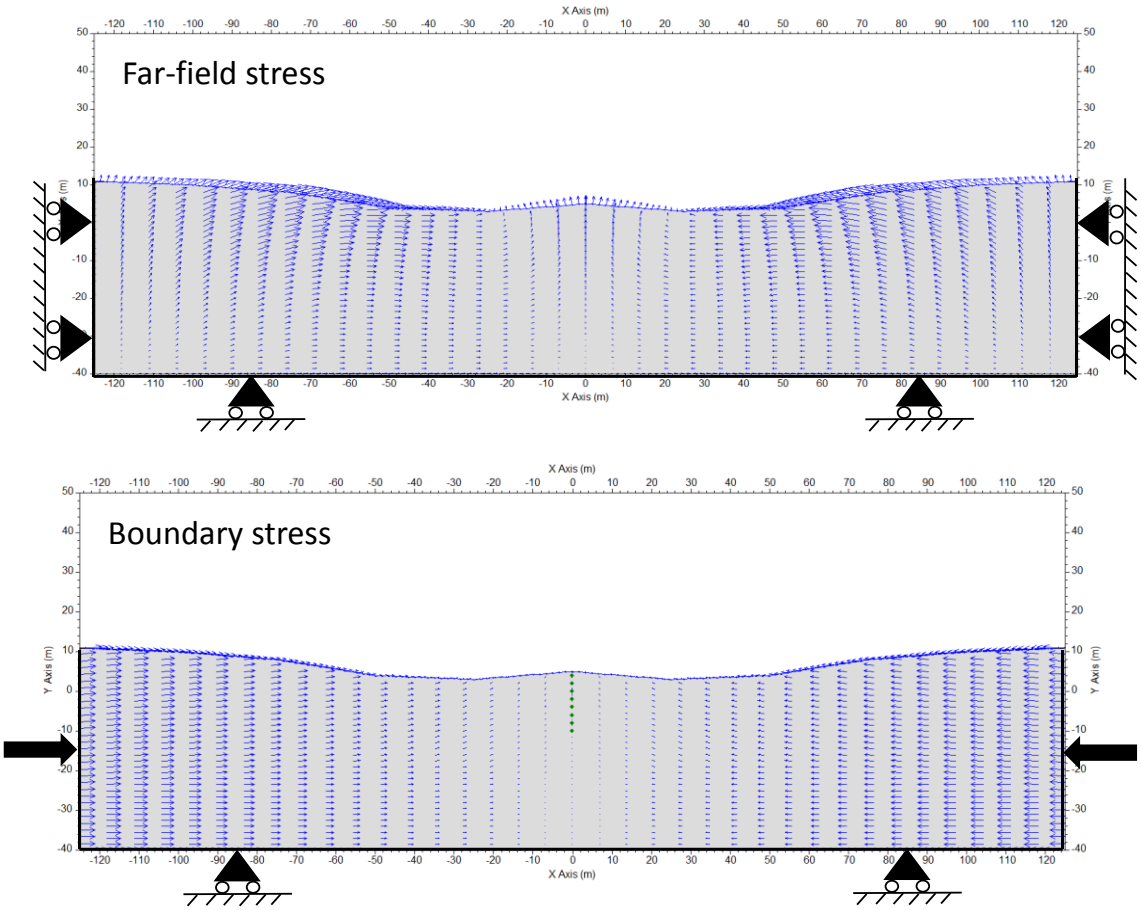

Figure 29. The difference in displacement behaviour between far-field stress function and the boundary stress function. While using the far-field stresses, the normal displacements are disabled from the side and the bottom boundaries. In boundary stress approach, the side boundaries are allowed to move also in the normal direction.

In this study, the boundary stress function was selected for further modelling, because the displacement behaviour was considered as more realistic. However, the boundary stress function increases stresses close to the boundaries where the compression is applied and for this reason, the fracture initiation at these areas was prevented.

4.3.2 Fracture initiation

The first task regarding model with fracturing was to reduce the rock mass strength to *in situ* scale in order to avoid the employment of unrealistically high stresses. The strength reduction was justified, because *in situ*, the stress history of the rock considerably reduces the strength of the mass. Moreover, the time-dependent degradation of the cohesion decreases the shear strength of the rock. (Martin 1997)

Overall strength degradation was decided to be used, because both tensile and shear strength were considered to be affected by the stress history of the Långören island. Furthermore, while the decreasing cohesion influences only to the shear strength, the tensile strength has been observed to be decreased by the thermal stresses (Kirkkomäki 2001) and by the saturated conditions (Augustinus 1995), which at Långören are potential due to the nearby seawater.

In FRACOD^{2D}, the overall stress reduction affects directly to the stress required for the fracture initiation. While in tensile conditions the strength is directly the inputted value, the shear strength is a function of the friction angle and cohesion (see equations 9 and

10). Thus, the overall strength degradation could be performed also by modifying these values.

Nevertheless, while the previous studies have demonstrated that the *in situ* rock strength is commonly less than 50 percent of the laboratory-tested values (Martin 1997), the corresponding strength reduction was performed for the Långören models. However, in this context, a calibration model was required in order to avoid fracturing prior to the application of exfoliation inducing factors.

The calibration model was constructed by creating a block with straight boundaries and using an *in situ* scale. Thus, no topography or any other stress-modifying agents were regarded in the analysis. As a result, 150-meter-wide and 100-meter-thick rectangular block was modelled and the 15 MPa horizontal boundary stress was applied. The top boundary was input as a free boundary representing the bedrock surface.

The rock mass strength was reduced until single elastic fracture elements initiated to the rock mass. The figure below presents the fracture initiation while the rock mass strength was 30 percent of the original value.

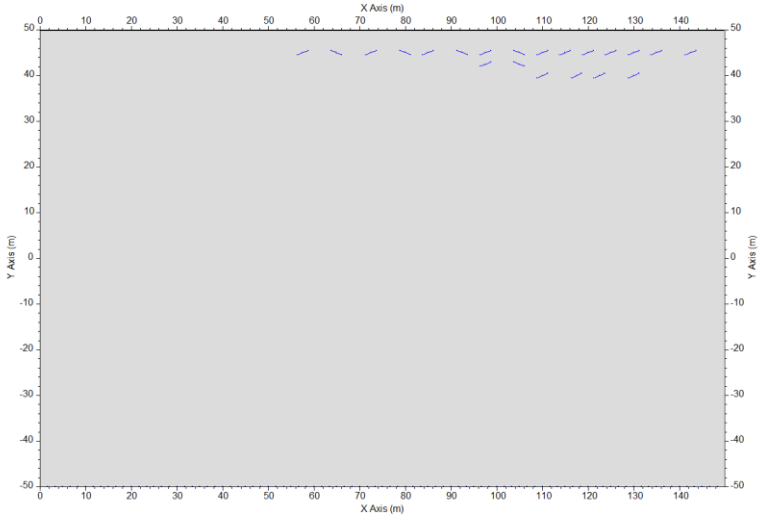

Figure 30. The single elastic fractures initiate near the free boundary while the rock mass strength was reduced to 30 percent of the original value.

While no fracture initiation was observed while using 40 percent of the original strength, this value was chosen to be employed as *in situ* strength modification. On the other hand, even the smaller strength values were unable to induce fracture propagation. Thus, the separate calibration was required to achieve proper fracture propagation.

4.3.3 Fracture propagation

In order to obtain propagating fractures under relatively low stresses, the fracture cohesion was decided to be decreased. The selection of the fracture cohesion as a fracture propagation affecting parameter was justified because it was determined as the most influencing factor in this context. In addition, similar to the rock mass cohesion, the fracture cohesion has been examined to decrease along time hence, being also related to the subcritical crack growth (Kemeny 2002). Therefore, while assuming that previous SCG might have occurred at Långören, the reduction of fracture cohesion was appropriate.

The fracture cohesion limit, where fractures started to propagate, was determined by employing models with simple convex topography and minimal horizontal compression for fracture initiation. Again, the cohesion values were reduced stepwise until the desirable fracture generation was obtained (Figure 31).

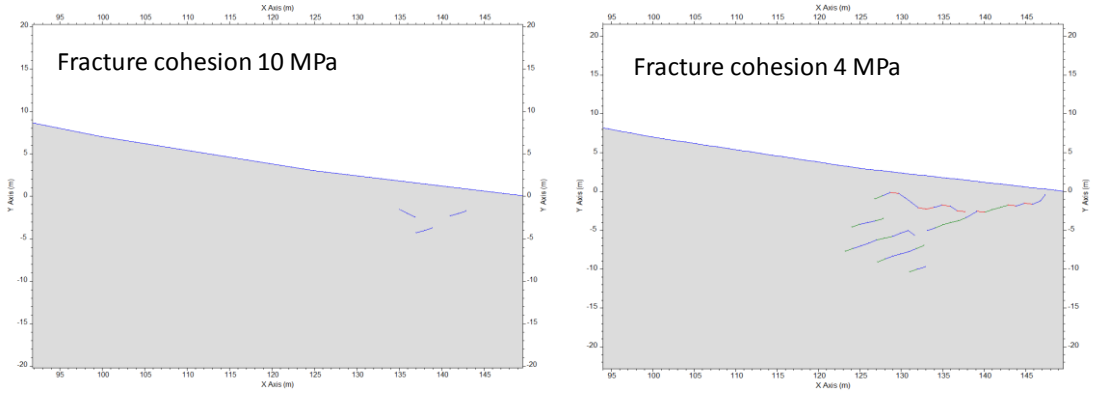

Figure 31. The difference between different fracture cohesions. In the left, the model has 10 MPa fracture cohesion and in the right, the fractures have 4 MPa cohesion, which was also the limit for the fracture propagation.

The limit for the fracture propagation was found at 4 MPa cohesion and this value was selected to the exfoliation fracturing analyses. Other fracture mechanics parameters were calibrated next in the fracture sensitivity section, because they were considered as more important variables while modifying fracture behaviour, not the occurrence of fracture propagation. On the other hand, the relationships and influences of different variables are complex and various approaches could have been used to calibrate the limit for fracture propagation.

4.3.4 Fracture sensitivity

In fracture sensitivity analysis, the influences of fracture stiffness, mode II fracture toughness and tensile strength of the rock mass were discovered. The modelled topography was selected to represent the simplified rock surface of the Långören island in order to examine the fracture behaviour in contrast to the exfoliation fracturing.

First, the fracture stiffness was decided to be evaluated. As the initial parameters were based on the laboratory tests, these values were decided to be reduced stepwise. While the values were reduced up to 0.5 percent from the initial value, the relationship between the normal stiffness K_n and shear stiffness K_s was however, kept constant (Figure 32).

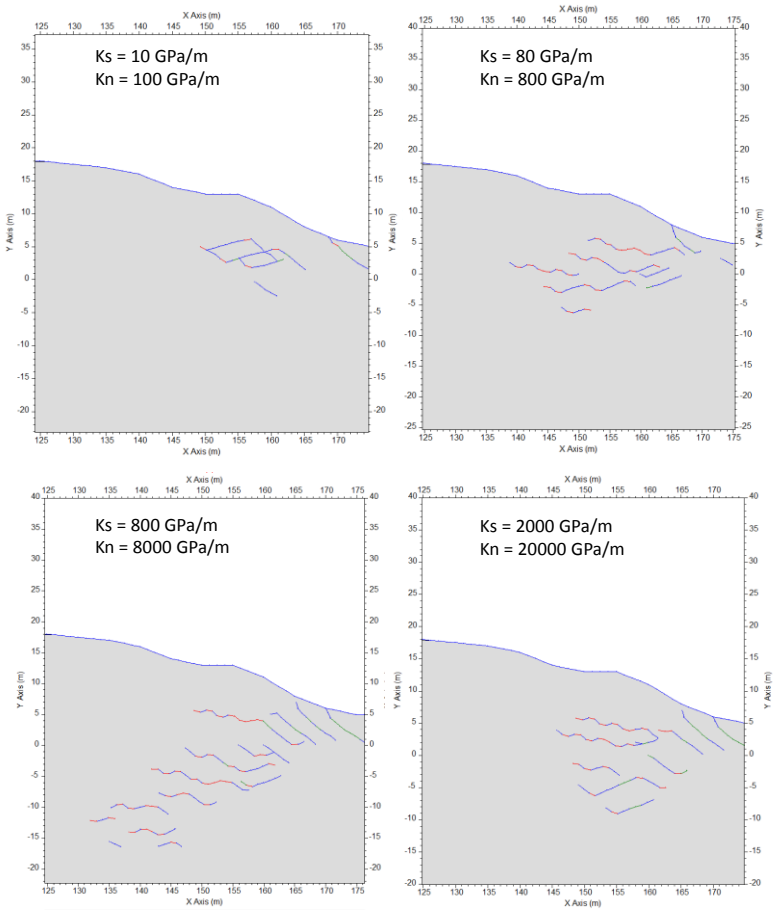

Figure 32. The effects of different fracture stiffness values. Although the values were varied in a wide range the relationship between the normal and shear stiffness was kept constant.

The stiffness was observed to affect mainly to the fracture occurrence. While excessively low values blocked the fracture initiation in further depths, the original laboratory values K_s = 2000 GPa/m and K_n = 20,000 GPa/m (Siren 2011), which were processed as the highest possible scenario, also reduced the amount of fracture generation. As a result, the K_s = 80 GPa/m and K_n = 800 GPa/m were selected as the most appropriate values regarding the exfoliation phenomenon. These values produced the best set of close spaced tensile fractures and they were considered relevant for *in situ* scale modelling.

Next, the mode II fracture toughness was varied. Mode I was disregarded in this analysis, because based on the laboratory measurements conducted with different size samples, the mode I fracture toughness stays constant while the mode II experience scale-dependency. Thus, the mode II fracture toughness increases with larger dimensions (Meier *et al.* 2015). In the analysis, the mean values 3.30 MPa$\sqrt{m}$ and 7.22 MPa$\sqrt{m}$ (Meier *et al.* 2015) of different size laboratory tests were employed together with one overestimated value of 11.22 MPa$\sqrt{m}$ (Figure 33).

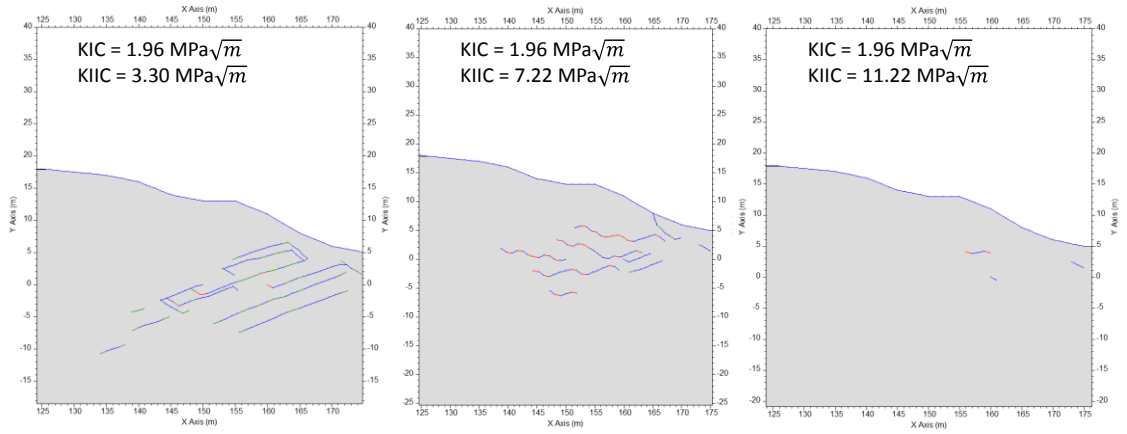

Figure 33. The effect of the mode II fracture toughness, as mode II was determined scale dependent parameter.

The performed examination indicates that mode II is especially important parameter behind *in situ* scale modelling of surface parallel fracturing, because it seems to determine the type of the fracture propagation. In fact, the smaller values completely prevented the tensile fracturing in the model. On the other hand, values set overly high blocked all the fracture generation with the employed stress conditions. As a result, the mode II toughness of 7.22 MPa$\sqrt{m}$ was estimated as the best choice for the further modelling.

The final explored parameter was the tensile strength of the rock mass. However, because the tensile strength was already reduced due to the overall strength reduction, a new approach was required to examine the effect of the tensile strength. As a result, the overall reduction was replaced with the corresponding reduction of rock mass cohesion. Now, the differences between the evaluated tensile stresses are presented in Figure 34.

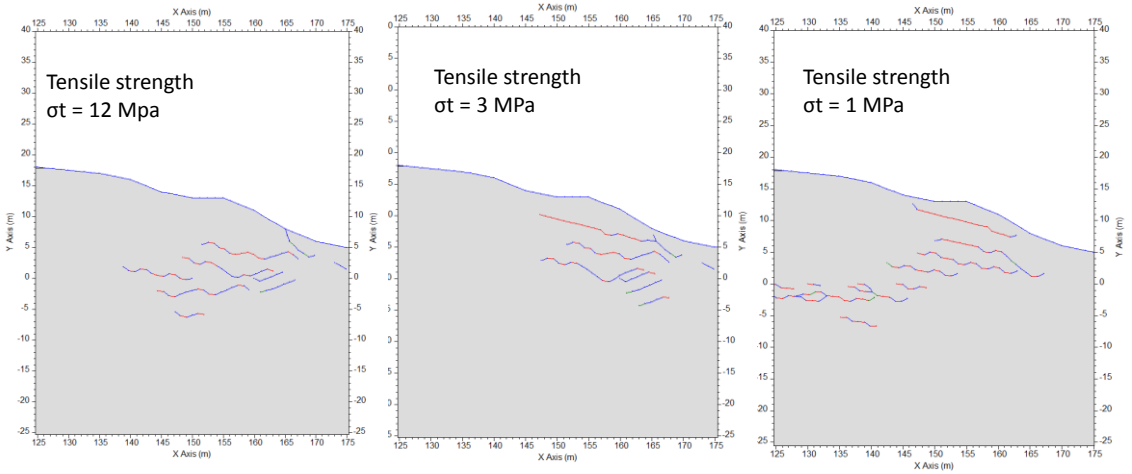

Figure 34. The effect of lower tensile strength in the fracture generation.

Between the 2 MPa and 12 MPa strength values, no effect was observed due to the degradation. However, the models with 1 MPa or smaller tensile strength values affected the fracturing considerably while these models experienced straight and almost lateral fracturing close to the surface. In 0.2 MPa tensile strength model, the fracture initiations occurred also closer to each other and the generated fractures appeared smaller compared to the higher strength models. The result indicates that with greater tensile strength values the shear mode is the controlling type in the fracture initiation. Moreover, the growing

fractures experience alternately shear and tensile deformations, which explains the undulating shape of the fractures. On the other hand, while the tensile strength was assessed extensively low the mode I was the dominant in fracture initiation and propagation.

As the tensile strength was already decreased due to the overall strength modification in the previous calibration, no further modification was decided to be made. In contrast, all the modified fracture parameters are now presented in Table 7 in the next section.

4.4 Fracture mechanics parameters

The initial fracture mechanics parameters were obtained from the previous FRACOD^{2D} analyses performed for Olkiluoto pegmatitic granite (Siren 2011) and the majority of these values were based on the laboratory testing. In this study the parameters were calibrated to be applicable for *in situ* scale analyses. Thermal properties were obtained directly from the works of Kukkonen *et al.* (2011) and Åkesson (2012). The complete table of the employed variables is presented below.

Table 7. Rock mechanics and fracture mechanics parameters for pegmatitic granite (after Siren 2011, p. 10)

Material	Parameter		Value
Intact rock	Young's modulus	E	55 GPa
	Poisson's ratio	v	0.20
	UCS	σ_c	115 MPa
	Rock mass strength	σ_{cm}	65.6 MPa
	Tensile strength	σ_t	12 MPa
	Cohesion	c	12.9 MPa
	Friction angle	φ	47° (degrees)
Fractures	Fracture toughness I	K_{IC}	1.96 MPa$\sqrt{m}$
	Fracture toughness II*	K_{IIC}	7.22 MPa$\sqrt{m}$
	Cohesion – tensile*	c	4 MPa
	Cohesion – shear*	c	4 MPa
	Friction angle – tensile	φ_t	35° (degrees)
	Friction angle – shear	φ_s	35° (degrees)
	Dilatation angle – tensile	ψ_t	2.5° (degrees)
	Dilatation angle – shear	ψ_s	2.5° (degrees)
	Normal stiffness – tensile*	k_n	800 GPa/m
	Normal stiffness – shear*	k_n	800 GPa/m
	Shear stiffness – tensile*	k_s	80 GPa/m
	Shear stiffness – shear*	k_s	80 GPa/m
	Initial aperture		$10 * 10^{-6}$ m
	Residual aperture		$1 * 10^{-6}$ m
Thermal properties	Coefficient of thermal expansion**	b_t	9.0 x 10^{-6} mm/mm°C
	Thermal conductivity***	c_t	3.20 W $m^{-1}K^{-1}$
	Specific heat capacity***	c_p	689 J kg^{-1} K^{-1}

*Modified value based on the calibration, **Åkesson 2012, ***Kukkonen *et al.* 2011

5 Examined models

This chapter reveals three modelling cases executed to examine exfoliation fracture development at Långören island. The boundary conditions, introduced in the previous chapter, were employed differently in each case. Case I concentrates on determining the effects of the topography and high compressive stress conditions without considering any other agents behind the fracture development. Case II models were constructed to simulate fracturing in the pressure release conditions. Furthermore, case III models were processed with thermal environment in order to generate thermal expansion induced fracturing to the rock.

5.1 Case I – Topography and high compression

5.1.1 Modelling procedure

The effect of topography under high compression was discovered by examining stress fields and fracture patterns generated in various topography conditions. First, the tensile stresses in each of the topography models were plotted while using the *in situ* compression of 15 MPa and not allowing any fracture initiation in the models.

Next, the fracture initiation was allowed in the models and the stress levels required for the fracturing were determined. Finally, the fracturing results were evaluated in contrast to the observed stresses and shapes of the topography.

5.1.2 Topography induced stress field

As the two-dimensional fracture mechanics analysis is employed, the modelled topography was dependent on the selection of the 2D-section. In this study, three different topographies were created to represent the simplified shape of the Långören island. The next topography shapes were modelled.

- Topography 1; continuous convex surface,
- topography 2; shallow convex surface with the flat part in the middle,
- topography 3; steep convex surface with flat part in the middle and in the beginning
- topography 4; shallow convex surface with steep concave part in the middle.

The topography 3 was estimated to represent the most realistic bedrock surface at Långören in the direction of the major principal stress component (see Figure 12). In contrast, the topographies 1 and 2 were created to in order to determine the influences of the surface discontinuity and steepness. Therefore, the topography 1 serves as an ideal convex surface and topography 2 as a more gently sloping interpretation compared to the topography 3. In addition, topography 4 was constructed to simulate Långören bedrock in the direction, which was estimated normal to the major principal stress component.

All the models were produced using the FRACOD^{2D} symmetry function, because fewer edges could be used and the rock mass volume could be doubled. After the 15 MPa compression was applied to the side edge, the tensile stress distributions were obtained as shown in Figure 35.

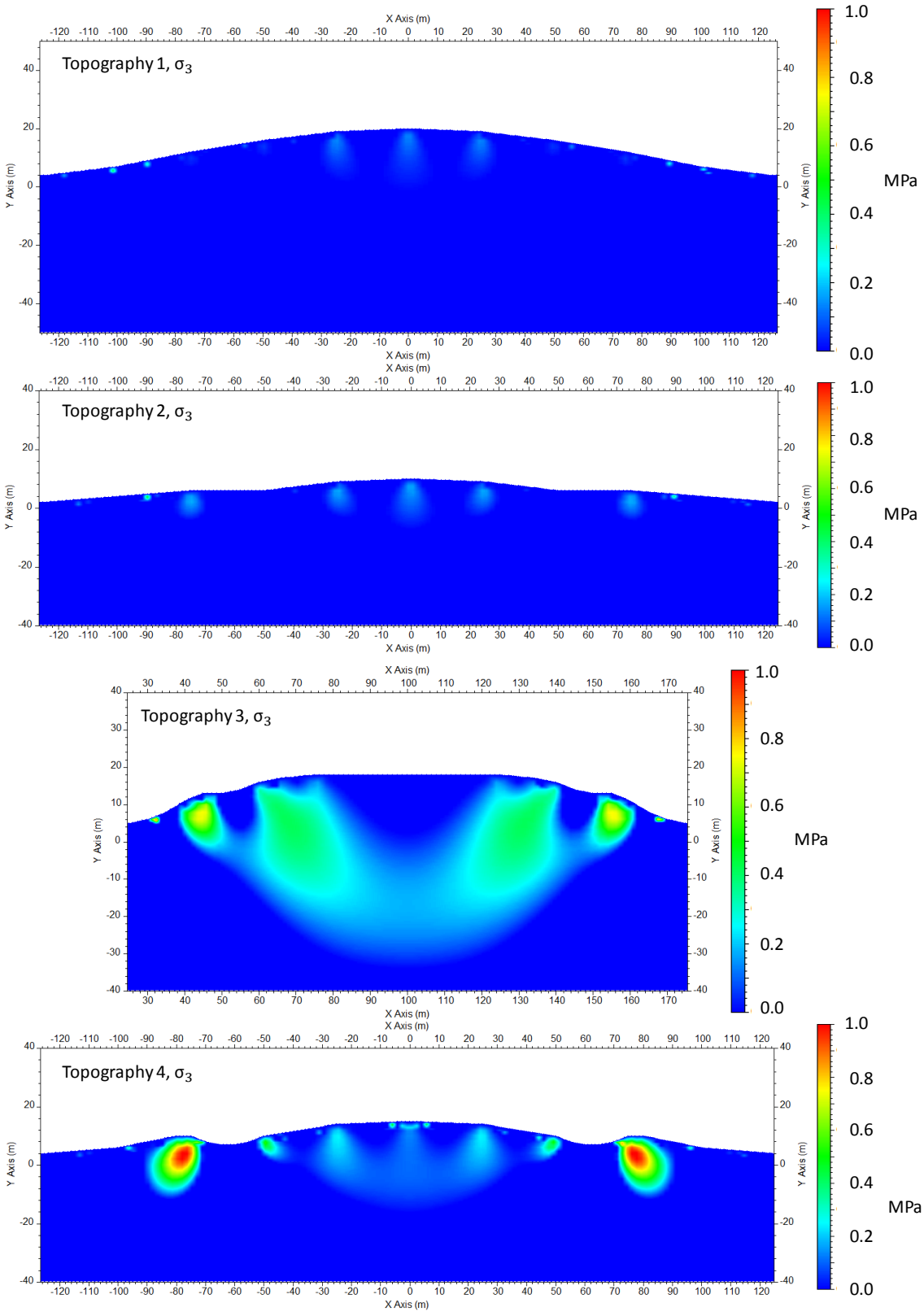

Figure 35. The tensile stress concentrations in the topography models. From top to bottom, the topography 1, topography 2, topography 3 and topography 4. In each of the topographies, the tensile stresses are highlighted and the magnitudes of stresses, in equal scale, are presented column on the right.

The topography 3 and 4 were examined to induce the largest tensile stresses. Thus, it seems that discontinuity and steepness of the convex topography shape is requisite for the more prominent tensile stresses, which in turn, could produce the appropriate conditions for surface parallel fracturing. While the real topography of the Långören island is certainly discontinuous at the area of the recorded exfoliation events, the generation of tensile stresses is also presumable.

5.1.3 Topography induced fracturing

Next, the fracture initiation was allowed in each of the modelled topographies and the fracturing was observed at the stress limit, which was minimal for the fracture generation. The generated fracture patterns were discovered to alternate greatly, as the discontinuous convex surfaces allowed improved conditions for tensile fracture propagations. The fracture initiation was restricted only close to the side boundaries while the depth of fracture initiation was not limited.

The topography 1 prevented tensile fractures almost completely, as the sliding fractures generated close to the lowest point of the topographic surface. For the overall fracture initiation, the topography 1 required also the largest amount of horizontal compression, which was determined to 21 MPa (Figure 36).

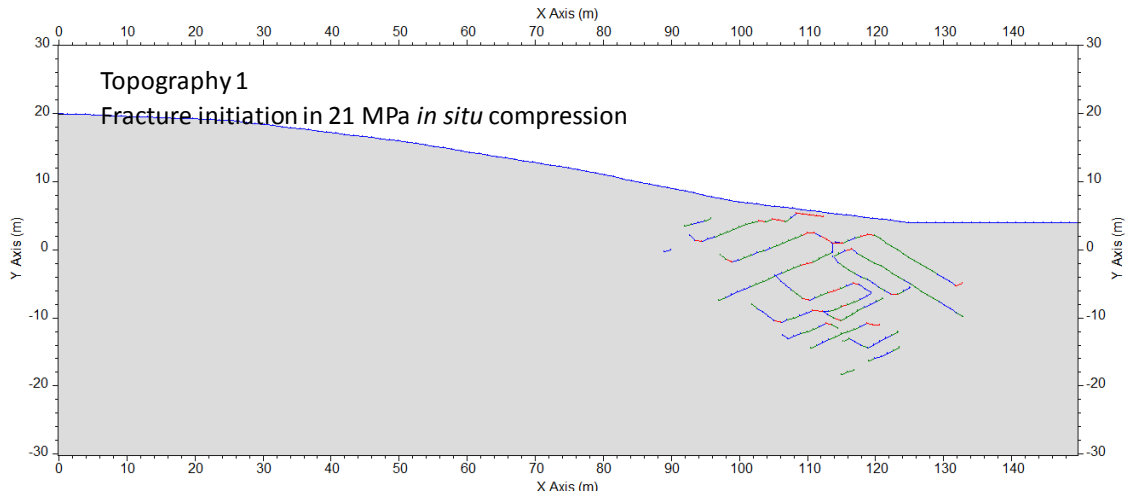

Figure 36. Fractures induced by the topography 1. The minimum required in situ compression for fracture initiation was 21 MPa.

The topography 2 experienced very similar fracture generation compared to the topography 1. However, the amount of tensile fracturing increased close to the rock surface and these fractures were also approximately parallel to the topography. In addition, the *in situ* stress for the fracture initiation reduced to 20 MPa (Figure 37).

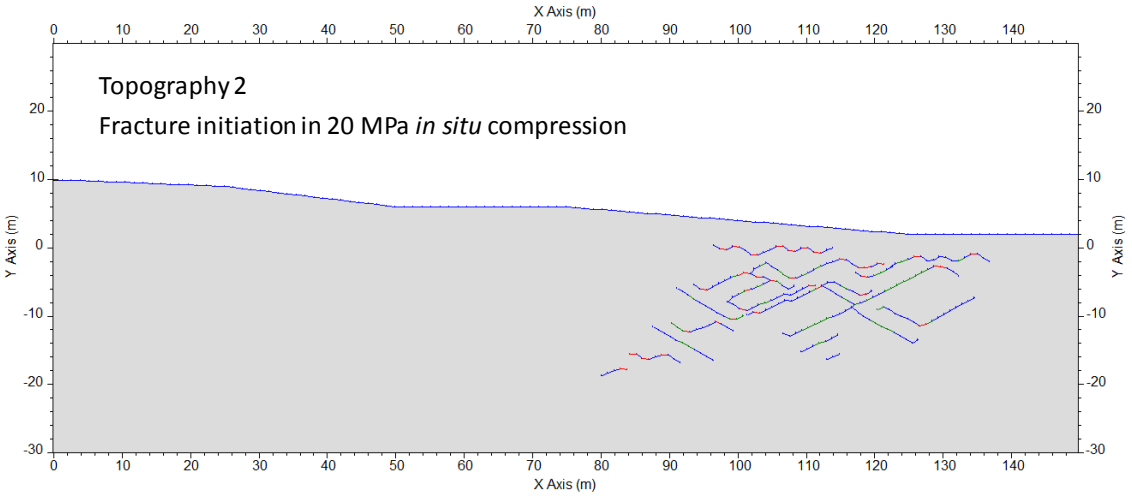

Figure 37. Fractures induced by the topography 2. The minimum required in situ compression for fracture initiation was 20 MPa.

In contrast to the previous models, the topography 3 induced mainly surface parallel fracturing and only a few sliding fractures generated to the rock mass. On the other hand, the total amount of fractures was apparently reduced. The required *in situ* compression was 19 MPa in this case.

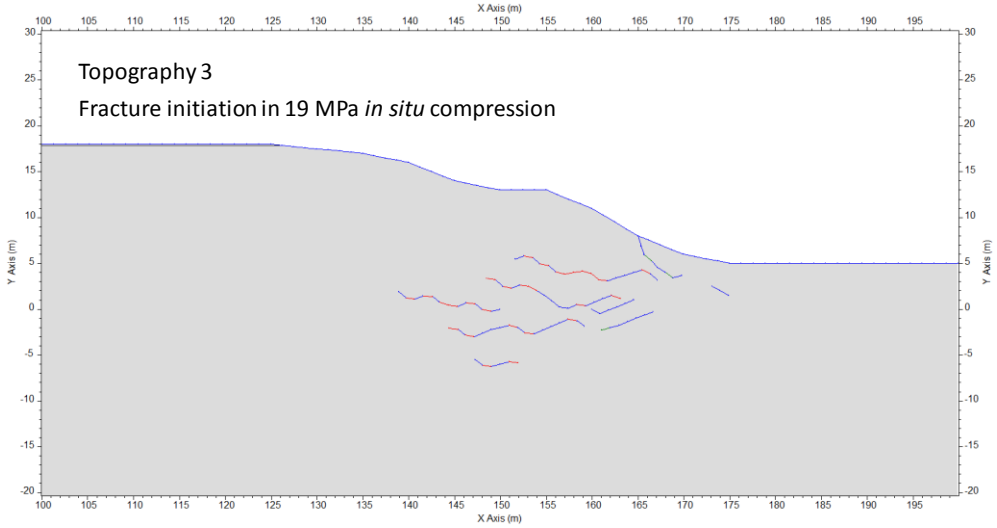

Figure 38. Fractures induced by the topography 3. The minimum required in situ compression for fracture initiation was 19 MPa.

In the topography 4, all the tensile fractures generated below the steep convex part of the topographical surface and few sliding fractures originated below the more lateral part of the model. The most remarkable fracture originated about five meters below the bedrock surface. This fracture appeared as an evident exfoliation fracture while it was smoothly parallel to the topography having no corresponding roughness compared to the beneath fracturing. In the topography 4, also 18 MPa compression was required for the fracture initiation, which was the smallest amount of the applied *in situ* stress in the examined models.

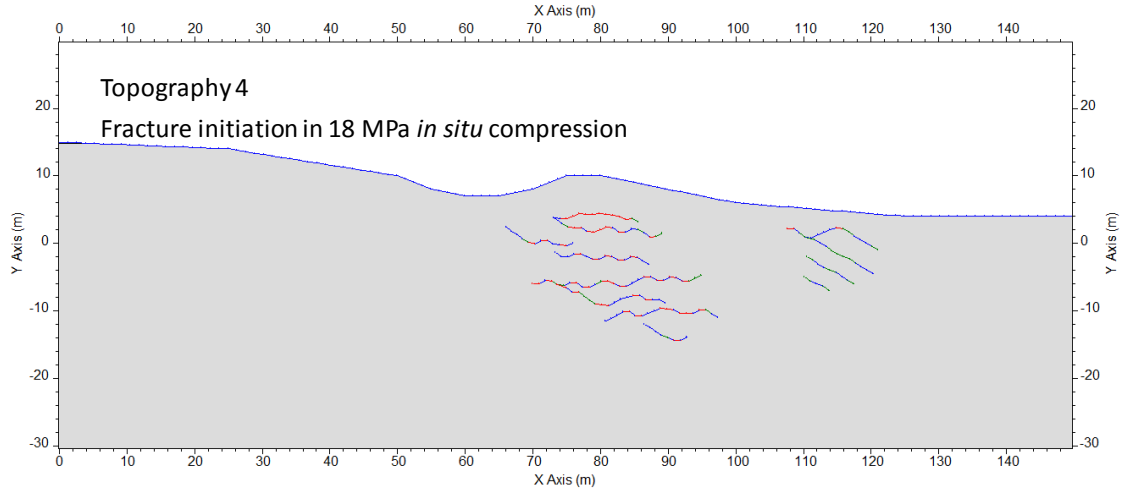

Figure 39. Fractures induced by the topography 4. The minimum required in situ compression for fracture initiation was 18 MPa.

5.1.4 Results

In the topography and high compression analysis, the tensile stress was determined as the controlling factor in the exfoliation development. The topography, which was the most efficient in producing tensile stress concentrations, was also the most capable of inducing exfoliation type of fracturing. Furthermore, the lowest *in situ* compression was required for the model with highest tensile stress concentration. Based on the simulations, it can be suggested that the undulating steep convex rock surface is the best alternative for the exfoliation development.

As a result, the topography 3 and 4 seemed to be the most prominent regarding exfoliation fracturing, because they restricted shear deformation while apparent surface parallel fracturing was observed in these models. Moreover, the least amount of compressive *in situ* stress was needed for the fracture initiation.

Although the exfoliation can be determined possible in surface parallel compression, the required near surface stresses for the fracture initiation were still slightly unrealistic. As the maximum possible near surface compression was previously in this thesis regarded as 15 MPa, even the lowest compression in the modelling exceeded this value by 3 MPa. Thus, additional factors are needed in order to produce exfoliation at lower *in situ* stresses. On the contrary, the case I did not produce fracturing below 20 meters and hence, probably even higher stresses would be needed for the development of deeper exfoliation.

5.2 Case II – pressure release

5.2.1 Modelling procedure

The pressure release modelling was performed by examining different ways to remove overburden pressure in FRACOD^{2D}. Because the software cannot consider viscoelasticity, only the effects of the remaining stresses were examined. Thicker layer of rock was also used in order to better account deeper deformations. In all of these models, the horizontal pressure, applied from the side edges, was kept constant during the vertical pressure release. In addition, all of the models were processed with the same topography, which was selected to be the topography 3 from the case I modelling. The two phases of pressure release (Figure 27) were also modelled similarly in each of the models.

Three different types of pressure release were considered. They were referred as symmetrical pressure release, surface normal pressure release and stepwise pressure release. In the symmetrical pressure release, all of the overburden pressure components were removed evenly. In the surface normal pressure release, the vertical pressure components were reduced evenly, but the surface parallel components, induced by the inclined edges, were kept unchanged through the modelling (Figure 40). Thus, in this pressure release model, the compression at the surface was the highest. In the stepwise pressure release, the pressure components were removed stepwise by reducing the overburden stress from one boundary at a time as each boundary has its own stress function. This model was created to simulate a moving glacier.

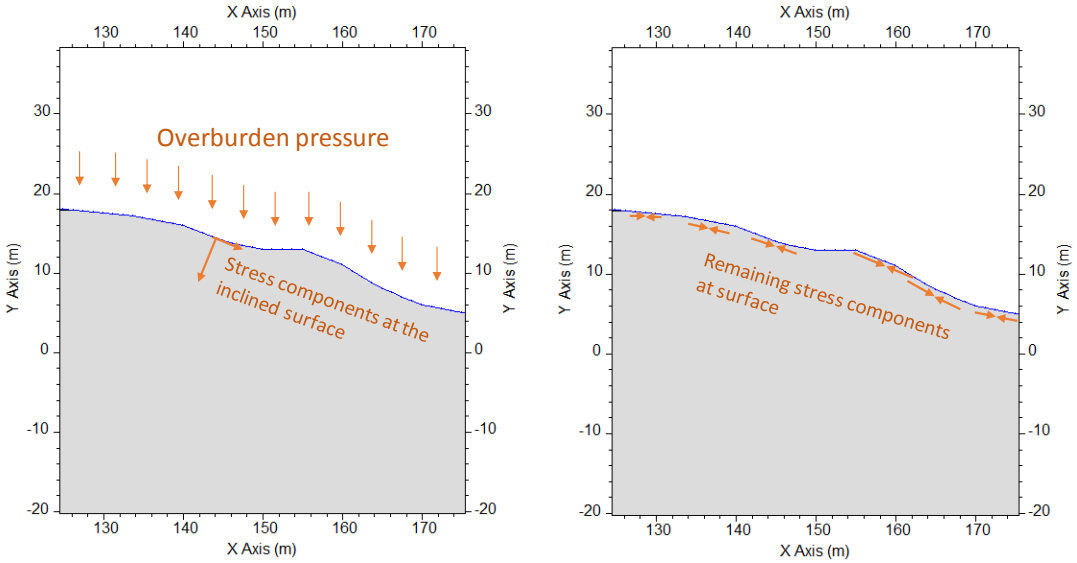

Figure 40. The surface normal pressure release modelling with the remaining surface parallel stress components. If the inclination of the surface is higher the surface parallel component is also higher.

5.2.2 Symmetrical pressure release

The symmetrical pressure release was performed by examining the fracturing in two different models. The difference in the models was the horizontal compression, which in the first model was 22 MPa similar to the vertical loading and in the second model 37 MPa.

In both of these models, no fracturing was observed to occur during the pressure release and the first fractures initiated after the full removal of the ice cover pressure. Therefore, the fracture patterns were induced only by the compression applied from the side edges of the model. In the model with 22 MPa horizontal pressure, only two surface parallel fractures were detected (Figure 43). However, the amount of fractures would have probably increased if more calculation cycles would have processed. In addition, while using the same number of calculation cycles, the total amount of fracturing was increased in the model with 37 MPa horizontal compression.

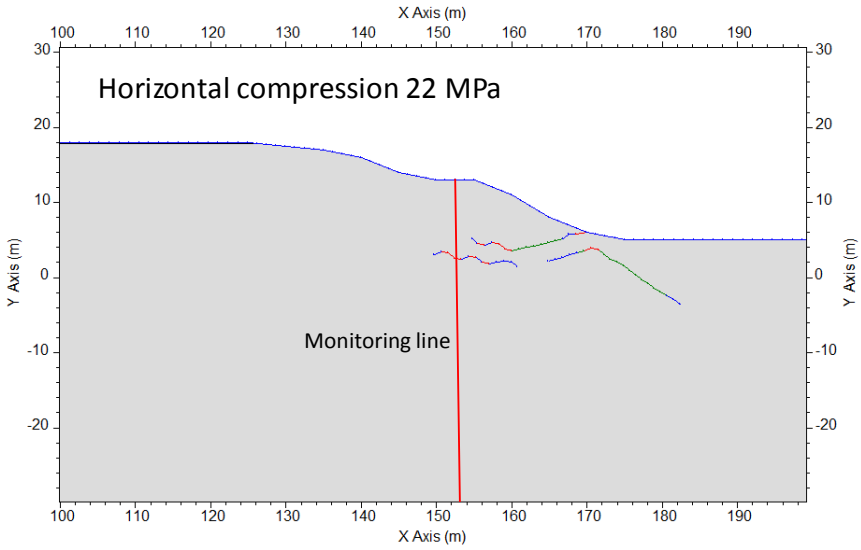

Figure 41. The fractures induced in the model with symmetrical pressure release although these fractures resulted only from the compression of 22 MPa after the full pressure release. The monitoring line for stress behaviour examination (Figure 43) is also illustrated.

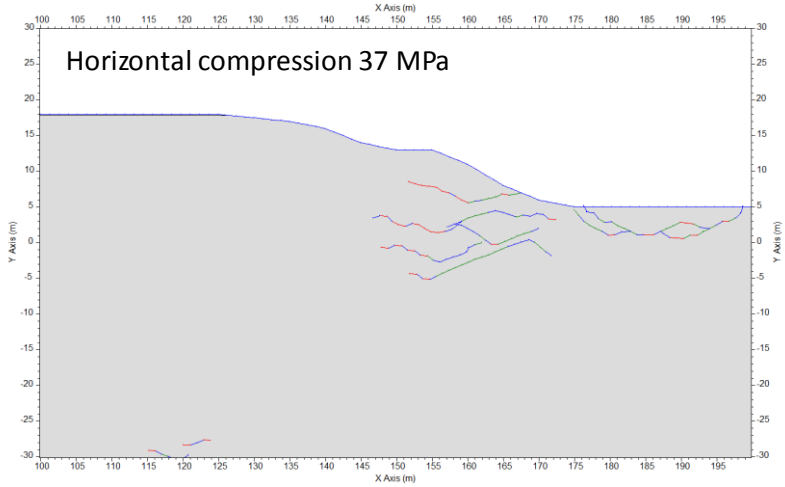

Figure 42. The fractures induced in the model with symmetrical pressure release. These fractures resulted only from the compression of 37 MPa after the full pressure release.

Stress behaviours in contrast to depth were found to have a sufficiently similar orientation after and during each phase of the pressure release with 22 MPa horizontal stress (Figure 43). This indicated that no significant variation occurs in the stress-field.

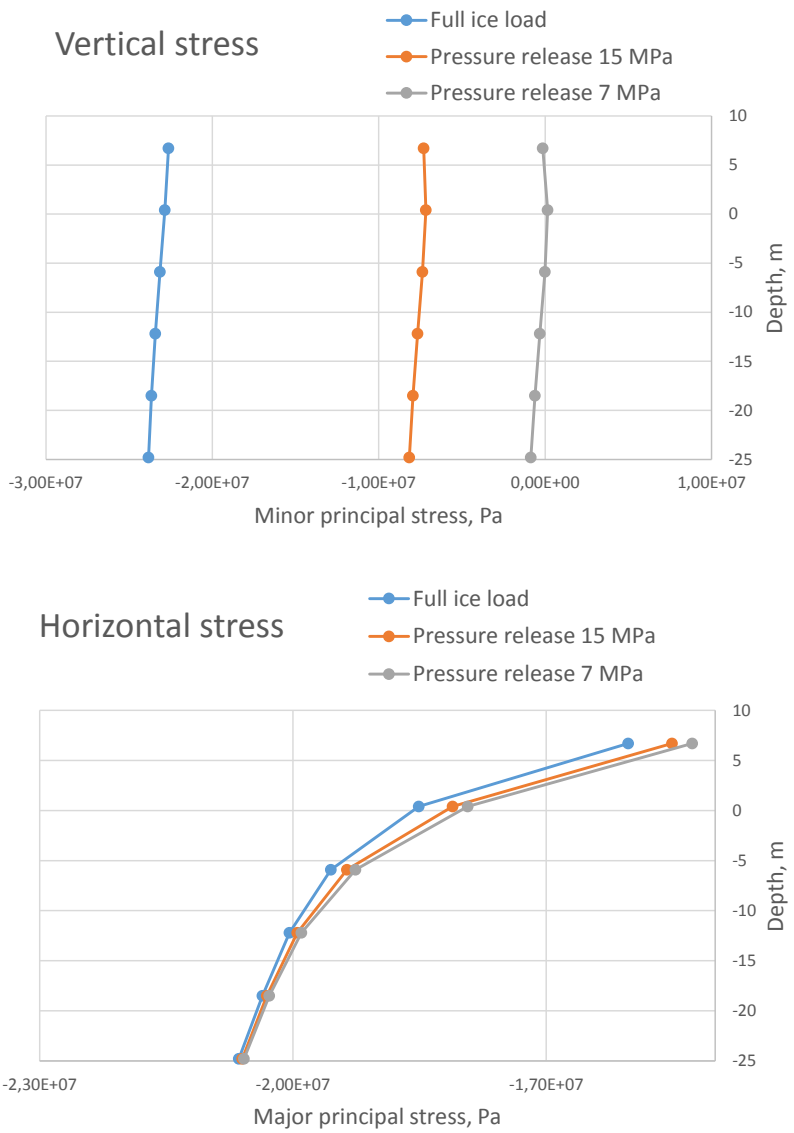

Figure 43. The stress behaviour from the monitoring line of the symmetrical pressure release model with 22 MPa horizontal compression. These figures indicate that no significant variation in stress fields occurred while the orientations of the stress components were nearly parallel.

5.2.3 Surface normal pressure release

In contrast to the previous pressure release modelling, the surface normal pressure release was executed by removing only the stress components, which were normal to the surface boundary. Therefore, at the inclined surface, the stress components parallel to the surface were left constant through the modelling (Figure 40).

The acquired fracturing was mainly parallel to the topography and the fluctuation in the fractures was sufficiently decreased compared to the previous models. Moreover, the observed fractures were closer to the rock surface (Figure 44) and the fracture initiation began after the first rebound phase.

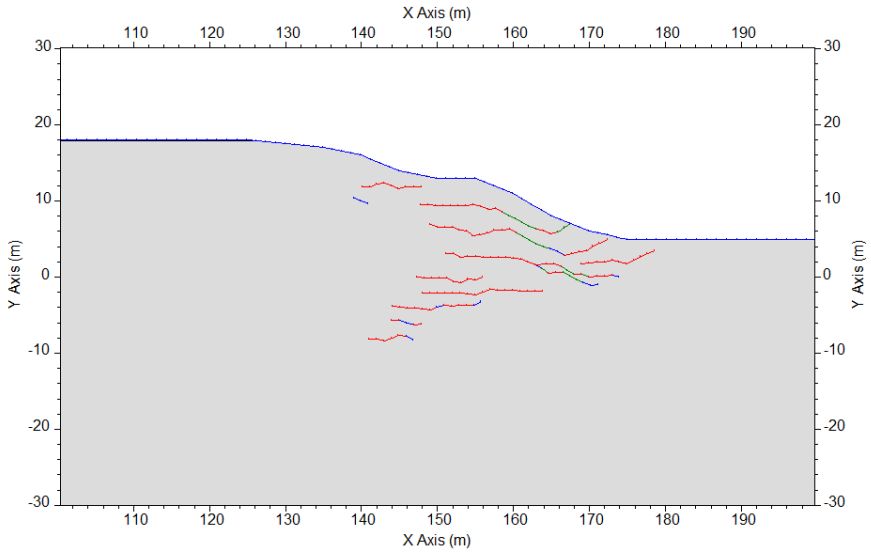

Figure 44. The fractures induced by the remaining surface stress in the uneven pressure release modelling.

Generally, the surface normal pressure release modelling demonstrates that compression, applied from the free surface, is probably one of the key factors behind rock exfoliation. On the other hand, the real behaviour of the glacial stresses at the inclined surface is not discovered further in the thesis and hence, the surface normal pressure release can be only regarded as one possibility for post-glacial fracturing environment.

5.2.4 Stepwise pressure release

In addition to the surface normal pressure release, the stepwise pressure release represents also one post glacial stress removal scenario. In this scenario, the pressure release occurs along the moving glacier. As a result, all the stress components were reduced stepwise to zero as each boundary pressure was released separately processing only one calculation cycle per edge (Figure 45).

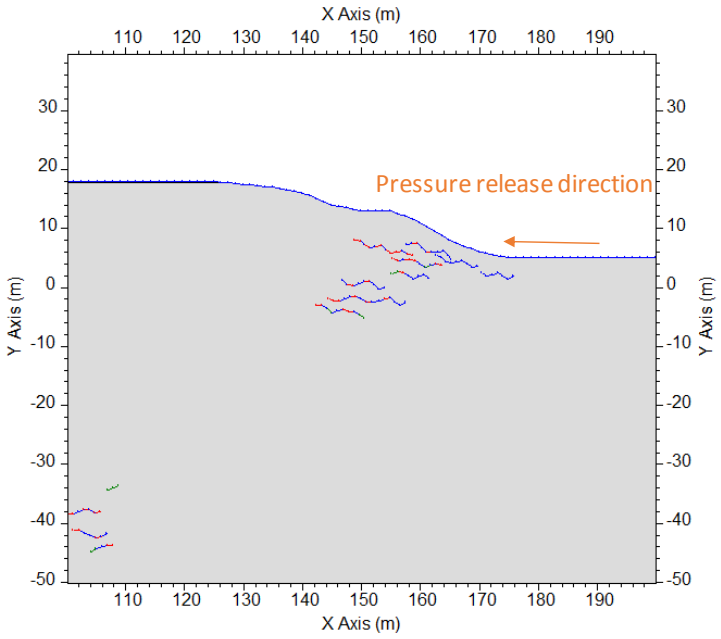

Figure 45. Fracturing induced by the stepwise pressure release. The direction of pressure removal is presented with arrow.

While the pressure was released starting from the right, surface parallel fracturing was observed. These fractures were however, rather serrated because after the first pressure removal phase, only elastic fractures were initiated and the tensile conditions were achieved in the final removal. On the other hand, smoother fracturing could have been achieved if more calculation cycles would have been used during each boundary pressure removal.

5.2.5 Results

According to the stress behaviour in the first pressure release model, the symmetrical removal of the glacial overburden in FRACOD^{2D} did not produce convenient alteration in the stress orientation behaviour while the fractures generated only due to the high compression after the complete removal of the loading. In this case, the higher *in situ* compression was however, more capable of inducing more fracturing, which appeared also closer to the rock surface.

On the other hand, the surface normal pressure release generated continuous surface parallel exfoliation. This indicates, that surface parallel compression, applied from the surface itself might be, in addition to naturally high *in situ* stresses, important factor behind exfoliation near the bedrock surface. In the pressure release FRACOD^{2D} modelling by Lanaro *et al.* (2007), the fracturing was observed also in greater depths, even below 200 meters. However, this results probably from the employment of very high stress states as pressure release due erosion was discovered.

The stepwise pressure release produced fracturing close to the surface, but these fractures were profoundly rough, which on the other hand, probably originates from the low number of the calculation cycles that were processed.

5.3 Case III – thermal expansion

5.3.1 Modelling procedure

The effect of the thermal expansion was modelled in two phases. In the first phase, the long-term thermal modelling was executed by employing the average temperatures of the past 10 weeks before the exfoliation event. As mentioned earlier this temperature was increased by 5 °C to overcome the difference between the average temperatures of the rock surface and the surrounding air. No fracturing was allowed in these models while only the stress behaviour was observed in order to examine the increase in the stress field. In the second phase, the short-term thermal modelling was conducted by employing the daily variations of the rock temperature. In addition to the long-term modelling, the stress behaviour was also studied and plotted in contrast to the previous results.

In the short term modelling, the boundary stress was determined in order to avoid fracturing prior to the thermal expansion. In two of the short-term thermal expansion models, the boundary stress was set differently. First, the boundary stress was estimated as close as possible to the fracture initiation level. Thus, the fracturing began instantly after the thermal stress was applied. This procedure allowed the longer observation of the thermally induced fracture generations.

Next, the boundary stress was assessed in order to avoid fracturing before the thermal time step, which corresponds to the actual date of the exfoliation event. In other words, the fracturing was allowed at the time step 13 corresponding to 27th July 2014 (Table 6).

Moreover, the reality of the required boundary stress in short-term modelling was evaluated in contrast to the long-term thermal stresses.

In all of the models, the stress behaviour was measured from the same monitoring line, which was input to the location of the most possible fracture initiation (Figure 46). The length of the monitoring line was 15 meters and it was enhanced with a 1-meter-deep accurate monitoring part at the rock surface.

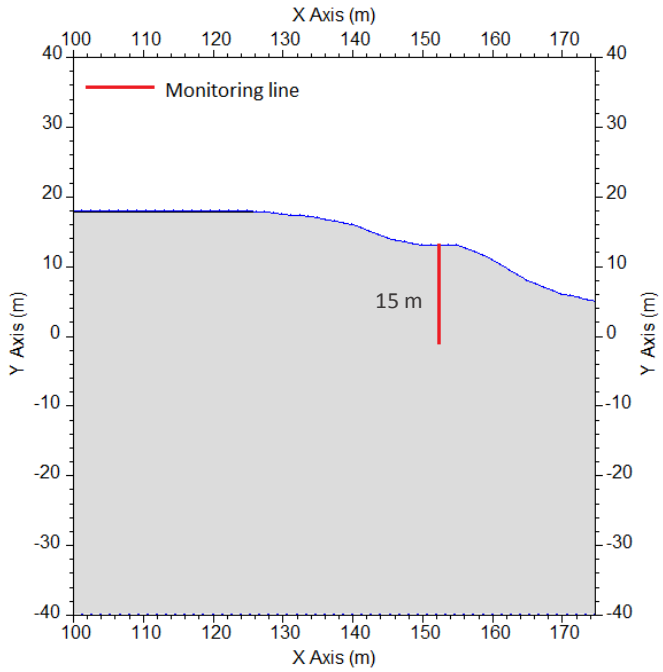

Figure 46. The location of the stress and temperature monitoring in the thermal expansion modelling.

All the models were processed with temperature boundaries with equal positions. In addition, the seawater temperature was applied to the straight boundary next to the side edges of the model and the rest of the topography was set as rock temperature boundary (Figure 47).

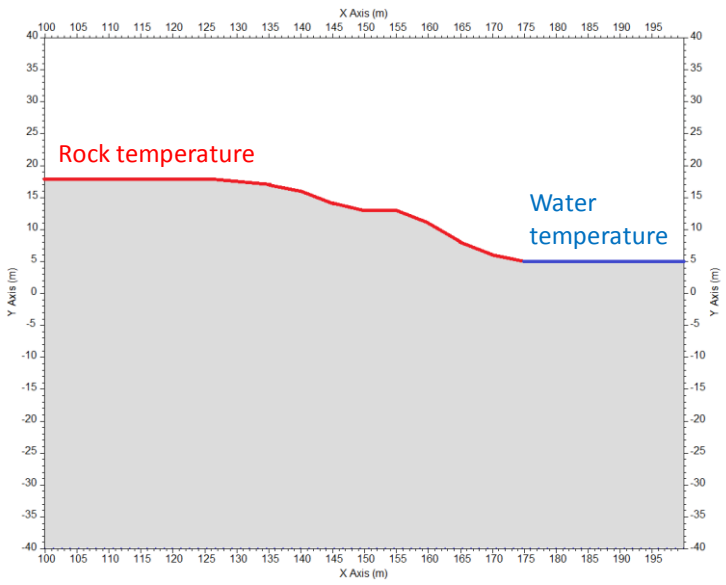

Figure 47. The temperature boundaries in the thermal expansion models.

5.3.2 Long-term modelling

In the long-term thermal expansion modelling, first, the long-term (10 week) thermal stress and *in situ* compression of 15 MPa were plotted in contrast to each other to describe the difference between the major principal stress component and the temperature induced additional compression (Figure 48). The introduced thermal expansion represents stress field at the end of the modelled thermal cycle in other words, at the end of the 10-week long thermal heating.

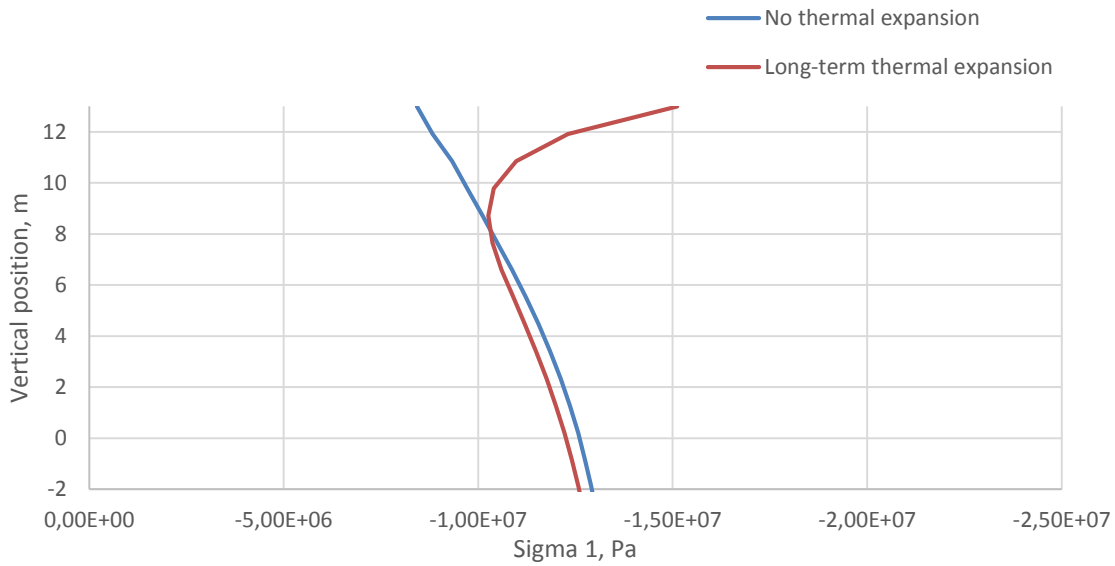

Figure 48. The additional horizontal thermal stress in contrast to the modelled stress behaviour with no thermal effects.

As seen from the figure, the long-term thermal expansion affects approximately four meters below the bedrock surface with nearly linearly decreasing compressive influence. In the surface, the additional increase in the stress was about 6.5 MPa while one meter deeper the same effect was 4 MPa and two meters from the surface 2.5 MPa. Thus, the average additional compression until four meters from the surface was 3.4 MPa.

In addition to the horizontal compression, the long-term thermal expansion affected to the vertical stress component (Figure 49). This influence was observed to extend deeper compared to the horizontal compression. The thermal expansion increased the tensile stress in the location of the monitoring line by approximately 0.15 MPa. However, until 2 meters from the surface, the change in the vertical stress component was minimal.

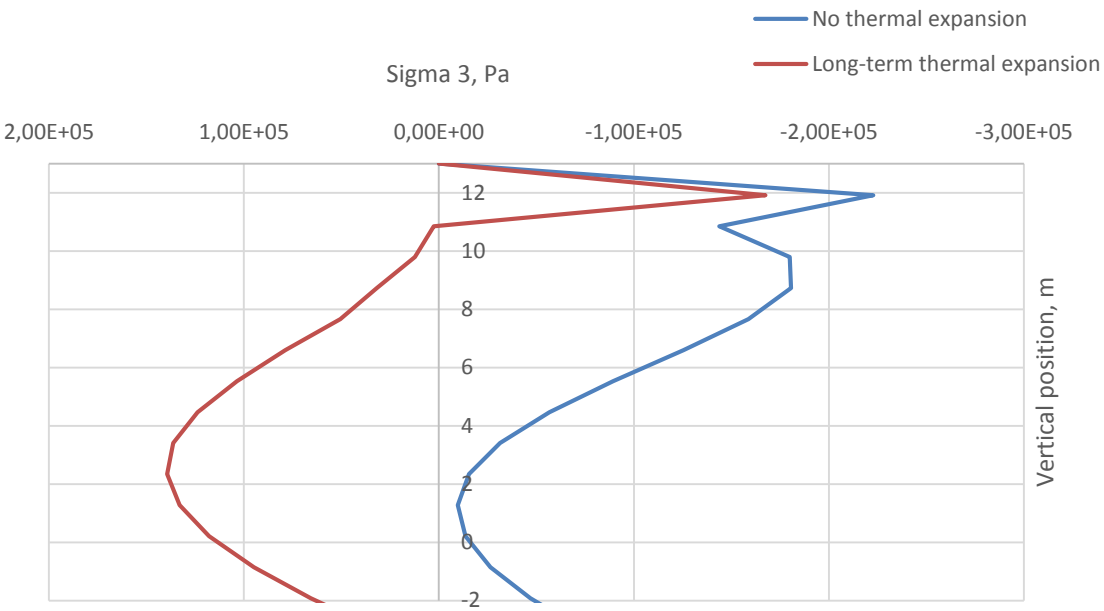

Figure 49. The vertical thermal stress in contrast to the modelled stress behaviour with no thermal effects.

In contrast to the rock stresses at the end of the long-term calculation, the additional temperature increase in rock is presented in the following figure. As can be noticed, while increasing temperatures were observed 20 meters below the surface, these additional temperatures were too low to induce additional compression below 4 meters.

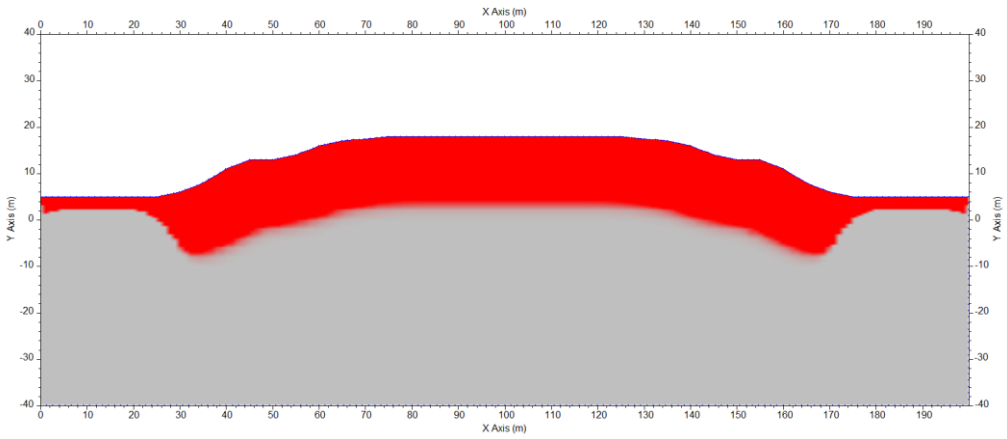

Figure 50. The range of the rock temperature increase in the long-term thermal modelling. The red color is the additional temperature, while the grey area represents the initial unchanged rock temperature.

5.3.3 Short-term modelling

The short-term thermal expansion was modelled using the daily temperature variations. First, similarly to the long-term modelling, the influence of the temperature on the stress field was discovered in shallow depths (Figure 51). Again, the presented situation corresponds to the end of the thermal calculation while the applied boundary stress was 15 MPa. In this case, only the horizontal stress component is introduced, because no significant variation was observed in the vertical stress component while modelling short-term thermal expansion.

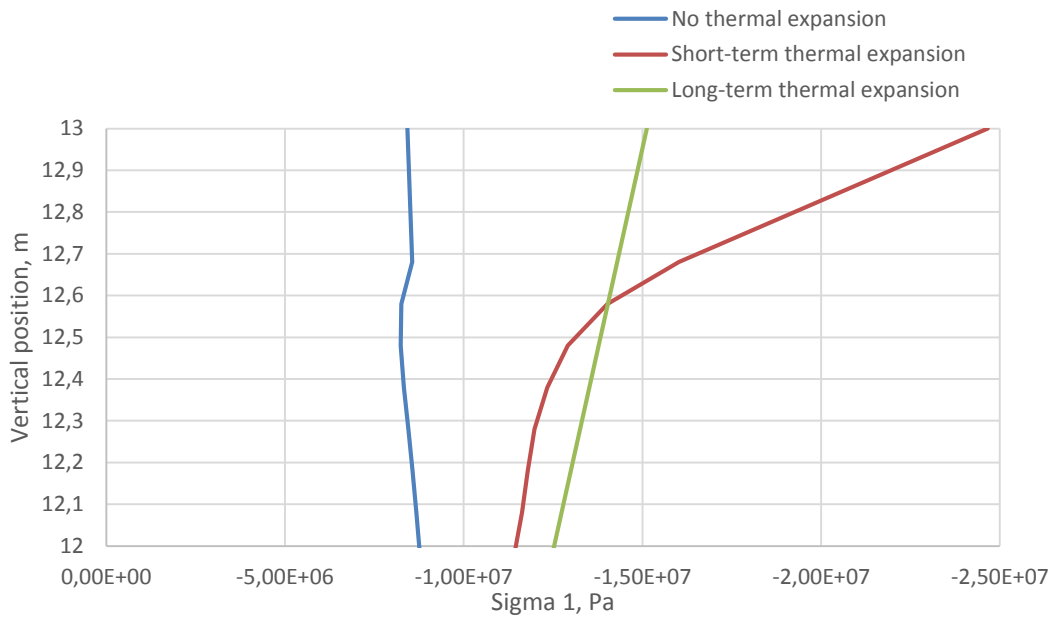

Figure 51. The modelled temperature profiles one meter from the surface. As can be seen, the short-term thermal expansion has a remarkable compression increasing effect very close to the surface.

As can be seen from the figure above, the short-term thermal expansion affected to the horizontal compression greatly very close to the surface, but below 0.4 meters the effect was overcome by the long-term heating. While the temperature profiles were examined, it was also noticed that temperature behaviour was almost directly in agreement with stress behaviour.

Including the *in situ* monitored temperature diagram, the temperature profiles are presented in Figure 52. The real temperature diagram is well aligned with the modelled temperature profile if the effect of existing fractures is ignored. The monitored diagram represents only the behaviour of the measured temperature, because during the monitoring period not as high temperatures were obtained as the modelled temperatures from 2014.

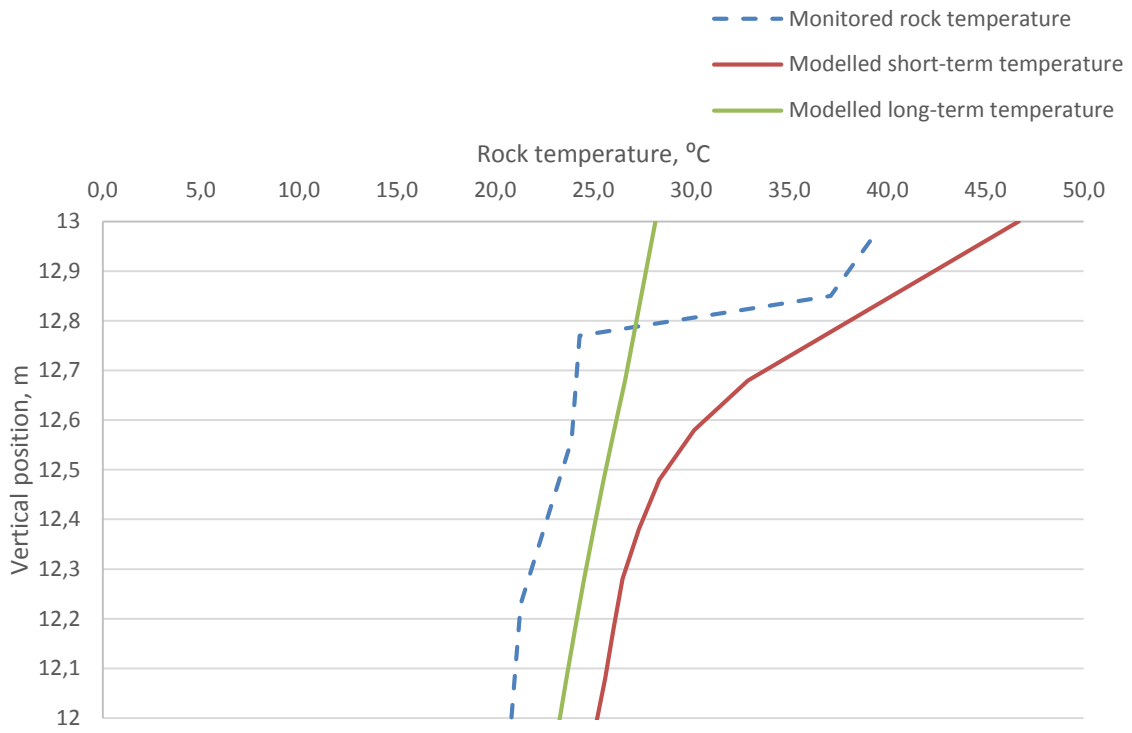

Figure 52. Modelled long-term and short-term temperature profiles in contrast to the in situ monitored temperature profile, where the effect of the existing fractures is apparent. It should be noticed that the initial surface temperatures are not the same.

In order to obtain information of the fracture pattern evolution under thermal stress, the fracture initiation was allowed and the boundary stress was determined as close to the fracture initiation as possible while using no thermal functions. This boundary stress was 18.93 MPa and the fractures started to generate at the second thermal time step. The fracture evolution is presented in the following figures.

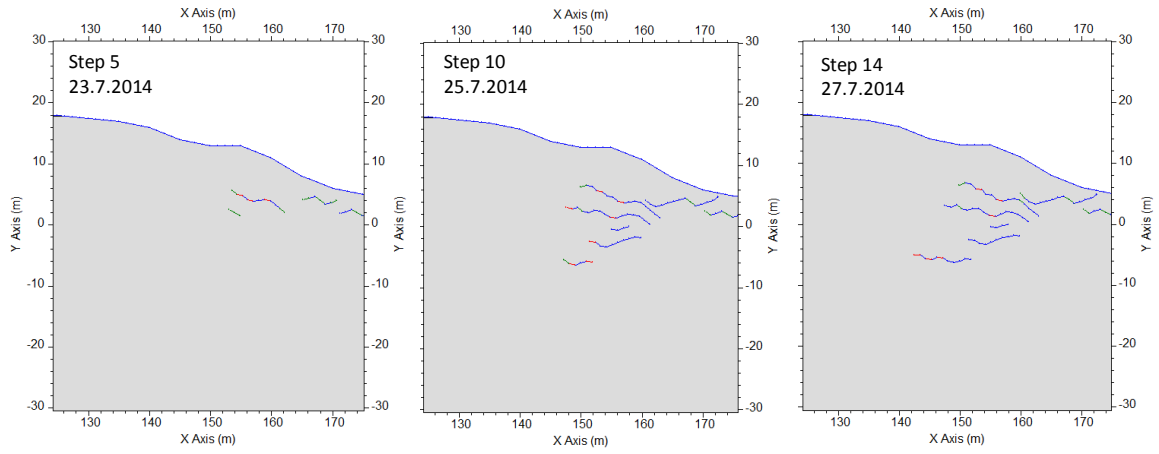

Figure 53. Fracture evolution under thermal loading and in situ compression of 18.93 MPa. The fracturing started at the second thermal time step.

The first fractures initiated about 8 meters from the surface and the fracture generation continued only below this first fracture. The deeper fractures propagated also slower compared to the fracture closest to the surface.

If accounting the additional temperature increase in the figures (Figure 54), it can be detected that the fractures begin to generate deeper compared to the area of the increasing temperatures.

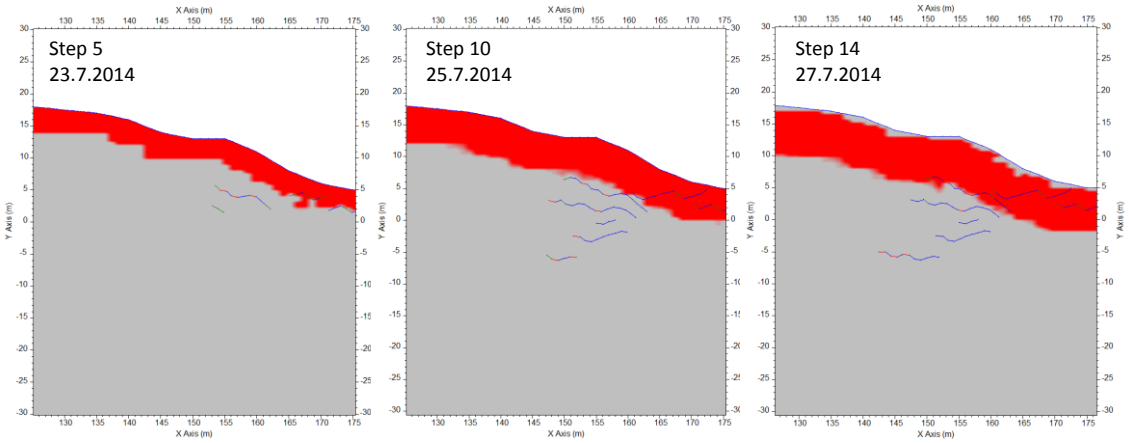

Figure 54. The range of the rock temperature increase in the short-term thermal modelling. The red color is the additional temperature, while the grey area represents the initial unchanged rock temperature.

In the following model, the *in situ* boundary stress was decreased in order to prevent fracturing before the 13th time step corresponding to the realistic fracture initiation at the date 27th July 2014. The modified *in situ* stress was now estimated to 18.58 MPa. Together with short-term thermal influence, the following fracturing was obtained.

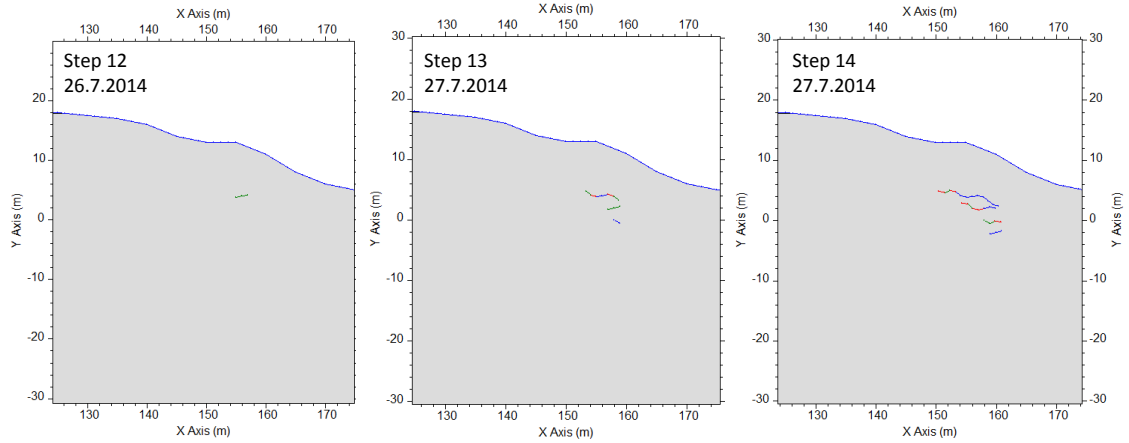

Figure 55. The fracture evolution under thermal loading and in situ compression of 18.58 MPa. The fracturing started at the 12th thermal time step.

In the model, the fracture initiations occurred also one below another order and the closest fracture appeared about 8 meters from the surface. At the end of the final time step four fractures were initiated one below another.

5.3.4 Results

The thermal expansion induced exfoliation was modelled by investigating the long-term and short-term thermal stresses and thermally triggered fracturing. The long-term thermal expansion was discovered to have a horizontal compression increasing influence up to 4 meters from the surface while the short-term thermal expansion affected only 0.4 meters from the surface. On the other hand, while regarding the vertical stress component, the

long-term heating induced additional tensile stresses deeper than 15 meters from the surface. Conversely, the short-term thermal environment did not affect to the vertical stresses. Thus, the long-term thermal expansion seems to be more prominent factor when the thermally induced exfoliation is considered, because it can increase the stress state very close to the fracture initiation limit also in further depths.

In the thermal expansion modelling, the first observed fractures originated approximately 8 meters below the bedrock surface, which does not correspond to the reality as all of the GPR monitored fractures (Figure 14) were located closer than two meters from the surface. This probably results from the accuracy of the processed models and the simplification of the topography.

In reality, the existing fractures would possibly prevent proper thermal conduction through them, which can be seen from the monitored temperature line in Figure 18 and Figure 52. Thus, the real fracture evolution could be reverse in contrast to the modelling where fractures initiated one below another. If the existing fractures prevent the thermal conduction at a certain depth, this would induce more thermal stress and higher temperatures at the area above the fractures.

6 Discussion

Previously, the three modelling cases were introduced, each of them investigating Långören exfoliation phenomenon based on a different exfoliation fracturing theory. The case I examined the effects of various topography conditions under high compressive stress state. The case II focused on the residual stresses during the post-glacial pressure release, and the case III investigated the influence of thermal expansion at the rock surface.

6.1 Topography and in situ stresses

In all of the cases, the results indicated that high compression and tensile stress producing topography are the essential requirements for the exfoliation. On the other hand, thermal or post-glacial conditions can increase the compressive stress state in rock thus, causing the fracture initiation.

The influence of the topography was discovered essential, as the continuous and shallow topographies with lesser tensile stress concentrations were unable to produce prominent surface parallel fracturing. These topographies also required higher stresses for the overall fracture initiation. The observed tensile stresses were the most appropriate if the convex surface was discontinuous having an undulating shape. Furthermore, steeper height alterations in the convex topography increased the tensile stresses.

While 2D modelling approach was employed, the 3D topography in contrast to the real stress field orientation could not be used in the work although 3D conditions might affect greatly to the obtained fracturing. The constructed 2D topographies were also rough approximations of the possible bedrock sections and the undersea conditions remained completely elusive. Nevertheless, while the real topography of the Långören island is considered, the location of the monitored exfoliation fractures is appropriate in contrast to the modelling as the shape of the sloping surface is distinctly varying at the area.

The *in situ* compression that was required for the fracture initiation was still rather high in all of the models in contrast to the measured maximum near-surface values in Southern Finland (Mononen 2005). However, in the post-glacial pressure release, the high residual stresses are realistic if the analysis is performed regarding the situation relatively close the ice-cover removal. Since currently the effect of the post-glacial stresses is estimated only to a few mega pascals, the post-glacial stresses are not liable factors in the exfoliation occurred in 2014. On the other hand, pressure release might have induced post-glacial fracturing that currently affects to the thermal conduction in the rock hence assisting in the present day fracture generations.

In addition to the fractures formed by the post-glacial stresses, subcritical crack growth, which was not modelled in this study, might propagate fractures slowly in the rock mass while the critical limit for the rapid fracture propagation has not been exceeded. Because all of the models were processed with an intact rock mass with no pre-existing discontinuities, the influence of the pre-input fractures remains to be discovered in the becoming exfoliation studies.

The surface normal pressure release with remaining surface parallel stress components was capable of producing the best set of evident exfoliation fractures. It is not however clear, if this type of residual stress behaviour would be realistic after the removal of the glacial loading. In this context, the existence of the surface parallel glacial stress components remains also to be discovered in the further analyses.

6.2 Thermal environment

In the case III, the short-term (daily) thermal expansion induced very high compressive stresses close to the bedrock surface where the temperature boundary was input. However, this compression was observed to decrease rapidly during the first half a meter depth, which corresponded also to the *in situ* measured temperature behaviour. On the other hand, the long-term (weekly) thermal expansion produced considerable compression apparently below the depth of 2 meters and furthermore, the vertical stress component experienced additional tensile conditions even below 15 meters. All the GPR measured fractures at the island were located only a few meters or less from the rock surface, which signifies that these fractures were in the range of long-term thermal expansion.

On the other hand, while the models suggest that fractures generate in one-below-another-order, the real fracture evolution at the Långören island is not known. The recorded fracturing in 2014 occurred apparently very close to the surface, but it is not certain if the fractures below initiated later or before the observed phenomenon. Hence, if only the nearest fractures generated at the time of the observation, the event could have been induced almost purely by the short-term thermal impact.

In this context, the influence between short-term and long-term thermal effects can be debated. While the short-term thermal expansion could induce fracturing very close to the surface due to sudden thermal impact, the long-term thermal expansion would reach the limit for fracture initiation along longer time. Thus, short-term thermal expansion could by itself generate fractures only above half a meter from the surface. In long-term thermal expansion, the sudden temperature variations are not important, but the high average temperature in contrast to the longer timespan is essential. The long-term thermal expansion can also induce fracturing in further depths, at least few meters from the surface, due to the slow thermal conduction of rock.

In reality, the observed exfoliation at Långören has probably been a combined result of the long-term and short-term thermal expansion. In the short-term thermal expansion modelling, approximately 18.5 MPa *in situ* stress was required, which was relatively close to the fracture initiation even without thermal expansion. Therefore, the long-term thermal stress has potentially been needed in order to adjust the stress state this close to the level of fracture initiation.

The first fractures in the short-term thermal modelling generated at the depth that was about 8 meters from the rock surface and the further fracturing occurred even deeper. Moreover, the increase in the rock temperature extended only close to the 8 meters depth while the additional temperatures at this area were extremely small. This indicates that the fractures may not necessarily generate at the areas of the largest thermal stresses, but the combined influence of the *in situ* stress and the thermal expansion is probably more crucial.

On the other hand, based on the topography induced stress fields, the tensile stresses seemed to control the location of exfoliation development. Hence, as the long-term thermal expansion was capable of increasing tensile stresses even below 15 meters depth, it can be regarded as more prominent factor for exfoliation fracturing compared to the short-term heating. None of the fractures initiated however, in tensile fracturing mode while the first fracture element appeared always in mode II.

6.3 Uncertainties and further remarks

The simulated fracturing did not appear as close to the surface in any of the modelling cases as the *in situ* observed fractures. This results perhaps from the inaccuracy of the FRACOD^{2D} models and the uncertainty of the realistic topography and stress conditions. It would have been possible to make models more accurate, as the employed grid point spacing was two meters, but the problem with the increasing accuracy would have been that it would have required recalibration of the modelling parameters and the calculation speed would have been decreased. Thus, fewer models could have been analysed. Moreover, the stress behaviour is hard to set realistic in case of the smaller scale modelling.

In addition to the topography conditions, some uncertainty exists in the modelled rock temperatures, because the monitoring results, which were used in the temperature estimation, were achieved in 2016 when the temperatures were certainly lower than the temperatures during the exfoliation in 2014. In addition, applied seawater temperatures represented the surface water temperatures while in reality, the deep water temperatures can be expected much colder. Moreover, the exact effect of the solar radiation on the rock temperatures could not be determined as the complete weather data from the *in situ* monitoring system was not available at the time this thesis was written.

In further *in situ* scale FRACOD^{2D} analyses, the setting of the correct rock and fracture mechanics parameters, as was discovered in this study, will be essential. Especially the scale-dependency of the mode II fracture toughness should be assessed, because the laboratory results (Meier *et al.* 2015) of 50 mm diameter samples prevented the tensile fracturing almost completely, while the results of 120 mm diameter samples produced almost opposite results. The rock mass strength and fracture cohesion are also vital to be set correctly, because they were determined as the most influencing factors regarding the stress limits for the fracture initiation and propagation.

In the future exfoliation modelling, the viscoelasticity and the direction dependent rock mass strength are also factors which should be considered, because the viscoelasticity might explain deeper exfoliation, according to the pressure release theory, and the foliation direction of the rock could assist surface parallel fracturing with smaller stresses. The effect of pre-existing fractures should be also considered in the thermal models.

Although the purpose of this thesis was not to discover the global origin of rock exfoliation, it seems that a topography, capable of inducing high tensile stresses, is the essential requirement for the surface parallel fracturing. Furthermore, the high stress levels for the exfoliation fracture generation can be achieved for example due to the thermal stresses, which can induce thermal expansion and additional stresses even up to 8 meters depth and increase the compressive stress directly at the bedrock surface extremely high.

7 Conclusions

The aim of this thesis was to explain the cause of the Långören exfoliation events in 2014. In this context, the fracture mechanics approach FRACOD^{2D} was employed in order to simulate the recorded fracturing. The validation of FRACOD^{2D} was justified, because the code was proved suitable in the previous exfoliation fracturing analyses and the majority of the prominent exfoliation theories were appropriate for the software.

As the thermal environment was considered important for the modelling, the thermal boundary conditions were obtained based on the historical weather data and the *in situ* monitoring at the Långören island. Moreover, the local stress field was estimated according to the highest near surface stresses measured in Southern Finland. The employed rock mechanics parameters were achieved from the laboratory tests of Olkiluoto pegmatitic granite, which was regarded sufficiently similar to Långören rock type, because at the time of the study, there did not exist rock mechanics data directly from the island.

The three modelling cases were conducted in order to simulate exfoliation fracturing based on the different exfoliation theories. These cases were the topography in high compression, the pressure release and the thermal expansion. The case I examined the influence of various topography conditions in high *in situ* stresses. The case II focused on the different ways to remove the glacial pressure and the case III determined the effects of the long-term and short-term thermal expansion.

As a result, the topography, capable of producing tensile stress concentrations was discovered essential requirement for the exfoliation fracturing. In these topography conditions, all the modelling cases were capable of producing exfoliation if the *in situ* stress was set high. In the employed conditions, this compression was 19 MPa. However, while the solely very high *in situ* stress seemed slightly unrealistic close to the bedrock surface and the post-glacial pressure release could not convincingly be included in the present day fracturing, the thermal expansion was considered as the most prominent source of the Långören exfoliation events.

While the long-term and the short-term thermal expansion models were analysed, it was discovered that the short-term thermal impact affects only above half a meter from the surface. In contrast, the long-term thermal expansion induced additional compression up to 4 meters depth and additional tensile stress at least up to 15 meters depth. This corresponds also to the deeper exfoliation fractures observed at Långören. On the other hand, it is not clear if the deeper exfoliation fractures generated at the time of the recorded near surface phenomenon or if they existed before the observed fracturing. In case of preexistence, they might have been induced by the post-glacial stresses or previous thermal expansion.

As a final conclusion, certain topography, capable of producing tensile stress concentrations, and the high compressive stress state are regarded as the definite reasons for the Långören exfoliation events in 2014. In addition, the critical level for the compressive stress was achieved due to the thermal stresses, which were anomalously high before the observed phenomenon.

The results of this thesis can be used in the future exfoliation studies. As the tentative topography and stress requirements were presented, the production of more accurate anal-

yses would be now possible. However, while regarding exfoliation at Långören, the accurate analyses would require the accurate rock mechanics and fracture mechanics parameters from the island. The *in situ* stress state should be also measured and evaluated in contrast to the 3D topography.

Bibliography

Amadei, B. & Stephansson, O. 1997. Rock stress and its measurement. London, United Kingdom. Chapman & Hall. 490 pages. ISBN 0412447002

Anderson, O. L. & Grew, P. C. 1977 Stress corrosion theory of crack propagation with applications to geophysics. Reviews of Geophysics. Vol. 15.1. pp. 77-104. DOI: 10.1029/RG015i001p00077. ISSN 1944-9208.

Atkinson, B. K. 1982. Subcritical crack propagation in rocks: theory, experimental results and applications. Journal of Structural Geology. Vol. 4:1. pp. 41-56. DOI:10.1016/ 0191-8141(82)90005-0. ISSN 0191-8141.

Atkinson, B. K. 1984. Subcritical crack growth in geological materials. Journal of Geophysical Research. Vol. 89:B6. pp. 4077-4114. DOI:10.1029/JB089iB06p04077. ISSN 2169-9356

Augustinus, P. C. 1995. Glacial valley cross-profile development: the influence of in situ rock stress and rock mass strength, with examples from the Southern Alps, New Zealand. Geomorphology. Vol. 14:2. pp. 87-97. DOI:10.1016/0169-555X(95)00050-X. ISSN 0169-555X

Backers, T. 2004. Fracture toughness determination and micromechanics of rock under mode I and mode II loading. Doctoral thesis. University of Potsdam, Germany. 92 pages

Backers, T. 2006. Experimental Determination of Subcritical Crack Growth Parameters. Postdam, Germany. GeoFrames GmbH. 62 pages. Report R101-1B06.

Bahat, D. & Grossenbacher, K. & Karasaki, K. 1999. Mechanism of exfoliation joint formation in granitic rocks, Yosemite national park. Journal of Structural Geology. Vol. 21:1. pp. 85–96. DOI:10.1016/S0191-8141(98)00069-8. ISSN 0191-8141.

Borchers, J. W. 1996. Ground-water resources and water-supply alternatives in the Wawona area of Yosemite national park, California. Sacramento, California, USA: U.S. Geological survey. 77 pages. Water-resources investigations report 95-4229

Bieniawski, Z. T. 1967. Mechanism of brittle fracture of rock - Part 1- Theory of the fracture process. International journal of rock mechanics and mining sciences. Vol 4:4. pp. 395-406. DOI :10.1016/0148-9062(67)90030-7. ISSN 1365-1609.

Blackwelder, E. 1925. Exfoliation as a phase of rock weathering. The Journal of Geology. Vol 33:8. pp. 793-806. Available: www.jstor.org/stable/30055637. ISSN 0022-1376 (Printed). ISSN: 1537-5269 (Online)

Bruttomesso, D. & Jacobs, L. & Costley, R. 1993. Development of interferometer for acoustic emission testing. Journal of engineering mechanics. Vol 119:11. pp. 2303-2316. DOI: 10.1061/(ASCE)0733-9399(1993)119:11(2303) ISSN 0733-9399 (Printed). ISSN 1943-7889 (Online)

Chapman, R. W. & Greenfield, M. A. 1949. Spheroidal weathering of igneous rocks. American journal of science. Vol. 247:6. pp. 407-249. DOI:10.2475/ajs.247.6.407. ISSN 0002-9599.

Charles, R. J. 1958. Static fatigue of glass II. Journal of applied physics. Vol 29:11. pp. 1549-1553. DOI:10.1063/1.1722992. ISSN 0021-8979 (Printed). ISSN: 1089-7550 (Online)

Evans, A.G. 1972. A method for evaluating the time-dependent failure characteristics of brittle materials – and its application to polycrystalline alumina. Journal of materials science. Vol. 7:10. pp. 1137-1146. DOI:10.1007/BF00550196. ISSN 0022-2461 (Printed). ISSN 1573-4803 (Online)

Fjeldskaar, W. & Lindholm, C. & Dehls, J. F. & Fjeldskaar, I. 2000. Postglacial uplift, neotectonics and seismicity in Fennoscandia. Quaternary Science Reviews. Vol. 19:14. pp. 1413-1422. DOI:10.1016/ S0277-3791(00)00070-6. ISSN 0277-3791

FMI, Finnish Meteorological Institute. 2016. The Finnish Meteorological Institute open data. www.en.ilmatieteenlaitos.fi/open-data

Griffith, A. A. 1920. The phenomena of rupture and flow in Solids. Philosophical transactions of the royal society A. Vol. 221:582-593. pp. 163-198. DOI:10.1098/rsta.1921.0006. ISSN 1471-2962.

Grosse, C.U. & Ohtsu, M. 2008. Acoustic emission testing - Basics for research - applications in civil engineering. Berlin, Germany. Springer. 404 pages. ISBN 978-3-540-69895-1 (Printed). ISBN 978-3-540-69972-9 (Online).

Hall, K. & Andre, M-F. 2001. New insights into rock weathering from high-frequency rock temperature data: an Antarctic study of weathering by thermal stress. Geomorphology. Vol. 41:1. pp. 23-35. DOI: 10.1016/S0169-555X(01)00101-5. ISSN 0169-555X

Harland, W. B. 1957. Exfoliation joints and ice action. Journal of glaciology. Vol. 3:21. pp. 8-10. ISSN 0022-1430.

Hencher, S. R. & Lee, S. G. & Carter, T. G. & Richards, L. R. 2010. Sheeting joints: characterisation, shear strength and engineering. Rock mechanics and rock engineering. Vol. 44:1. pp. 1-22. DOI:10.1007/s00603-010-0100-y. ISSN 0723-2632 (Printed) ISSN 1434-453X (Online).

Holzhausen, G. R. 1978. Sheet structure in rock and some related problems in rock mechanics. Ph. D. Thesis. Stanford university, astrophysics. Stanford, California, USA. 515 pages.

Hökmark, H. & Fälth, B. 2014. Approach to assessing the stability of Olkiluoto deformation zones during a glacial cycle. Eurajoki, Finland: Posiva Oy. 74 pages. Posiva working report 2013-37.

Irwin, G. R. 1957. The stresses and strains near the tip of a crack traversing a plate. Journal of Applied Mechanics. Vol. 24:1957. pp. 361-364.

Jahns, R. H. 1943. Sheet structure in granites: Its origin and use as a measure of glacial erosion in New England. The journal of geology. Vol. 51:2. pp. 71-98. DOI:10.1086/625130. ISSN 0022-1376 (Printed) ISSN 1537-5269 (Online).

Kemeny, J. M. 2002. The time-dependent reduction of sliding cohesion due to rock bridges along discontinuities: a fracture mechanics approach. Rock Mechanics and Rock Engineering. Vol. 36:1. pp. 27-38. DOI:10.1007/s00603-002-0032-2. ISSN 0723-2632 (Printed). ISSN 1434-453X (Online)

Kirkkomäki, T. 2001. Laboratory testing of marble. Espoo, Finland. Helsinki University of Technology, Laboratory of Rock Engineering. 80 pages. A Research Report 29. ISSN 1239-6788. ISBN 951-22-5525-1

Kukkonen, I. & Kivekäs, L. & Vuoriainen, S. & Kääriä, M. 2011. Thermal properties of rocks in Olkiluoto: results of laboratory measurements 1994–2010. Eurajoki, Finland. 96 pages. Posiva working report 2011-17.

Lambeck, K. & Purcell, A. 2003. Glacial rebound and crustal stress in Finland. Eurajoki, Finland. 84 pages. Posiva Report 2003-10. ISSN 1239-3096. ISBN 951-652-124-X

Lanaro, F. & Amemiya, K. & Yamada, A. 2007. Modelling the formation of sheeting joints with FRACOD^{2D} (FRActure propagation CODe). BEM-DDM modelling of rock damage and its implications on rock laboratory strength and in-situ stress. pp. 149-177. Japan: Japan Atomic Energy Agency. JAEA-Research 2007-093.

Lockner, D. A. & Byerlee, J. D. & Kuksenko, V. & Ponomarev, A. & Sidorin, A. 1992. Observations of quasistatic fault growth from acoustic emissions. In publication: Brace, W. F. Fault mechanics and transport properties of rock. London, England: Academic press. pp. 3-31. ISBN 978-0-12-243780-9.

Lund, B. & Schmidt, P. & Hieronymus, C. 2009. Stress evolution and fault stability during the Weichselian glacial cycle. Stockholm, Sweden: Svensk kärnbränslehantering AB. 106 pages. SKB technical report 09-15. ISSN 1404-0344.

Martel, S. J. 2006. Effect of topographic curvature on near-surface stresses and application to sheeting joints. Geophysical research letters. Vol. 33:1. LO1308. DOI:10.1029/2005GL024710. ISSN 1944-8007

Martel, S. J. 2011. Mechanics of curved surfaces, with application to surface-parallel cracks. Geophysical research letters. Vol. 38:20. L20303. DOI:10.1029/ 2011GL049354. ISSN 1944-8007

Martin, C. D. 1997. Seventeenth Canadian geotechnical colloquium: the effect of cohesion loss and stress path on brittle rock strength. Canadian Geotechnical Journal. Vol. 34:5. pp. 698-725. DOI:10.1139/t97-030. ISSN 0008-3674 (Printed). ISSN 1208-6010 (Online)

Meier, T. & Kluge, C. & Backers, T. 2015. ONKALO POSE Experiment Laboratory fracture toughness test results. Eurajoki, Finland: Posiva Oy. 24 pages. Posiva working report 2015-15.

Mononen, S. 2005. Jännitystilan huomioon ottaminen rakennuskiven louhinnassa. Licentiate thesis. Helsinki University of Technology, Rock Engineering. 54 pages.

Nichols, T.C. 1980. Rebound, its nature and effect on engineering works. Journal of Engineering Geology and Hydrogeology. Vol. 13:3. pp. 133-152. DOI: 10.1144/GSL.QJEG.1980.013.03.01. ISSN 1470-9236 (Printed). ISSN 2041-4803 (Online)

Rinne, M. 2008. Fracture mechanics and subcritical crack growth approach to model time-dependent failure in brittle rock. Helsinki, Finland. Helsinki University of Technology, rock engineering. 150 pages. ISSN 1795-2239 (Printed). ISSN 1795-4584 (Online). ISBN 978-951-22-9434-3 (Printed). ISBN 978-951-22-9435-0 (Online).

Shen B. & Stephansson O. 1993. Numerical analysis of mixed mode I and mode II fracture propagation. International journal of rock mechanics and mining sciences & geomechanics abstracts. Vol 30:7. pp. 861-867. DOI:10.1016/0148-9062(93)90037-E. ISSN 0148-9062.

Shen, B. & Stephansson, O. & Rinne, M. 2014. Modelling rock fracturing processes, a fracture mechanics approach using FRACOD. Dordrecht, Netherlands. Springer. 173 pages. ISBN 978-94-007-9603-8

Siren, T. 2011. Fracture mechanics prediction for Posivas's Olkiluoto spalling experiment (POSE). Eurajoki, Finland: Posiva Oy. 30 pages. Posiva working report 2011-23.

Siren, T. 2015. ONKALO in situ concrete spalling experiment - fracture mechanics prediction. Eurajoki, Finland: Posiva Oy. 23 pages. Posiva working report 2013-48.

Steffen, H. & Wu, P. 2011. Glacial isostatic adjustment in Fennoscandia — A review of data and modeling. Journal of Geodynamics. Vol. 52:3-4. pp. 169-204. DOI: 10.1016/j.jog.2011.03.002. ISSN 0264-3707

SYKE, Finnish Environment Institute. 2016. Finnish Environment Institute open data. www.syke.fi/en-US/Open_information

Terzaghi, K. 1962. Dam foundation on sheeted granite. Géotechnique. Vol. 12:3. pp. 199–208. DOI:10.1680/geot.1962.12.3.199. ISSN 0016-8505 (Printed) ISSN 1751-7656 (Online).

Twidale, C. R. 1973. On the origin of sheet jointing. Rock mechanics. Vol. 5:3. pp. 163-187. ISSN 0035-7448.

Wakasa, S. & Matsuzaki, H. & Tanaka, Y. & Matskura, Y. 2006. Estimation of episodic exfoliation rates of rock sheets on a granite dome in Korea from cosmogenic nuclide analysis. Earth surface processes and landforms. Vol. 31:10. pp. 1246–1256. DOI:10.1002/esp.1328. ISSN 1096-9837

Wiederhorn, S. M. & Johnson, H. & Diness, A.M. & Heuer, A.H. 1974. Fracture of glass in vacuum. Journal of American Ceramic Society. Vol. 57:8. pp. 336-341. DOI:10.1111/j.1151-2916.1974.tb10917.x. ISSN 1551-2916

Whittaker B.N. & Singh R.N. & Sun G. 1992. Rock fracture mechanics, principles, design and applications. Amsterdam, the Netherlands. Elsevier. 570 pages. ISBN 0-444-896848

Wilkins, B.J.S. 1980. Slow crack growth and delayed failure of granite. International journal of rock mechanics and mining sciences. Vol 17:6. pp. 365-369. DOI:10.1016/0148-9062(80)90520-3. ISSN 1365-1609.

Åkesson, U. 2012. Laboratory measurements of the coefficient of thermal expansion of Olkiluoto drill core samples. Eurajoki, Finland: Posiva Oy. 31 pages. Posiva working report 2012-14.

Appendices

Appendix 1. Stress field of the topography 1

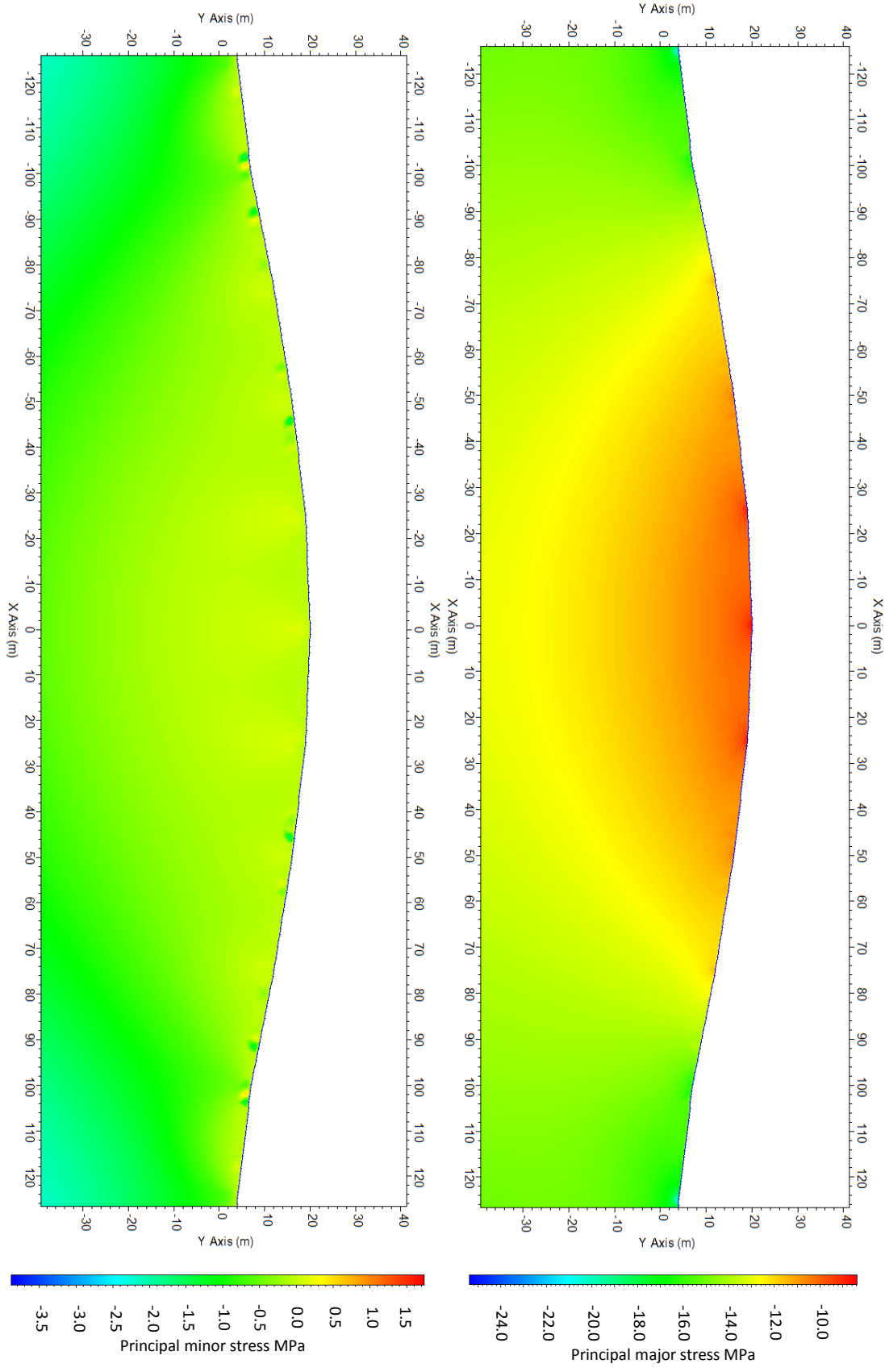

Appendix 2. Stress field of the topography 2

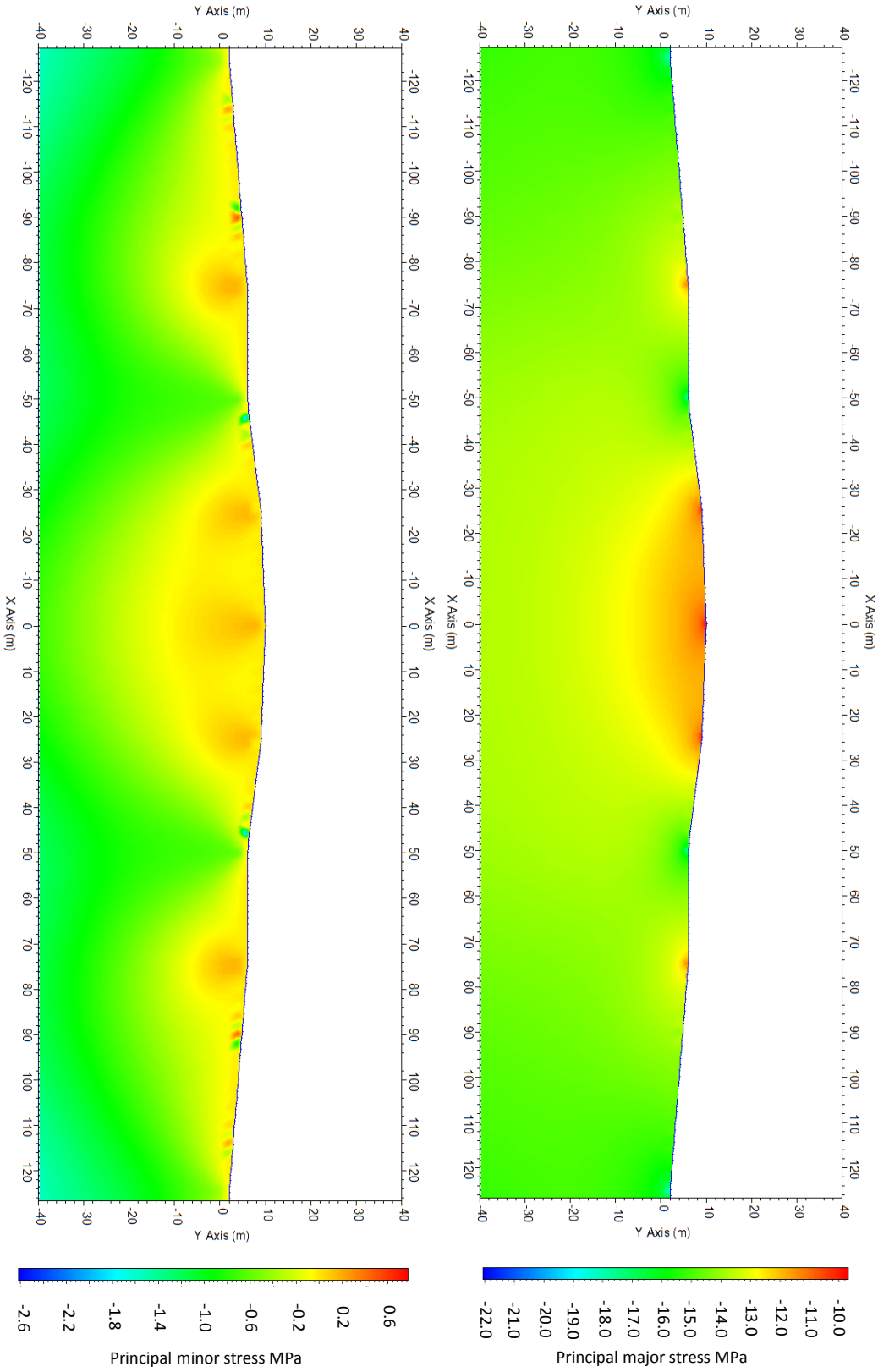

Appendix 3. Stress field of the topography 3

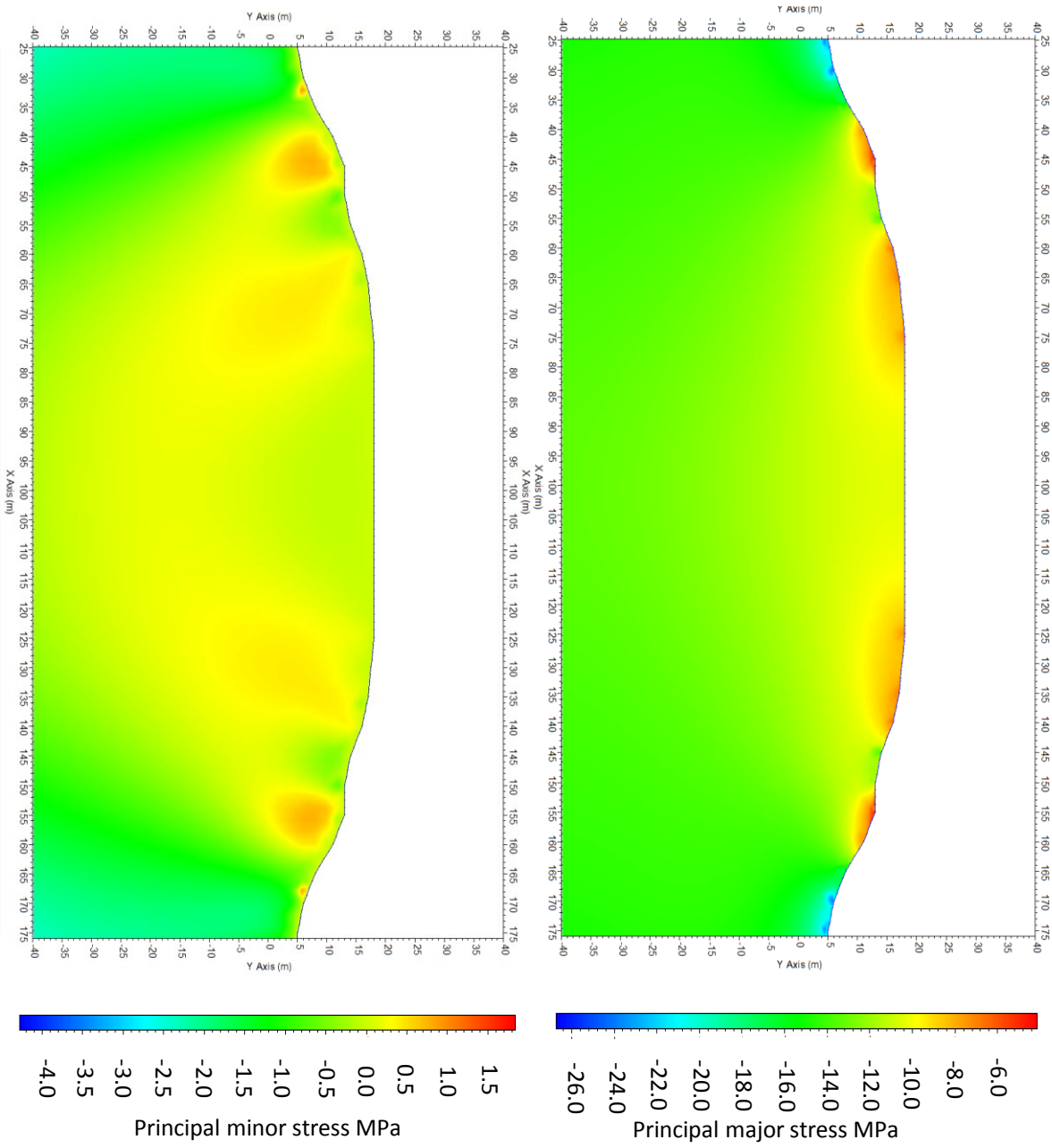

Appendix 4. Stress field of the topography 4

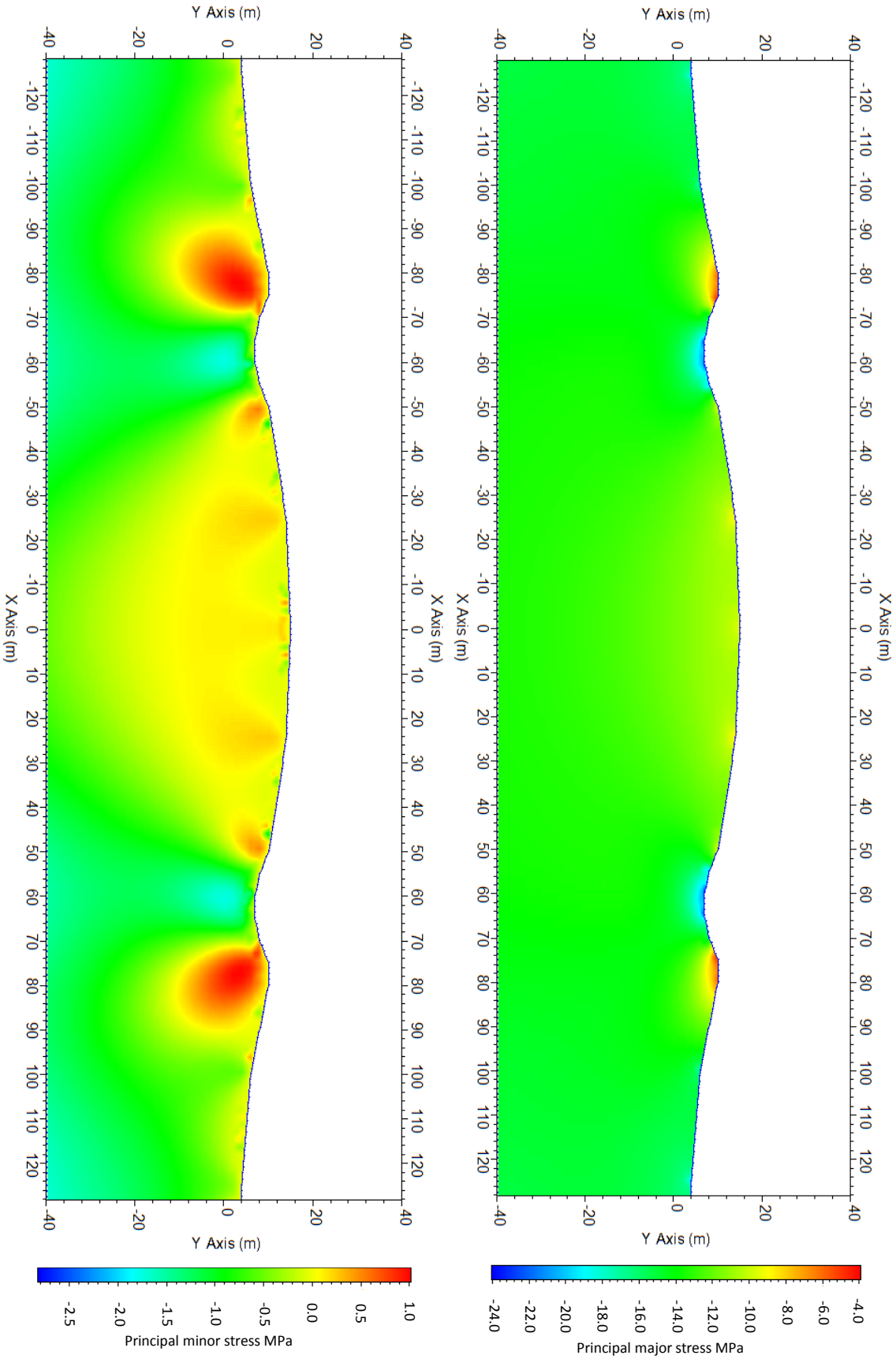

Appendix 5. FRACOD^{2D} code for thermal expansion

```
TITLE
Thermal expansion

SYMMETRY -- Model symmetry
1 100 0

TOUK -- Rock mass -- Kic and Kiic, mat
1.96e6 7.22e6 1

MODULUS -- Poisson's Ratio and Young's modulus
0.20 55e+9 1

PROPERIES -- Old joints -- jmat, ks. kn,phi,coh, dila, initial aperture, residual Aperture
01 80E+9 800E+9 35.0 4E+6 2.5 10e-6 1e-6

PROPERIES --- Tensile fractures -- jmat, ks. kn,phi,coh, dila, initial aperture, residual aperture
11 80E+9 800E+9 35.0 4E+6 2.5 10e-6 1e-6

PROPERIES --- Shear fractures -- jmat, ks. kn,phi,coh, dila, initial aperture, residual aperture
12 80E+9 800E+9 35.0 4E+6 2.5 10e-6 1e-6

STRESSES -- sxx,syy,sxy
-0e+06 0e+06 0

GRAVITY -- dens_rock,gy,sh_sv_ratio,y_surf
2650,-10,0.33,18

ROCK - rphi rcoh rst mat
47 12.9e+6 12e+6 1

SWINDOW -- xll,xur,yll,yur,numx,numy
0 200 -40 40 100 40

IWINDOW
25 175 -30 30

RANDOM fracture initiation - f_ini0,l_rand (initiation level, random or not)
0.40 0

SETF -- 1 ONLY ~ONE FRACTURE INITIATES ONCE
1.0

SETE -- If factor_e=0.0, all elastic fracture tips will be checked; (default factor_e=0.5)
0.5

SETT -- fracture tip is too close to the existing element. If so, they are either ignored, or merged to the
existing elements. (default tolerance=1.0)
1.0

ISIZE
2.0


**** THERMAL BOUNDARY CONDITION
```

TTIME -- 0 days --
561600 0 13

THERMAL -- Rock mass -- bt=thermal expansion factor,k=ct=thermal conductivity,density,cp=specific heat capacity,temp0,material
9.00e-6 3.20 2650 689 20 1

TBOU ! xt1,xt2,yt1,yt2,kode_t,value_t
25 100 -39 20 1

0	0	43
1	43200	-8
2	86400	90.2
3	129600	-59.4
4	172800	147.2
5	216000	-107.8
6	259200	197.2
7	302400	-161.8
8	345600	251.4
9	388800	-215
10	432000	303
11	475200	-264.8
12	518400	353.8
13	561600	-313.4

TBOU ! xt1,xt2,yt1,yt2,kode_t,value_t
1 25 -39 20 1

0	0	20
1	43200	20
2	86400	20
3	129600	20
4	172800	20
5	216000	20
6	259200	20
7	302400	20
8	345600	20
9	388800	20
10	432000	20
11	475200	20
12	518400	20
13	561600	20

TFRA ! xt1,xt2,yt1,yt2,kode_t,value_t
0 200 -40 20 3

0	0	0
1	43200	0
2	86400	0
3	129600	0
4	172800	0
5	216000	0
6	259200	0
7	302400	0
8	345600	0
9	388800	0
10	432000	0
11	475200	0
12	518400	0
13	561600	0

*** MONITORNG LINES

MONL
47.5 12.98 47.5 11.98 10

MONL
47.5 12.98 47.5 -2.98 15

**** GEOMETRY

EDGE - num,xbeg,ybeg,xend,yend,kode,bvs,bvn,mat,gradsy,gradny
4 70 17.5 75 18 1 0 0e6 1

EDGE - num,xbeg,ybeg,xend,yend,kode,bvs,bvn,mat,gradsy,gradny
4 65 17 70 17.5 1 0 0e6 1

EDGE - num,xbeg,ybeg,xend,yend,kode,bvs,bvn,mat,gradsy,gradny
4 60 16 65 17 1 0 0e6 1

EDGE - num,xbeg,ybeg,xend,yend,kode,bvs,bvn,mat,gradsy,gradny
4 55 14 60 16 1 0 0e6 1

EDGE - num,xbeg,ybeg,xend,yend,kode,bvs,bvn,mat,gradsy,gradny
4 50 13 55 14 1 0 0e6 1

EDGE - num,xbeg,ybeg,xend,yend,kode,bvs,bvn,mat,gradsy,gradny
4 45 13 50 13 1 0 0e6 1

EDGE - num,xbeg,ybeg,xend,yend,kode,bvs,bvn,mat,gradsy,gradny
4 40 11 45 13 1 0e6 1

EDGE - num,xbeg,ybeg,xend,yend,kode,bvs,bvn,mat,gradsy,gradny
4 35 8 40 11 1 0 0e6 1

EDGE - num,xbeg,ybeg,xend,yend,kode,bvs,bvn,mat,gradsy,gradny
4 30 6 35 8 1 0 0e6 1

EDGE - num,xbeg,ybeg,xend,yend,kode,bvs,bvn,mat,gradsy,gradny
4 25 5 30 6 1 0 0e6 1

EDGE - num,xbeg,ybeg,xend,yend,kode,bvs,bvn,mat,gradsy,gradny
33 0 -40 0 5 1 0 -18.53e6 1

EDGE - num,xbeg,ybeg,xend,yend,kode,bvs,bvn,mat,gradsy,gradny
19 75 18 100 18 1 0e6 0 1

EDGE - num,xbeg,ybeg,xend,yend,kode,bvs,bvn,mat,gradsy,gradny
19 0 5 25 5 1 0e6 0 1

EDGE - num,xbeg,ybeg,xend,yend,kode,bvs,bvn,mat,gradsy,gradny
75 100 -40 0 -40 4 0e6 0 1

CYCL 1

***INITIATION

INTERNAL FRAC INITATION

***THERMAL TIME STEPS

TTIME -- 21.07.2014
561600 1 13
CYCL 2 -- 2 cycle --

TTIME -- 22.07.2014
561600 2 13
CYCL 2 -- 2 cycle --

TTIME -- 22.07.2014
561600 3 13
CYCL 2 -- 2 cycle --

TTIME -- 23.07.2014
561600 4 13
CYCL 2 -- 2 cycle --

TTIME -- 23.07.2014
561600 5 13
CYCL 2 -- 2 cycle --

TTIME -- 24.07.2014
561600 6 13
CYCL 2 -- 2 cycle --

TTIME -- 24.07.2014
561600 7 13
CYCL 2 -- 2 cycle --

TTIME -- 25.07.2014
561600 8 13
CYCL 2 -- 2 cycle --

TTIME -- 25.07.2014
561600 9 13
CYCL 2 -- 2 cycle --

TTIME -- 26.07.2014
561600 10 13
CYCL 2 -- 2 cycle --

TTIME -- 26.07.2014
561600 11 13
CYCL 2 -- 2 cycle --

TTIME -- 27.07.2014
561600 12 13
CYCL 2 -- 2 cycle --

TTIME -- 27.07.2014
561600 13 13
CYCL 2 -- 2 cycle –

endfile